



Applied Research and Innovation Branch

# Dynamic Modulus of Cold-in-Place Recycling (CIR) Material

Md Rashadul Islam, Sylvester A. Kalevela and Jill A. Rivera

Report No. CDOT 2018-13  
May 2018

The contents of this report reflect the views of the authors, who are responsible for the facts and accuracy of the data presented herein. The contents do not necessarily reflect the official views of the Colorado Department of Transportation or the Federal Highway Administration. This report does not constitute a standard, specification, or regulation.

**Technical Report Documentation Page**

1. Report No. CDOT 2018-13		2. Government Accession No.		3. Recipient's Catalog No.	
4. Title and Subtitle Dynamic Modulus of Cold In-Place Recycling (CIR) Material				5. Report Date May 2018	
				6. Performing Organization Code	
7. Author(s) Md Rashadul Islam, Sylvester A. Kalevela and Jill A. Rivera				8. Performing Organization Report No. CDOT 2018-13	
9. Performing Organization Name and Address Colorado State University – Pueblo Department of Engineering Technology 2200 Bonforte Blvd Pueblo, CO 81001				10. Work Unit No. (TRAIS)	
				11. Contract or Grant No. CDOT 415.02	
12. Sponsoring Agency Name and Address Colorado Department of Transportation - Research 4201 E. Arkansas Ave. Denver, CO 80222				13. Type of Report and Period Covered Final Report, June 2016 – September 2017	
				14. Sponsoring Agency Code	
15. Supplementary Notes Prepared in cooperation with the US Department of Transportation, Federal Highway Administration					
16. Abstract  <p>This study investigates the dynamic modulus of Cold-in-Place Recycling (CIR) pavement material and its performance using pavement performance data, field testing, laboratory testing, and Pavement Mechanistic-Empirical Design Guide (PMED) software analysis. Colorado Department of Transportation (CDOT) has 37 projects with over 8 million square yards using CIR materials. Sites from ten projects were selected to monitor the performances, and collect samples for laboratory testing. Field sampling, R-value testing of base/subgrade, and resilient modulus of base/subgrade were conducted. Dynamic moduli testing on the CIR cores were conducted by the CDOT. PMED software analysis was conducted using the data to examine the CDOT-calibrated PMED software for overlay design with CIR data. Results show measured distresses of CIR rehabilitation techniques are mostly below the threshold values during the service period. International Roughness Index, rutting, and transverse cracking never exceeded the threshold values during the studied period. Only two CIR pavements exceeded the threshold values for fatigue cracking after 8-10 years of service. Measured distresses of CIR rehabilitation techniques are similar to conventional pavement. The laboratory test results show CIR has about 50% less dynamic modulus compared to the traditional asphalt mixture. The CDOT-calibrated PMED software predicts the International Roughness Index (IRI) and the rutting of CIR overlaid pavement well but underestimates fatigue cracking.</p> <p><u>Implementation Statement</u> The results of this research will be presented to the Materials Advisory Committee (MAC) for review and approval for incorporation into the CDOT Pavement Design Manual and the PMED software program if found favorable. Considering the field performances of tested CIR pavements, this research recommends CDOT use the data derived from this study to support and implement the continued deployment of this recycling technology.</p>					
17. Keywords Cold-in-Place Recycling, Performance, Dynamic Modulus, PMED			18. Distribution Statement This document is available on CDOT's website <a href="http://www.coloradodot.info/programs/research/pdfs">http://www.coloradodot.info/programs/research/pdfs</a>		
19. Security Classif. (of this report) Unclassified		20. Security Classif. (of this page) Unclassified		21. No. of Pages 136	22. Price

## **ACKNOWLEDGEMENTS**

The Colorado State University-Pueblo (CSU-Pueblo) research team would like to express its sincere gratitude and appreciation to Jay Goldbaum and Michael Stanford for being the Study Panel Leaders and Colorado Department of Transportation (CDOT) Champions for this project and for their regular support and suggestions. We appreciate the valuable administration and support of the Applied Research and Innovation Branch (ARIB) Deputy Director and Research Program Area Manager, Dr. Aziz Khan. The CSU-Pueblo research team would like to thank the Study Panel Members James Chang (Region 1 Materials), Melody Perkins (Pavement Design Program), Keith Uren (Pavement Design Engineer), Vincent Battista (Support Engineer), Skip Outcalt, and Craig Wieden (Region 2 Materials) for their valuable suggestions during the project. We are also grateful to Dave Weld and Paul Smith for their help in the field, Tim Luscombe and Nick Andrade of Ground Engineering for their help in sample collection and laboratory testing, and Marshall Shackelford of Suncor Energy (USA), Inc. who performed additional reviews of the draft report. The CSU-Pueblo research team would also like to thank Dahir Egal, the Federal Highway Administration (FHWA) - Colorado Division contact, and Bill Schiebel, the Research and Implementation Council (RIC) Sponsor. Special thanks go to Numan Mized and Roberto E. DeDios for their keen interest in the project and timely operational support, and to Jessica Weatherby, the CDOT Librarian, for grammar and document review. Finally, the authors would like to thank the ARIB Director, Amanullah Mommandi for his overall support.

## **Executive Summary and Implementation Statement**

Due to the advancement of milling equipment and rise in asphalt binder's price, pavement rehabilitation has become very popular in pavement design and roadway construction. Although several rehabilitation technologies are available, Cold-in-Place Recycling (CIR) technology may be the cheapest and environment-friendliest. Prior to adopting this technology, CIR's properties and performance data must be evaluated. Currently, Colorado Department of Transportation (CDOT) does not have specific dynamic modulus and performance information for Cold-in-Place Recycling (CIR) pavement layers/materials. In addition, the CDOT Mechanistic Empirical (M-E) Pavement Design Manual has not established recommendations for appropriate CIR modulus values to use for design. Prior to using the Pavement Mechanistic-Empirical Design (PMED) program, reliable dynamic modulus values representative of the type, source of CIR materials used in pavement construction, and the performance expectation must be established. The goal of this study is to develop modulus values for various CIR materials that can be confidently and effectively used by CDOT pavement designers when using the Mechanistic and Empirical Design approach. This study also aims to develop and implement new standards that could improve the performance of CIR pavements and make future CIR pavements more feasible and cost-effective.

Since 2000, CDOT has built 37 projects with over 8 million square yards using the CIR process. Sites from ten projects were selected to monitor the performances, collect asphalt, base, and subgrade samples for laboratory testing. Field sampling, R-Value testing of base/subgrade, and resilient modulus of base/subgrade were conducted by Ground Engineering. Dynamic modulus testing on the CIR cores were conducted for the sites by CDOT. PMED software analysis was conducted using laboratory test data to examine CDOT CIR software calibrations.

Field performance data collected by CDOT for time periods between the year CIR projects were completed and 2016. Four types of data were collected: fatigue cracking, rutting, transverse cracking, and International Roughness Index (IRI) also known as smoothness. Measured distresses of CIR rehabilitation techniques are mostly below the threshold values during the service period. IRI, rutting, and transverse cracking never exceeded the threshold values during the studied period. Only two CIR pavements exceeded the threshold values for fatigue cracking after 8-10 years of

service. Control test sites with similar climate, traffic, and geometry were identified for each of the 10 sites. Analysis of field performance data collected at the control sites showed that CIR technology had comparable performance levels to conventional rehabilitation techniques or conventional pavement. The CIR performance was better at three sites, similar at one site, and worse at six sites compared to the control projects for fatigue cracking. Results of rutting show CIR performed better at four sites, similar at two sites, and worse at four sites compared to the control sites. For transverse cracking, CIR performed better at five sites, and worse at five sites compared to the control projects. CIR performed better at four sites, and worse at six sites compared to the control projects for IRI. Considering all of these field performances, it can be said that measured distresses of CIR rehabilitation techniques are similar to conventional pavements. Laboratory test results show the dynamic modulus of CIR is about 50% of the dynamic modulus of a conventional asphalt mixture. PMED software analysis shows that the CDOT-calibrated PMED software for overlay design is an acceptable tool for predicting IRI and rutting distress, but not for fatigue cracking. Considering the fore-mentioned field performance results, this study suggests that the use of CIR technology for pavement design can be an effective solution.

# TABLE OF CONTENTS

Acknowledgements.....	i
Table Of Contents.....	iv
List Of Figures.....	viii
List Of Tables.....	xiv
<b>SECTION 1: INTRODUCTION.....</b>	<b>1</b>
Background.....	1
Objectives.....	1
<b>SECTION 2: LITERATURE REVIEW.....</b>	<b>3</b>
Background.....	3
Benefits.....	3
Comparison with Conventional HMA.....	3
Field Evaluation.....	4
Application.....	4
Miscellaneous Evaluations.....	5
Literature Summary.....	6
<b>SECTION 3: SELECTED SITES.....</b>	<b>7</b>
Introduction.....	7
Selected Test Sites.....	7
Site #1: SH 9 Fairplay to Alma.....	7
Site #2: SH 9 Hoosier Pass (Northbound).....	9
Site #3: SH 86 East of Franktown.....	11
Site #4: SH 86 Kiowa (Eastbound).....	12
Site #5: I-25 South of Colorado City to Cedarwood.....	14
Site #6: SH 50 Cerro Summit Paving.....	15
Site #7: I-70 West of Mack.....	17
Site #8: I-70 Fruita to Clifton.....	18
Site #9: SH 92 Delta (Eastbound).....	20
Site #10: SH 133 North of Hotchkiss.....	21

Selected Control Sites .....	23
Control Site #1 .....	23
Control Site #2 .....	24
Control Site #3 .....	25
Control Site #4 .....	25
Control Site #5 .....	26
Control Site #6 .....	26
Control Site #7 .....	27
Control Site #8 .....	28
Control Site #9 .....	28
Control Site #10 .....	29
<b>SECTION 4: PERFORMANCE DATA .....</b>	<b>31</b>
General .....	31
Site #1 SH 9 Fairplay to Alma .....	32
Site #2 SH 9 Hoosier Pass (Northbound) .....	35
Site #3 SH 86 East of Franktown .....	37
Site #4 SH 86 Kiowa (Eastbound) .....	40
Site #5 I-25 South of Colorado City to Cedarwood .....	43
Site #6 SH 50 Cerro Summit Paving .....	46
Site #7 I-70 West of Mack .....	49
Site #8 I-70 Fruita to Clifton .....	52
Site #9 SH 92 Delta (Eastbound) .....	55
Site #10 SH 133 North of Hotchkiss .....	58
Pavement Performance Summary .....	61
<b>SECTION 5: MATERIALS COLLECTION AND TESTING .....</b>	<b>65</b>
Background .....	65
Materials Collection .....	65
Characterization of CIR .....	67
Dynamic Modulus (E*) Testing .....	67
Resilient Modulus Testing .....	68
Classification of Base and Subgrade Courses .....	69

Maximum Dry Density and Optimum Moisture Content Testing for Base Course .....	70
R-Value (California Bearing Ratio) Testing.....	70
Maximum Dry Density and Optimum Moisture Content Testing for Subgrade Course .....	70
<b>SECTION 6: SUMMARY OF RESULTS AND DISCUSSION.....</b>	<b>71</b>
General.....	71
Dynamic Modulus Test Results .....	71
Site #1 SH 9 From Fairplay to Alma .....	71
Site #2 Hoosier Pass (Northbound).....	73
Site #3 SH 86 East of Franktown.....	75
Site #4 SH 86 Kiowa (Eastbound).....	77
Site #5 I-25 South of Colorado City to Cedarwood.....	79
Site #6 Cerro Summit Paving .....	81
Site #7 West of Mack.....	83
Site #8 Fruita to Clifton .....	85
Site #9 Delta (Eastbound).....	87
Site #10 SH 133 North of Hotchkiss.....	89
Development of Dynamic Modulus Data for the PMED.....	91
Properties of Base/Subgrade.....	95
Classification, R-Value and Proctor Results.....	95
Resilient Modulus of Base/Subgrade.....	96
<b>SECTION 7: PMED SOFTWARE ANALYSIS .....</b>	<b>109</b>
General.....	109
PMED Analysis .....	109
Site #1 SH 9 from Fairplay to Alma .....	110
Site #2 SH 9 Hoosier Pass (Northbound) .....	112
Site #3 SH 86 East of Franktown.....	114
Site #4 SH 86 Kiowa (Eastbound).....	117
Site #5 I-25 South of Colorado City .....	119
Site #6 SH 50 Cerro Summit .....	121
Site #7 I-70 West of Mack .....	124
Site #8 I-70 Fruita to Clifton.....	126

Site #9 SH 92 Delta (Eastbound).....	128
Site #10 SH 133 North of Hotchkiss.....	130
Summary.....	132
<b>SECTION 8: CONCLUSIONS AND RECOMMENDATIONS .....</b>	<b>133</b>
Conclusions.....	133
Recommendations for Future Studies.....	134
Implementation Plans.....	134
<b>SECTION 9: REFERENCES .....</b>	<b>135</b>

## LIST OF FIGURES

Figure 1. Cross Section of Pavement Structure at the SH 9 Fairplay to Alma Site.....	8
Figure 2. View of the SH 9 Fairplay to Alma Site Looking North.....	8
Figure 3. Location of the SH 9 Fairplay to Alma Site (Google Maps).....	9
Figure 4. Cross Section of Pavement at the SH 9 Hoosier Pass (Northbound) .....	10
Figure 5. View of the SH 9 Hoosier Pass (Northbound) Site Looking North .....	10
Figure 6. Location of the SH 9 Hoosier Pass (Northbound) Site (Google Maps) .....	10
Figure 7. Cross Section of Pavement Structure at the SH 86 East of Franktown.....	11
Figure 8. View of the SH 86 East of Franktown Site Looking East.....	12
Figure 9. Location of the SH 86 East of Franktown Site (Google Maps) .....	12
Figure 10. Cross Section of Pavement Structure at the SH 86 Kiowa (Eastbound) .....	13
Figure 11. View of the SH 86 Kiowa (Eastbound) Site Looking East .....	13
Figure 12. Location of the SH 86 Kiowa (Eastbound) Site (Google Maps).....	14
Figure 13. Cross Section of Pavement Structure at the I-25 South of Colorado City to Cedarwood .....	14
Figure 14. View of the I-25 South of Colorado City to Cedarwood Site Looking South .....	15
Figure 15. Location of the I-25 South of Colorado City to Cedarwood Site (Google Maps) .....	15
Figure 16. Cross Section of Pavement Structure at the SH 50 Cerro Summit.....	16
Figure 17. View of the SH 50 Cerro Summit Looking East.....	16
Figure 18. Location of the SH 50 Cerro Summit Site (Google Maps) .....	16
Figure 19. Cross Section of Pavement Structure at the I-70 West of Mack .....	17
Figure 20. View of the I-70 West of Mack Site Looking West.....	17
Figure 21. Location of the I-70 West of Mack Site (Google Maps).....	18
Figure 22. Cross Section of Pavement Structure at the I-70 Fruita to Clifton.....	19
Figure 23. View of the I-70 Fruita to Clifton Site .....	19
Figure 24. Location of the I-70 Fruita to Clifton Site (Google Maps) .....	20
Figure 25. Cross Section of Pavement Structure at the SH 92 Delta (Eastbound) .....	20
Figure 26. View of the SH 92 Delta (Eastbound) Site Looking West.....	21
Figure 27. Location of the SH 92 Delta (Eastbound) Site (Google Maps).....	21
Figure 28. Cross Section of Pavement Structure at the SH 133 North of Hotchkiss.....	22
Figure 29. View of the SH 133 North of Hotchkiss Site .....	22
Figure 30. Location of the SH 133 North of Hotchkiss Site (Google Maps) .....	23
Figure 31. Cross-section of Pavement Structure at Control Site #1 .....	24
Figure 32. Cross-section of Pavement Structure at Control Site #2 .....	24
Figure 33. Cross-section of Pavement Structure at Control Site #3 .....	25
Figure 34. Cross-section of Pavement Structure at Control Site #4 .....	25
Figure 35. Cross-section of Pavement Structure at Control Site #5 .....	26
Figure 36. Cross-section of Pavement Structure at Control Site #6 .....	27
Figure 37. Cross-section of Pavement Structure at Control Site #7 .....	27

Figure 38. Cross-section of Pavement Structure at Control Site #8 .....	28
Figure 39. Cross-section of Pavement Structure at Control Site #9 .....	29
Figure 40. Cross-section of Pavement Structure at Control Site #10 .....	30
Figure 41. Fatigue Cracking at Site #1 SH 9 Fairplay to Alma Showing Amount of Cracking at the Control Site, Test Site, and Whole Project .....	32
Figure 42. Rutting at Site #1 SH 9 Fairplay to Alma Showing Amount of Rutting at the Control Site, Test Site, and Whole Project .....	33
Figure 43. Transverse Cracking at Site #1 SH 9 Fairplay to Alma Showing Amount of Cracking at the Control Site, Test Site, and Whole Project .....	34
Figure 44. IRI at Site #1 SH 9 Fairplay to Alma Showing Amount of IRI at the Control Site, Test Site, and Whole Project.....	34
Figure 45. Fatigue Cracking at Site #2 SH 9 Hoosier Pass (Northbound) Showing Amount of Cracking at the Control Site, Test Site, and Whole Project.....	35
Figure 46. Rutting at Site #2 SH 9 Hoosier Pass (Northbound) Showing Amount of Rutting at the Control Site, Test Site, and Whole Project .....	36
Figure 47. Transverse Cracking at Site #2 SH 9 Hoosier Pass (Northbound) Showing Amount of Cracking at the Control Site, Test Site, and Whole Project.....	36
Figure 48. IRI at Site #2 SH 9 Hoosier Pass (Northbound) Showing Amount of IRI at the Control Site, Test Site, and Whole Project .....	37
Figure 49. Fatigue Cracking at Site #3 SH 86 East of Franktown Showing Amount of Cracking at the Control Site, Test Site, and Whole Project .....	38
Figure 50. Rutting at Site #3 SH 86 East of Franktown Showing Amount of Rutting at the Control Site, Test Site, and Whole Project .....	38
Figure 51. Transverse Cracking at Site #3 SH 86 East of Franktown Showing Amount of Cracking at the Control Site, Test Site, and Whole Project.....	39
Figure 52. IRI at Site #3 SH 86 East of Franktown Showing Amount of IRI at the Control Site, Test Site, and Whole Project.....	40
Figure 53. Fatigue Cracking at Site #4 SH 86 Kiowa (Eastbound) Showing Amount of Cracking at the Control Site, Test Site, and Whole Project .....	41
Figure 54. Rutting at Site #4 SH 86 Kiowa (Eastbound) Showing Amount of Rutting at the Control Site, Test Site, and Whole Project .....	41
Figure 55. Transverse Cracking at Site #4 SH 86 Kiowa (Eastbound) Showing Amount of Cracking at the Control Site, Test Site, and Whole Project.....	42
Figure 56. IRI at Site #4 SH 86 Kiowa (Eastbound) Showing Amount of IRI at the Control Site, Test Site, and Whole Project.....	43
Figure 57. Fatigue Cracking at Site #5 I-25 South of Colorado City to Cedarwood Showing Amount of Cracking at the Control Site, Test Site, and Whole Project .....	44
Figure 58. Rutting at Site #5 I-25 South of Colorado City to Cedarwood Showing Amount of Rutting at the Control Site, Test Site, and Whole Project .....	45

Figure 59. Transverse Cracking at Site #5 I-25 South of Colorado City to Cedarwood Showing Amount of Cracking at the Control Site, Test Site, and Whole Project .....	45
Figure 60. IRI at Site #5 I-25 South of Colorado City to Cedarwood Showing Amount of IRI at the Control Site, Test Site, and Whole Project .....	46
Figure 61. Fatigue Cracking at Site #6 SH 50 Cerro Summit Paving Showing Amount of Cracking at the Control Site, Test Site, and Whole Project.....	47
Figure 62. Rutting at Site #6 SH 50 Cerro Summit Paving Showing Amount of Rutting at the Control Site, Test Site, and Whole Project .....	47
Figure 63. Transverse Cracking at Site #6 SH 50 Cerro Summit Paving Showing Amount of Cracking at the Control Site, Test Site, and Whole Project.....	48
Figure 64. IRI at Site #6 SH 50 Cerro Summit Paving Showing Amount of IRI at the Control Site, Test Site, and Whole Project .....	49
Figure 65. Fatigue Cracking at Site #7 I-70 West of Mack Showing Amount of Cracking at the Control Site, Test Site, and Whole Project .....	50
Figure 66. Rutting at Site #7 I-70 West of Mack Showing Amount of Rutting at the Control Site, Test Site, and Whole Project.....	51
Figure 67. Transverse Cracking at Site #7 I-70 West of Mack Showing Amount of Cracking at the Control Site, Test Site, and Whole Project .....	51
Figure 68. IRI at Site #7 I-70 West of Mack Showing Amount of IRI at the Control Site, Test Site, and Whole Project.....	52
Figure 69. Fatigue Cracking at Site #8 I-70 Fruita to Clifton Showing Amount of Cracking at the Control Site, Test Site, and Whole Project .....	53
Figure 70. Rutting at Site #8 I-70 Fruita to Clifton Showing Amount of Rutting at the Control Site, Test Site, and Whole Project .....	54
Figure 71. Transverse Cracking at Site #8 I-70 Fruita to Clifton Showing Amount of Cracking at the Control Site, Test Site, and Whole Project .....	54
Figure 72. IRI at Site #8 I-70 Fruita to Clifton Showing Amount of IRI at the Control Site, Test Site, and Whole Project.....	55
Figure 73. Fatigue Cracking at Site #9 SH 92 Delta (Eastbound) Showing Amount of Cracking at the Control Site, Test Site, and Whole Project .....	56
Figure 74. Rutting at Site #9 SH 92 Delta (Eastbound) Showing Amount of Rutting at the Control Site, Test Site, and Whole Project .....	57
Figure 75. Transverse Cracking at Site #9 SH 92 Delta (Eastbound) Showing Amount of Cracking at the Control Site, Test Site, and Whole Project.....	57
Figure 76. IRI at Site #9 SH 92 Delta (Eastbound) Showing Amount of IRI at the Control Site, Test Site, and Whole Project.....	58
Figure 77. Fatigue Cracking at Site #10 SH 133 North of Hotchkiss Showing Amount of Cracking at the Control Site, Test Site, and Whole Project.....	59
Figure 78. Rutting at Site #10 SH 133 North of Hotchkiss Showing Amount of Rutting at the Control Site, Test Site, and Whole Project .....	59

Figure 79. Transverse Cracking at Site #10 SH 133 North of Hotchkiss Showing Amount of Cracking at the Control Site, Test Site, and Whole Project.....	60
Figure 80. IRI at Site #10 SH 133 North of Hotchkiss Showing Amount of IRI at the Control Site, Test Site, and Whole Project .....	61
Figure 81. Approximate Coring Locations at Each Site.....	66
Figure 82. Coring Operation at SH 86 Kiowa East .....	66
Figure 83. Cored Asphalt Samples from the SH 86 Kiowa East.....	66
Figure 84. AMPT Sample Preparation and Test Setup.....	67
Figure 85. AMPT Test Setup.....	68
Figure 86. Resilient Modulus Sample Preparation .....	68
Figure 87. Resilient Modulus Test Setup on a Soil Sample .....	69
Figure 88. Dynamic Moduli of Samples from SH 9 From Fairplay to Alma.....	73
Figure 89. Dynamic Moduli of Samples from Hoosier Pass (Northbound) .....	75
Figure 90. Dynamic Moduli of Samples from SH 86 East of Franktown .....	77
Figure 91. Dynamic Moduli of Samples from Kiowa (Eastbound).....	79
Figure 92. Dynamic Moduli of Samples from I-25 South of Colorado City to Cedarwood .....	81
Figure 93. Dynamic Moduli of Samples from Cerro Summit Paving.....	83
Figure 94. Dynamic Moduli of Samples from West of Mack .....	85
Figure 95. Dynamic Moduli of Samples from Fruita to Clifton.....	87
Figure 96. Dynamic Moduli of Samples from Delta East .....	89
Figure 97. Dynamic Moduli of Samples from North of Hotchkiss .....	91
Figure 98. Dynamic Moduli of all Mixes Including Conventional Mixtures.....	95
Figure 99. Resilient Modulus of the Blended Base and Subgrade at SH 9 from Fairplay to Alma Subgrade .....	97
Figure 100. Resilient Modulus of the Subgrade at SH 9 Hoosier Pass.....	98
Figure 101. Resilient Modulus of the Subgrade at SH 86 Franktown.....	99
Figure 102. Resilient Modulus of the Subgrade at SH 86 Kiowa (Eastbound).....	100
Figure 103. Resilient Modulus of the Subgrade at I-25 South of Colorado City. ....	101
Figure 104. Resilient Modulus of the Subgrade. ....	102
Figure 105. Resilient Modulus of the Subgrade at I-70 West of Mack. ....	103
Figure 106. Resilient Modulus of the Subgrade at I-70 Fruita to Clifton.....	104
Figure 107. Resilient Modulus of the Subgrade at SH 92 Delta (Eastbound) .....	105
Figure 108. Resilient Modulus of the Base at SH 92 Delta (Eastbound) .....	106
Figure 109. Resilient Modulus of the Subgrade at SH 133 Hotchkiss. ....	107
Figure 110. Resilient Modulus of the Base at SH 133 Hotchkiss.....	108
Figure 111. IRI at SH 9 from Fairplay to Alma Showing Amount of Measured and PMED Predicted IRI.....	110
Figure 112. Total Rutting at SH 9 from Fairplay to Alma Showing Amount of Measured and PMED Predicted Rutting .....	111

Figure 113. Fatigue Cracking at SH 9 from Fairplay to Alma Showing Amount of Measured and PMED Predicted Cracking.....	112
Figure 114. IRI at Hoosier Pass (Northbound) Showing Amount of Measured and PMED Predicted IRI.....	113
Figure 115. Total Rutting at Hoosier Pass (Northbound) Showing Amount of Measured and PMED Predicted Rutting .....	113
Figure 116. Fatigue Cracking at Hoosier Pass (Northbound) Showing Amount of Measured and PMED Predicted Cracking.....	114
Figure 117. IRI at SH 86 East of Franktown Showing Amount of Measured and PMED Predicted IRI.....	115
Figure 118. Total Rutting at SH 86 East of Franktown Showing Amount of Measured and PMED Predicted Rutting .....	116
Figure 119. Fatigue Cracking at SH 86 East of Franktown Showing Amount of Measured and PMED Predicted Cracking.....	116
Figure 120. IRI at SH 86 Kiowa (Eastbound) Showing Amount of Measured and PMED Predicted IRI.....	117
Figure 121. Total Rutting at SH 86 Kiowa (Eastbound) Showing Amount of Measured and PMED Predicted Rutting .....	118
Figure 122. Fatigue Cracking at SH 86 Kiowa (Eastbound) Showing Amount of Measured and PMED Predicted Cracking.....	118
Figure 123. IRI at I-25 South of Colorado City Showing Amount of Measured and PMED Predicted IRI.....	119
Figure 124. Total Rutting at I-25 South of Colorado City Showing Amount of Measured and PMED Predicted Rutting .....	120
Figure 125. Fatigue Cracking at I-25 South of Colorado City Showing Amount of Measured and PMED Predicted Cracking.....	121
Figure 126. IRI at SH 50 Cerro Showing Amount of Measured and PMED Predicted IRI.....	122
Figure 127. Total Rutting at SH 50 Cerro Summit Showing Amount of Measured and PMED Predicted Rutting .....	122
Figure 128. Fatigue Cracking at SH 50 Cerro Summit Showing Amount of Measured and PMED Predicted Cracking.....	123
Figure 129. IRI at I-70 West of Mack Showing Amount of Measured and PMED Predicted IRI .....	124
Figure 130. Total Rutting at I-70 West of Mack Showing Amount of Measured and PMED Predicted Rutting .....	125
Figure 131. Fatigue Cracking at I-70 West of Mack Showing Amount of Measured and PMED Predicted Cracking.....	125
Figure 132. IRI at I-70 Fruita to Clifton Showing Amount of Measured and PMED Predicted IRI .....	126

Figure 133. Total Rutting at I-70 Fruita to Clifton Showing Amount of Measured and PMED Predicted Rutting .....	127
Figure 134. Fatigue Cracking at I-70 Fruita to Clifton Showing Amount of Measured and PMED Predicted Cracking.....	127
Figure 135. IRI at SH 92 Delta (Eastbound) Showing Amount of Measured and PMED Predicted IRI .....	128
Figure 136. Total Rutting at SH 92 Delta (Eastbound) Showing Amount of Measured and PMED Predicted Rutting .....	129
Figure 137. Fatigue Cracking at SH 92 Delta (Eastbound) Showing Amount of Measured and PMED Predicted Cracking.....	129
Figure 138. IRI at SH 133 North of Hotchkiss Showing Amount of Measured and PMED Predicted IRI .....	130
Figure 139. Total Rutting at SH 133 North of Hotchkiss Showing Amount of Measured and PMED Predicted Rutting .....	131
Figure 140. Fatigue Cracking at SH 133 North of Hotchkiss Showing Amount of Measured and PMED Predicted Cracking.....	131

## LIST OF TABLES

Table 1. Selected CIR Locations from Different Regions .....	7
Table 2. Measured Maximum Distresses .....	62
Table 3. Recommended Threshold Values of Performance Criteria for Rehabilitation of Flexible Pavement Projects .....	62
Table 4. CIR Performance Compared to Conventional Pavement .....	63
Table 5. Test Protocols for Measuring Material Properties .....	65
Table 6. Dynamic Moduli of Two Samples from SH 9 from Fairplay to Alma.....	72
Table 7. Dynamic Moduli of Two Samples from Hoosier Pass (Northbound) .....	74
Table 8. Dynamic Moduli of Two Samples from SH 86 East of Franktown .....	76
Table 9. Dynamic Moduli of Two Samples from Kiowa (Eastbound).....	78
Table 10. Dynamic Moduli of Two Samples from I-25 South of Colorado City to Cedarwood .	80
Table 11. Dynamic Moduli of Two Samples from Cerro Summit Paving .....	82
Table 12. Dynamic Moduli of Two Samples from West of Mack .....	84
Table 13. Dynamic Modulus of Two Samples from Fruita to Clifton.....	86
Table 14. Dynamic Moduli of Two Samples from Delta (Eastbound).....	88
Table 15. Dynamic Moduli of Two Samples from SH 133 North of Hotchkiss .....	90
Table 16. Average Raw Dynamic Moduli of Ten Sites.....	93
Table 17. Fitted Dynamic Modulus of CIR Material.....	94
Table 18. Test Results Summary for Base/Subgrade.....	96
Table 19. Resilient Modulus of SH 9 from Fairplay to Alma Subgrade .....	97
Table 20. Resilient Modulus of SH 9 Hoosier Pass Subgrade.....	98
Table 21. Resilient Modulus of SH 86 Franktown Subgrade .....	99
Table 22. Resilient Modulus of SH 86 Kiowa (Eastbound) Subgrade .....	100
Table 23. Resilient Modulus of I-25 South of Colorado City Subgrade .....	101
Table 24. Resilient Modulus of SH 50 Cerro Summit Subgrade.....	102
Table 25. Resilient Modulus of I-70 West of Mack Subgrade .....	103
Table 26. Resilient Modulus of I-70 Fruita to Clifton Subgrade .....	104
Table 27. Resilient Modulus of SH 92 Delta (Eastbound) Subgrade .....	105
Table 28. Resilient Modulus of SH 92 Delta (Eastbound) Base.....	106
Table 29. Resilient Modulus of SH 133 Hotchkiss Subgrade .....	107
Table 30. Resilient Modulus of SH 133 Hotchkiss Base.....	108

This page is left intentionally blank

## **SECTION 1: INTRODUCTION**

### **Background**

Colorado Department of Transportation (CDOT) does not have state specific dynamic modulus information on Cold-in-Place Recycling (CIR) pavement layers/materials. Currently, the dynamic modulus design assumptions for values used by CDOT to estimate the structural support provided by CIR layers remain empirical and unreliable. As such, CDOT's Mechanistic-Empirical (M-E) Pavement Design Manual does not have recommendations derived from local calibration of state CIR for design.

The Pavement Mechanistic-Empirical Design (PMED) program is very versatile and allows the designer to use global or locate state calibration for its analysis. History has shown that better and more economic designs are made if local calibration information is used. Thus, 37 projects using CIR methods were used for local calibration of CIR's dynamic modulus. Prior to implementation of PMED for CIR, a small study was performed by a consultant based on some empirical correlations to determine a modulus value for CDOT. However, with CIR becoming a more popular rehabilitation/reconstruction among pavements with good subgrade support. CDOT needs to establish reliable and locally calibrated CIR dynamic modulus values to better evaluate and predict CIR's performance.

The goal of the study is to develop modulus values for various CIR materials that can be used by CDOT pavement designers as reliable PMED input. Additionally, this study aims to develop new standards that would improve the performance of CIR pavements and make future CIR projects more feasible and cost-effective.

### **Objectives**

The main objective of this research is to evaluate the effectiveness of CIR in Colorado's highway pavements. Specific objectives are listed below:

1. A comprehensive literature to review various factors that affect the dynamic modulus values of CIR materials and long-term pavement performance, and to develop a synthesis of past CIR research studies.
2. Investigate the dynamic modulus properties of CDOT's CIR pavements.
3. Correlate the CIR dynamic modulus values with the performance of the pavements if possible.
4. Establish a range of reliable dynamic modulus values for CIR materials that CDOT may use as input to the PMED program.
5. Examine if PMED predictive equations for CIR are appropriate for use at CDOT.

## **SECTION 2: LITERATURE REVIEW**

### **Background**

Recycling of Hot-Mix Asphalt (HMA) has increased in popularity since the late 1970s, primarily due to increased oil prices. Previously, the cost of recycling old pavements was greater than placing new HMA (1). The invention of milling machines allowed asphalt recycling to become more cost-effective compared to new construction (2). Cold-in-Place Recycling (CIR) is the processing and treatment of existing HMA pavements to restore the pavement without heating the asphaltic materials (3). The deteriorated top 2 to 4 inches of HMA are removed by a milling machine and the milled material is crushed and screened on-site to produce a specified gradation. Binding additives such as emulsion, cement, lime, or fly ash are mixed into the milled material. The mixture is then placed back on the roadway and graded to the final elevation. After compaction of the mixture, a fog seal or thin overlay may be applied if traffic volume is relatively high (3).

### **Benefits**

CIR is economically and environmentally beneficial as it uses less aggregates, does not need transportation of materials to and from the site, and involves less energy consumption. The use of CIR is environment friendly as it may decrease carbon dioxide emission by up to 9% compared to conventional HMA mixes on the whole lifecycle; the carbon dioxide emission is 54% less considering only the phase of rehabilitated pavement construction (4). Another study by Schwartz (5) showed that CIR technology decreases the green-house gas emission by 80% compared to conventional HMA application. Additionally, CIR technology saves 60% asphalt binder compared to HMA.

### **Comparison with Conventional HMA**

Cross and Jakatimath (2) compared the properties and performances of CIR to conventional HMA mixtures used in Oklahoma by laboratory and field investigation and found that CIR material is

comparable with conventional HMA mixture. In laboratory samples, they found that CIR mixtures were not as stiff as typical HMA mixtures. CIR mixtures showed the same increase in stiffness with long-term oven aging as did conventional HMA samples. Field evaluation consisted of rehabilitating two sections with CIR and slurry crack injection to retard reflection cracking. A third section was rehabilitated with a more conventional treatment of a fabric interlayer and HMA overlay. They conducted field distress surveys for three years at which times the two CIR test sections had less transverse cracking than the conventional test section. Based on this research, CIR appears to be a viable procedure for rehabilitation of transverse cracked pavements. Schwartz (5) showed the dynamic modulus of CIR is approximately 50% of the conventional HMA. The study also determined that CIR is 18% lighter than conventional HMA, and requires an additional 25% of thickness to obtain the same strength of HMA.

## **Field Evaluation**

Bhavsar (6) conducted laboratory tests and field observation for long-term CIR performance using two different Reclaimed Asphalt Pavement (RAP) mixtures. The purpose of this study was to compare two types of CIR materials: 1) full CIR and 2) CIR with conventional asphalt mixtures. Using visual inspections, Bhavsar found large amounts of deteriorations where greater number of trucks, poor drainage, and low speeds were prevalent. This study did not show a difference in laboratory or field performance between the two mixtures. Based on a field survey, Kim et al (7) found, CIR roads would last between 21 and 25 years based on the best-fit regression model where the roads were predicted to reach a fair pavement condition. Average service life of CIR roads with good subgrade support was predicted to last up to 34 years, whereas that of CIR roads with poor subgrade support was predicted to last up to 22 years.

## **Application**

CIR is applicable for lower volume roads that may only require a simple surface treatment. A cracked pavement may be restored by CIR if it is structurally sound and has well drained bases and subgrade. CIR is generally not appropriate for pavement with excessive rutting, unstable base-

subgrade, and moisture related damage that cannot be fully recycled by the depth of the CIR treatment applied to the roadway. (6-7).

## **Miscellaneous Evaluations**

Ma et al (8) conducted scanning electron microscope and split tensile tests in the laboratory to evaluate the influences of RAP, emulsified asphalt, and cement on CIR. The researchers determined the following:

- The aggregates' inner structure and strength are much different from aggregates.
- The strength of RAP has an effect on the strength of cold recycled asphalt mixture.
- New aggregates and fine gradation improve the bonding between RAP and binder.
- Emulsified asphalt samples with slow setting of asphalt gave sufficient time for cement to hydrate.
- The high viscosity of asphalt can improve the early strength of cold recycled asphalt mixture. Cement is an efficient additive to improve the strength by promoting demulsification of emulsified asphalt and producing cement hydrates.

Kim et al (9) found the following:

- An increase in foamed asphalt content from 1.0 to 3.0%, air voids in the CIR-foam mixtures decreased gradually.
- Curing the samples at higher temperature requires a shorter set-period resulting the optimum foamed asphalt contents to be between 1.5 and 2.5 percent.
- The flat and elongation ratio of RAP materials did not influence the indirect tensile strength of the CIR-foam mixtures.
- The optimum foamed asphalt content was not affected by the residual asphalt content.
- The stiffer residual asphalt would require more foamed asphalt, whereas the higher residual asphalt content would not require a smaller amount of foamed asphalt.
- Raveling test result is very sensitive to the curing time and the foamed asphalt content.
- Kim et al (9) recommended the material characterization tests such as penetration and dynamic shear rheometer tests be performed for the residual asphalt in RAP materials.

Kim et al (10) conducted dynamic modulus and repeated load tests on CIR foam mixtures with RAP materials collected from different CIR project sites. It was found that both dynamic modulus and flow number were dependent on the RAP sources and foamed asphalt constituents.

Kim and Lee (12) conducted dynamic modulus, flow number, flow time and raveling tests to evaluate the performance of CIR emulsion mixtures at various temperatures and loading conditions. They determined the following:

- Cationic slow setting emulsion in CIR emulsion mixtures produces higher dynamic modulus, flow number, and flow time compared to those produced by the high-float medium-setting emulsion modified with a polymer.
- Flow number, and flow time of CIR emulsion mixtures with softer residual asphalt was higher than those of CIR emulsion mixtures using harder residual asphalt.

Kim and Lee (12) prepared foamed CIR samples at different temperatures and conducted indirect tensile strength tests to determine whether the RAP temperature would affect the strength of the CIR materials. After testing the samples, they found that temperature of RAP materials has a significant impact on the wet indirect tensile strength of CIR foam mixtures and the optimum foam content differs with the temperature.

## **Literature Summary**

From the above discussion, the mechanical properties and performance of CIR is dependent on RAP sources and properties, and the residual binders. Local study is essential to determine the performance and measurement of CIR's effectiveness.

## SECTION 3: SELECTED SITES

### Introduction

Field asphalt and unbound materials were collected from ten pavement project sites in Colorado. The samples were tested by Ground Engineering and at CDOT materials laboratories. Field performance data were collected for the sites to evaluate the performance of the CIR application.

### Selected Test Sites

Ten pavement sites where CIR has been used were selected for this research and listed in Table 1.

**Table 1. Selected CIR Locations from Different Regions**

Location	Region	Roadway
SH 9 from Fairplay to Alma	1	SH 9
SH 9 Hoosier Pass (Northbound)	1	SH 9
SH 86 East of Frantown	1	SH 86
SH 86 Kiowa (Eastbound)	1	SH 86
I-25 South of Colorado City to Cedarwood	2	I-25
SH 50 Cerro Summit Paving	3	SH 50
I-70 West of Mack	3	I-70
I-70 Fruita to Clifton	3	I-70
SH 92 Delta (Eastbound)	3	SH 92
SH 133 North of Hotchkiss	3	SH 133

#### *Site #1: SH 9 Fairplay to Alma*

Located on State Highway 9 in Park County, Colorado, this roadway is classified as a minor arterial with an elevation of 10,228 feet, longitude of 39°15'16.45"N, and latitude of 106°02'20.50"W. The CIR project was constructed in 2007 (CDOT Project Number STA 0091-030, 15967) and started at milepost (MP) 66.4 and ended at MP 70.4. The 2015 average annual daily traffic (AADT), single unit trucks, and combination trucks were 4,000, 100, and 90, respectively. For the purpose of this

study, core samples were collected from MP 68.3 to MP 68.5. The cross-section, and the current view of the current CIR pavement section at SH 9 Fairplay to Alma are shown in Figure 1 and Figure 2 respectively. The Google map of the site is shown in Figure 3. The emulsion (CSS-Special) content used in the CIR layer is 2.0% by weight of the mix.

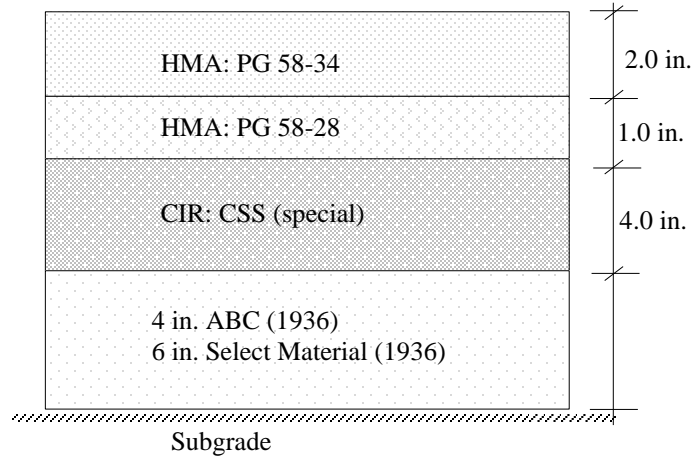


**Figure 1. Cross Section of Pavement Structure at the SH 9 Fairplay to Alma Site**



**Figure 2. View of the SH 9 Fairplay to Alma Site Looking North**

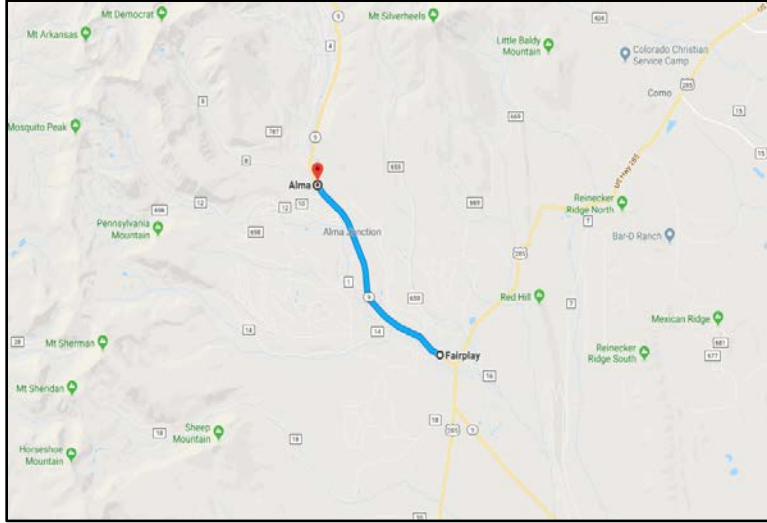


**Figure 3. Location of the SH 9 Fairplay to Alma Site (Google Maps)**

*Site #2: SH 9 Hoosier Pass (Northbound)*

The roadway is located on State Highway 9 in Summit County, Colorado as shown in Figure 4. This roadway is classified as a minor arterial with an elevation of 10,428 feet, longitude of 39°23'34.89"N, and latitude of 106°03'10.61"W. The CIR project was constructed in 2008 (CDOT Project Number STA 009A-001, 16,366) and started at MP 79.0 and ended at MP 82.0. The 2015 AADT, single unit trucks, and combination trucks were 4,800, 150, and 120, respectively. For the purpose of the study, core samples were collected from MP 80.0 to MP 80. The cross-section, and the current view of the current CIR pavement section at SH 9 Hoosier Pass (Northbound) are shown in Figure 4, and Figure 5 respectively. Figure 6 shows the Google map of the site location. The emulsion (CSS-1P) content used in the CIR layer is 2.25% by weight of the mix.

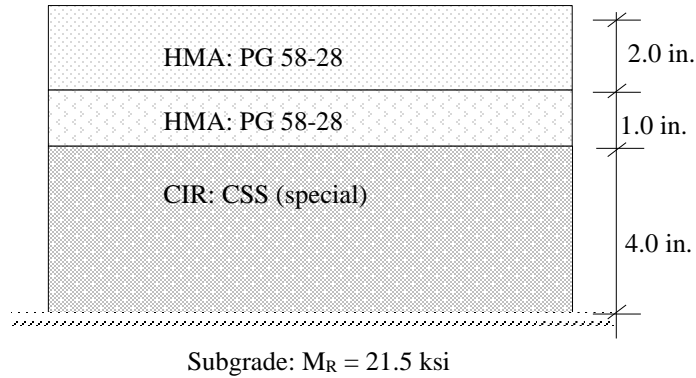


**Figure 4. Cross Section of Pavement at the SH 9 Hoosier Pass (Northbound)**



**Figure 5. View of the SH 9 Hoosier Pass (Northbound) Site Looking North**

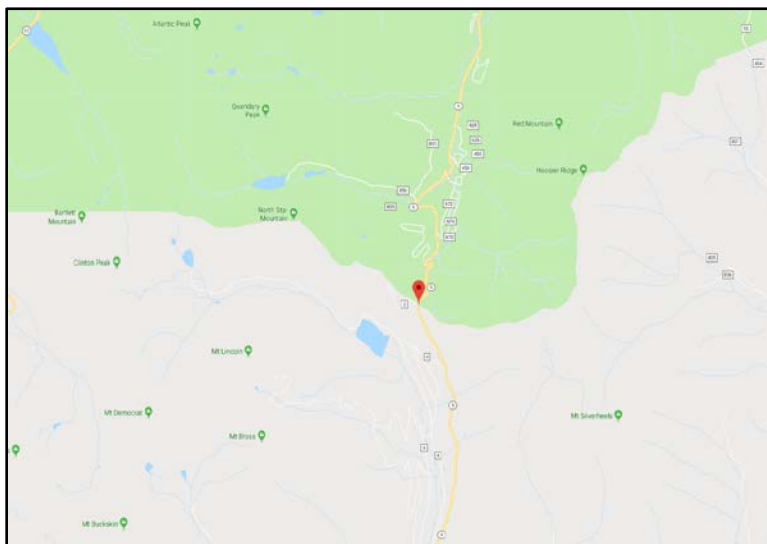


**Figure 6. Location of the SH 9 Hoosier Pass (Northbound) Site (Google Maps)**

*Site #3: SH 86 East of Franktown*

The SH 86 East of Franktown site is located on State Highway 86 in Douglas County, Colorado. This roadway is classified as a minor arterial with an elevation of 6,714 feet, longitude of 39°22'07.64"N, and latitude of 104°40'43.26"W. The CIR project was constructed 2007 (CDOT Project Number STA 086A-045, 15710) and started at MP 6.9 and ended at MP 12.2. The 2015 AADT, single unit trucks, and combination trucks were 11,000, 250, and 120, respectively. For the purpose of the study, core samples were collected from MP 11.4 to MP 11.6. The cross-section, and the current view of the current CIR pavement section at SH 86 East of Franktown are shown in Figure 7, and Figure 8 respectively. The Google map of the site is shown in Figure 9. The emulsion (HFMS-2sp) content used in the CIR layer is 1.7% by weight of the mix.

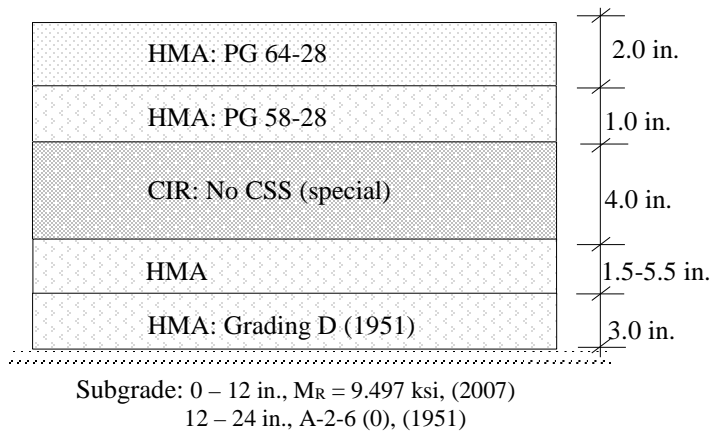


**Figure 7. Cross Section of Pavement Structure at the SH 86 East of Franktown**



**Figure 8. View of the SH 86 East of Franktown Site Looking East**

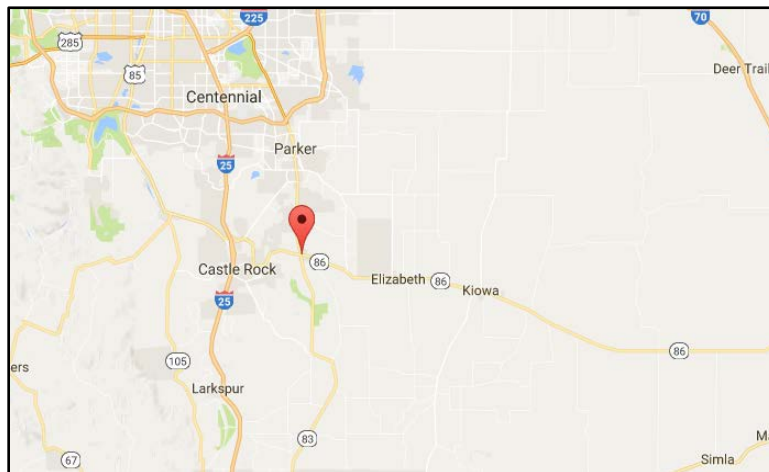


**Figure 9. Location of the SH 86 East of Franktown Site (Google Maps)**

*Site #4: SH 86 Kiowa (Eastbound)*

The SH 86 Kiowa (Eastbound) of Franktown site is located on State Highway 86 in Elbert County, Colorado. This roadway is classified as a minor arterial with an elevation of 6,343 feet, longitude of 39°18'46.91"N, and latitude of 104°21'56.06"W. The CIR project was constructed in 2011 (CDOT Project Number STA 086A-049, 17764) and started at MP 23.5 and ended at MP 31.1. The 2015 AADT, single unit trucks, and combination trucks were 2,200, 70, and 120, respectively. In the current research, core samples were collected from MP 28.9 to MP 29.1. The cross-section,

and the current view of the current CIR pavement section at SH 86 Kiowa (Eastbound) Alma are shown in Figure 10, and Figure 11 respectively. Figure 12 shows the Google map of the site. The emulsion (CSS-1P) content used in the CIR layer is 2.5% by weight of the mix.

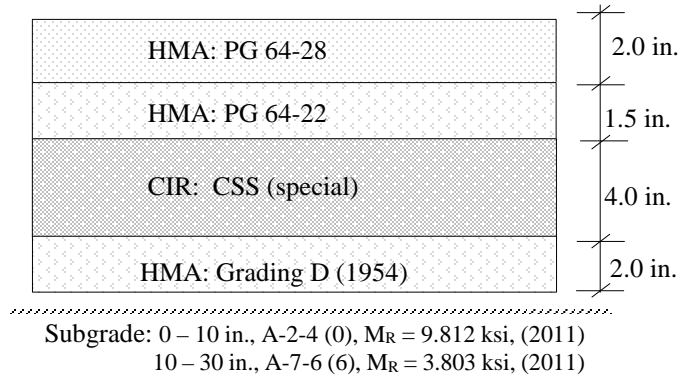


**Figure 10. Cross Section of Pavement Structure at the SH 86 Kiowa (Eastbound)**

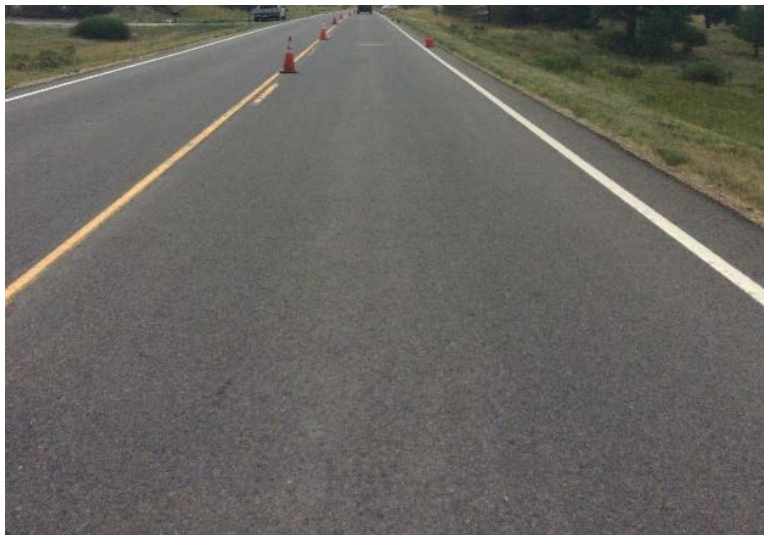


**Figure 11. View of the SH 86 Kiowa (Eastbound) Site Looking East**

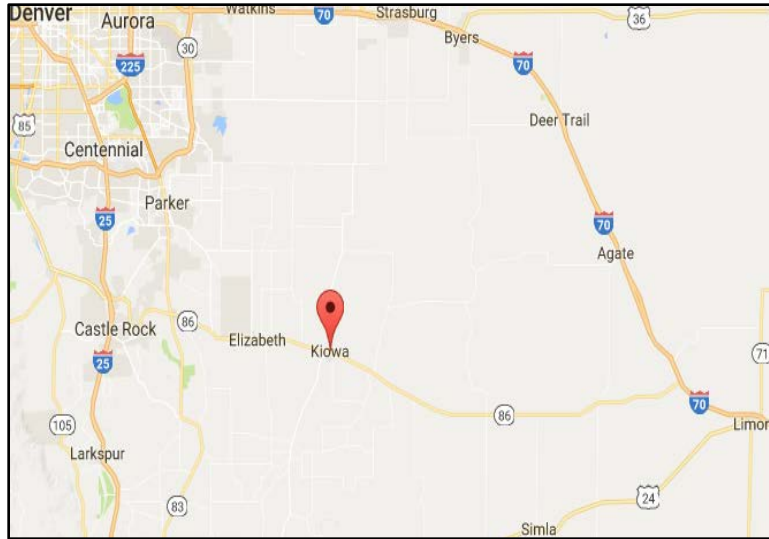


**Figure 12. Location of the SH 86 Kiowa (Eastbound) Site (Google Maps)**

*Site #5: I-25 South of Colorado City to Cedarwood*

The South of Colorado City to Cedarwood site is located on Interstate 25 in Pueblo County, Colorado with an elevation of 5,323 feet, longitude of 38°05'01.97"N, and latitude of 104°42'04.56"W. The CIR project was constructed in 2008 (CDOT Project Number STU 0251-329, 16076B) and started at MP 79.6 and ended at MP 87.6. The 2015 AADT, single unit trucks, and combination trucks were 19,000, 840, and 1,700, respectively. For the purpose of the study, core samples were collected from MP 84.5 to MP 84.7. The cross-section, and the current view of the current CIR pavement section at I-25 South of Colorado City to Cedarwood are shown in Figure 13, and Figure 14 respectively. The Google map of the site is shown in Figure 15.

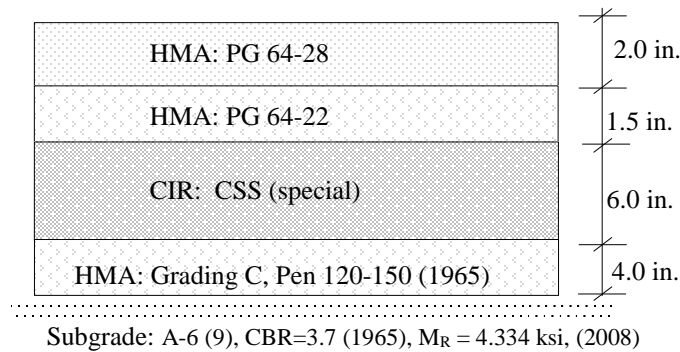


**Figure 13. Cross Section of Pavement Structure at the I-25 South of Colorado City to Cedarwood**



**Figure 14. View of the I-25 South of Colorado City to Cedarwood Site Looking South**



**Figure 15. Location of the I-25 South of Colorado City to Cedarwood Site (Google Maps)**

*Site #6: SH 50 Cerro Summit Paving*

The SH 50 Cerro Summit Paving site is located on State Highway 50 in Montrose County, Colorado. This roadway is classified as a principal arterial with an elevation of 7,623 feet, longitude of 38°26'36.58"N, and latitude of 107°36'41.21"W. The CIR project was constructed in 2006 (CDOT Project Number NH 0501-050, 15433). The project started at MP 103.0 and ended at MP 109.3. The 2015 AADT, single unit trucks, and combination trucks were 3,000, 90, and 250, respectively. For the purpose of the study, core samples were collected from MP 109.1 to MP 109.3. The cross-section, and the current view of the current CIR pavement section at SH 50 Cerro

Summit Paving are shown in Figure 16, and Figure 17 respectively. The Google map of the site is shown in Figure 18.

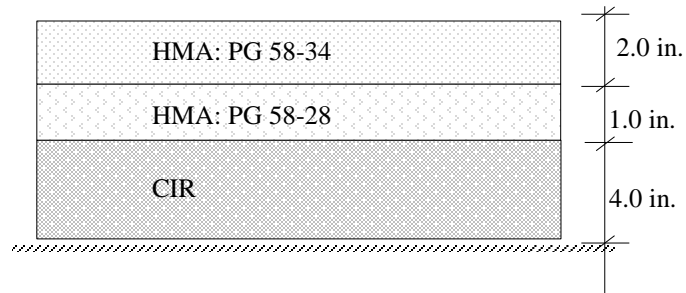


**Figure 16. Cross Section of Pavement Structure at the SH 50 Cerro Summit**



**Figure 17. View of the SH 50 Cerro Summit Looking East**



**Figure 18. Location of the SH 50 Cerro Summit Site (Google Maps)**

*Site #7: I-70 West of Mack*

The I-70 West of Mack site is located on Interstate 70 in Mesa County, Colorado with an elevation of 4,804 feet, longitude of 39°13'34.70"N, and latitude of 10855'36.51"W. The CIR project was constructed in 2005 (CDOT Project Number IM 0701-171, 15032). It started at MP 5.0 and ended at MP 11.6. The 2015 AADT, single unit trucks, and combination trucks were 7,400, 350, and 1,500 respectively. For the purpose of the study, core samples were collected from MP 7.0 to MP 7.2. The cross-section, and the current view of the current CIR pavement section at I-70 West of Mack are shown in Figure 19, and Figure 20 respectively. The Google map of the site is shown in Figure 21.

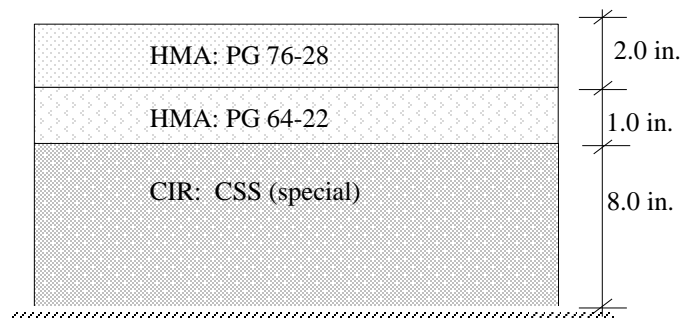


**Figure 19. Cross Section of Pavement Structure at the I-70 West of Mack**



**Figure 20. View of the I-70 West of Mack Site Looking West**



**Figure 21. Location of the I-70 West of Mack Site (Google Maps)**

*Site #8: I-70 Fruita to Clifton*

The I-70 Fruita to Clifton site is located on Interstate 70 in Mesa County, Colorado with an elevation of 4,516 feet, longitude of 37°07'16.44"N, and latitude of 108°40'37.28"W. The CIR project was constructed in 2004 (CDOT Project Number IM 0701-157, 13535). It started at MP 22.0 and ended at MP 37.0. In 2014, a 1.5-inch overlay was placed from MP 16 to MP 37 (CDOT Project Number NHPP 0701-222, 19677). The 2015 AADT, single unit trucks, and combination trucks were 20,000, 560, and 2000 respectively. For the purpose of the study, core samples were collected from MP 23.5 to MP 23.7. The cross-section, and the current view of the current CIR pavement section at I-70 Fruita to Clifton are shown in Figure 22, and Figure 23 respectively. The Google map of the site is shown in Figure 24.

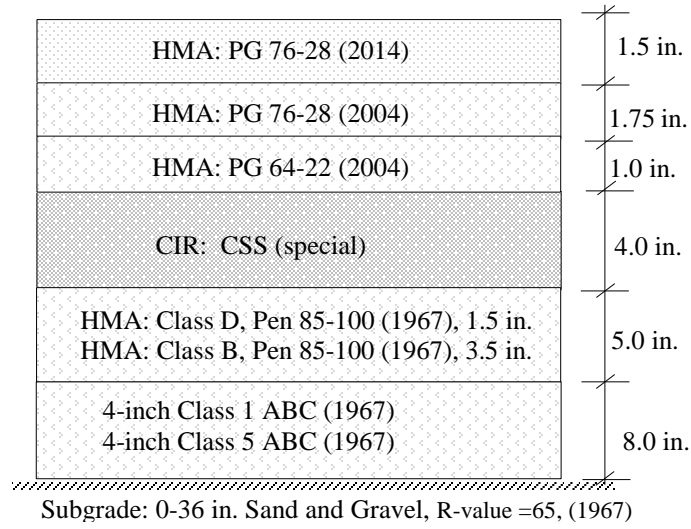


**Figure 22. Cross Section of Pavement Structure at the I-70 Fruita to Clifton**



**Figure 23. View of the I-70 Fruita to Clifton Site**



**Figure 24. Location of the I-70 Fruita to Clifton Site (Google Maps)**

*Site #9: SH 92 Delta (Eastbound)*

The SH 92 Delta (Eastbound) site is located on State Highway 92 in Delta County Colorado. This roadway is classified as a principal arterial with an elevation of 5,004 feet, longitude of 38°45'30.70"N, and latitude of 108°01'37.53"W. The CIR project was constructed in 2003 (CDOT Project Number STA 092A-016, 14217) and started at MP 0.2 and ended at MP 4.2. The 2015 AADT, single unit trucks, and combination trucks were 12,000, 340, and 160 respectively. For the purpose of the study, core samples were collected from MP 3.0 to MP 3.2. The cross-section, and the current view of the current CIR pavement section at SH 92 Delta (Eastbound) are shown in Figure 25, and Figure 26 respectively. The Google map of the site is shown in Figure 27.

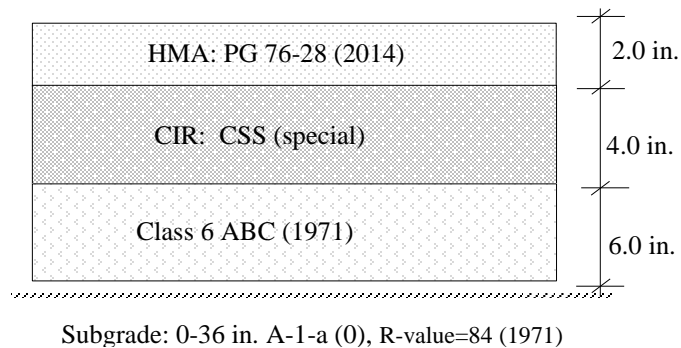


**Figure 25. Cross Section of Pavement Structure at the SH 92 Delta (Eastbound)**



**Figure 26. View of the SH 92 Delta (Eastbound) Site Looking West**



**Figure 27. Location of the SH 92 Delta (Eastbound) Site (Google Maps)**

*Site #10: SH 133 North of Hotchkiss*

The SH 133 North of Hotchkiss site is located on State Highway 133 in Delta County, Colorado. This roadway is classified as a minor arterial with an elevation of 5,741 feet, longitude of 38°52'55.59"N, and latitude of 107°35'32.98"W. The CIR project was constructed in 2008 (CDOT Project Number STA 133A-034, 16445) and started at MP 0.0 and ended at MP 11.4. The 2015 AADT, single unit trucks, and combination trucks were 12,000, 340, and 160, respectively. For the purpose of the study, core samples were collected from MP 9.2 to MP 9.4. The cross-section, and the current view of the current CIR pavement section at SH 133 North of Hotchkiss are shown

in Figure 28, and Figure 29 respectively. The Google map of the site is shown in Figure 30. The emulsion content used is the CIR layer is 2.5% by weight of the mix.

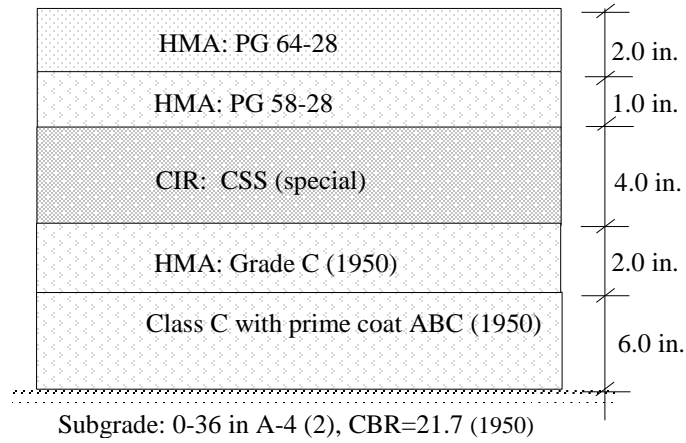


**Figure 28. Cross Section of Pavement Structure at the SH 133 North of Hotchkiss**



**Figure 29. View of the SH 133 North of Hotchkiss Site**



**Figure 30. Location of the SH 133 North of Hotchkiss Site (Google Maps)**

## **Selected Control Sites**

A control site was selected for each test site for comparison of the CIR pavement versus conventional HMA pavement. The control sites were selected by CDOT and were chosen for being the best fit to pavement location, materials, geometry, climate, traffic volume, and time of construction (i.e., the projects were built during the same year or close to the year. The control test sites were located near the CIR sites and deemed acceptable for comparison by CDOT. It is important to mention that the control sites were not constructed using CIR technology, rather conventional HMA, thus will not be an exact match to the test sites. The control sites are described below:

### *Control Site #1*

Control Site #1 is located on State Highway 135 in Gunnison County, Colorado (CDOT Project Number HB 135A-024, 16446), and was constructed in 2008 from MP 18.8 to 27.2. Control Site #1 will be compared with the CIR Site #1 SH 9 Fairplay to Alma. This roadway is classified as a minor arterial with an elevation of 8,781 feet, longitude of 38°49'37.46"N, and latitude of 106°55'15.89"W. The 2015 AADT, single unit trucks, and combination trucks were 3,200, 100, and 160 respectively. A cross-section of the pavement structure is shown in Figure 31.

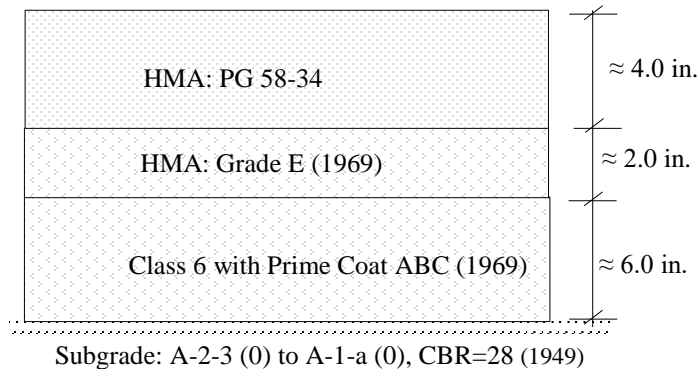


**Figure 31. Cross-section of Pavement Structure at Control Site #1**

*Control Site #2*

Control Site #2 is located on State Highway 9 in Park County, Colorado (CDOT Project Number STA 009-027, 17048) constructed in 2009 from MP 73.0 to 76.0. Control Site #2 will be compared with the CIR Site #2 SH 9 Hoosier Pass (Northbound). This roadway is classified as a minor arterial with an elevation of 11,010 feet, longitude of 39°20'11.98"N, and latitude of 106°3'8.33"W. The 2015 AADT, single unit trucks, and combination trucks were 5,800, 160, and 140 respectively. A cross-section of the pavement structure is shown in Figure 32.

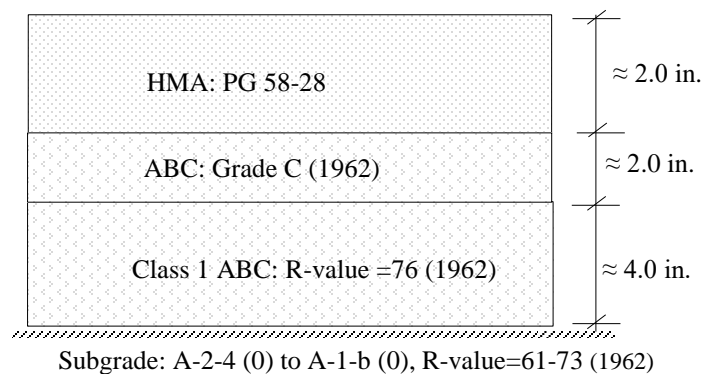


**Figure 32. Cross-section of Pavement Structure at Control Site #2**

*Control Site #3*

Control Site #3 is located on State Highway 83 in El Paso County, Colorado (CDOT Project Number STA 0831-105, 16028) constructed in 2007 from MP 33.1 to 41.2. Control Site #3 will be compared with the CIR Site #3 SH 86 East of Franktown. This roadway is classified as a principal arterial with an elevation of 6,829 feet, longitude of 39°13'33.94"N, and latitude of 104°42'0.31"W. The 2015 AADT, single unit trucks, and combination trucks were 3,700, 120, and 240 respectively. A cross-section of the pavement structure is shown in Figure 33.

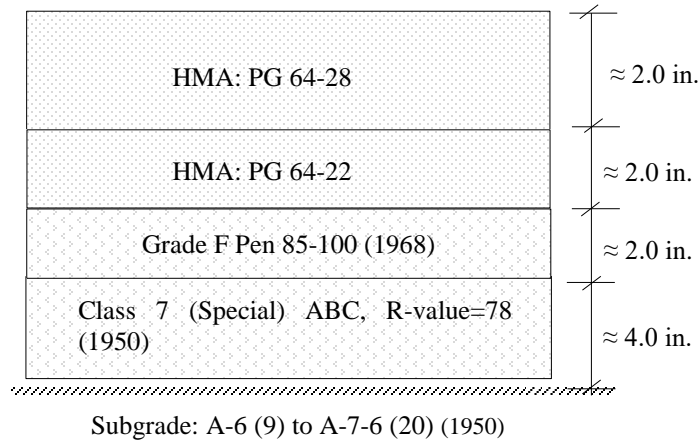


**Figure 33. Cross-section of Pavement Structure at Control Site #3**

*Control Site #4*

Control Site #4 is located on US Highway 24 in Elbert County, Colorado (CDOT Project Number ES1 0243-079, 17616) constructed in 2010 from MP 364.6 to 375.4. Control Site #4 will be compared with the CIR Site #4 SH 86 Kiowa (Eastbound). This roadway is classified as a principal arterial with an elevation of 5,786 feet, longitude of 39°13'1.37"N, and latitude of 103°49'1.25"W. The 2015 AADT, single unit trucks, and combination trucks were 2,900, 90, and 220 respectively. A cross-section of the pavement structure is shown in Figure 34.

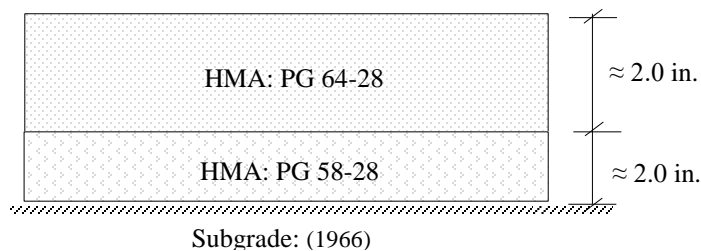


**Figure 34. Cross-section of Pavement Structure at Control Site #4**

*Control Site #5*

Control Site #5 is located on Interstate 25 in Pueblo County, Colorado (CDOT Project Number IM 0252-378, 15160) constructed in 2006 from MP 102.6 to 109.0 with an elevation of 4,891 feet, longitude of 38°44'51.59"N, and latitude of 104°37'10.64"W. Control Site #5 will be compared with the CIR Site #5 I-25 South of Colorado City to Cedarwood. The 2015 AADT, single unit trucks, and combination trucks were 31,000, 990, and 2,700 respectively. A cross-section of the pavement structure is shown in Figure 35.

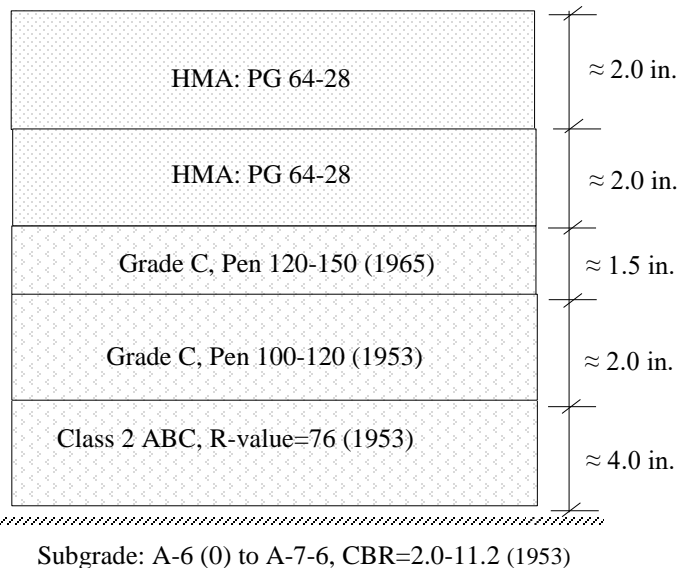


**Figure 35. Cross-section of Pavement Structure at Control Site #5**

*Control Site #6*

Control Site #6 is located on State Highway 131 in Routt County, Colorado (CDOT Project Number STR 131A-029, 14214) constructed in 2006 from MP 61.4 to 64.5. Control Site #6 will be compared with the CIR Site #6 SH 50 Cerro Summit Paving. This roadway is classified as a minor arterial with an elevation of 6,906 feet, longitude of 40°21'59.1"N, and latitude of 106°50'52.8"W. The 2015 AADT, single unit trucks, and combination trucks were 4,300, 100, and 40 respectively. A cross-section of the pavement structure is shown in Figure 36.

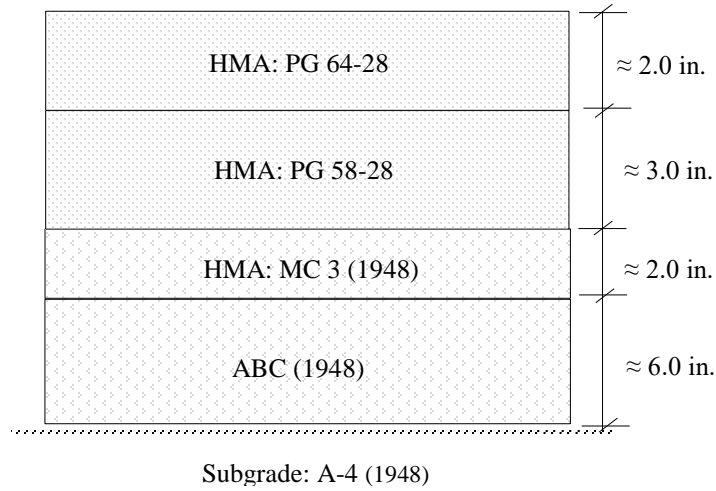


**Figure 36. Cross-section of Pavement Structure at Control Site #6**

*Control Site #7*

Control Site #7 is located on Interstate 70 in Garfield County, Colorado (CDOT Project Number IM 0701-179, 15320) constructed in 2006 from MP 110.0 to 118.5 with an elevation of 5,722 feet, longitude of 39°33'41.48"N, and latitude of 107°22'0.83"W. Control Site #7 will be compared with the CIR Site #7 I-70 West of Mack. The 2015 AADT, single unit trucks, and combination trucks were 21,000, 480, and 2,100, respectively. A cross-section of the pavement structure is shown in Figure 37.

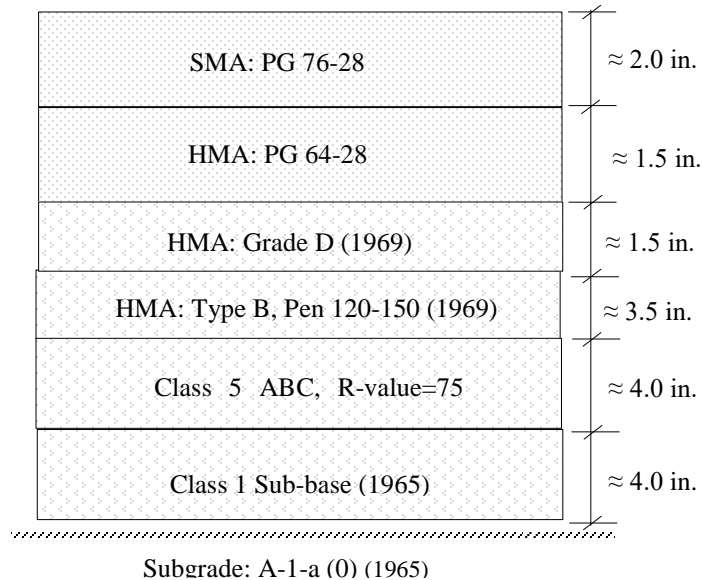


**Figure 37. Cross-section of Pavement Structure at Control Site #7**

*Control Site #8*

Control Site #8 is located on Interstate 70 in Mesa County, Colorado (CDOT Project Number HB 0701-173, 15065) constructed in 2007 from MP 37.0 to 43.4 with an elevation of 4,814 feet, longitude of 39°7'4.23"N, and latitude of 108°23'16.39"W. Control Site #8 will be compared with the CIR Site #8 I-70 Fruita to Clifton. The 2015 AADT, single unit trucks, and combination trucks were 22,000, 570, and 2,400 respectively. A cross-section of the pavement structure is shown in Figure 38.

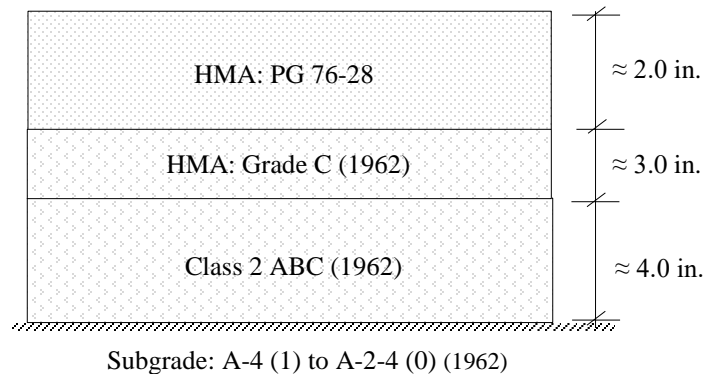


**Figure 38. Cross-section of Pavement Structure at Control Site #8**

*Control Site #9*

Control Site #9 is located on US Highway 50 in Montrose County, Colorado (CDOT Project Number NH 0502-053, 13472) constructed in 2004 from MP 109.4 to 112.0. This roadway is classified as a principal arterial with an elevation of 7,287 feet, longitude of 38°26'16.93"N, and latitude of 107°35'16.94"W. Control Site #9 will be compared with the CIR Site #9 SH 92 Delta (Eastbound). The 2015 AADT, single unit trucks, and combination trucks were 3,000, 90, and 250 respectively. A cross-section of the pavement structure is shown in Figure 39.

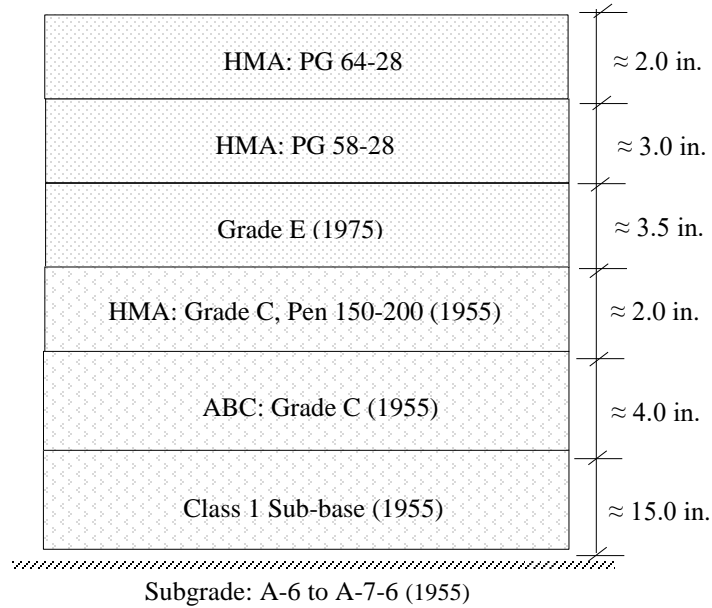


**Figure 39. Cross-section of Pavement Structure at Control Site #9**

*Control Site #10*

Control Site #10 is located on US Highways 50 in Gunnison County, Colorado (CDOT Project Number NH 0501-055, 15924) constructed in 2007 from MP 156.0 to 158.0. Control Site #10 will be compared with the CIR Site #10 SH 133 North of Hotchkiss. This roadway is classified as a principal arterial with an elevation of 7,708 feet, longitude of 38°32'39.83"N, and latitude of 106°56'7.72"W. The 2015 AADT, single unit trucks, and combination trucks were 2,800, 80, and 30 respectively. A cross-section of the pavement structure is shown in Figure 40.

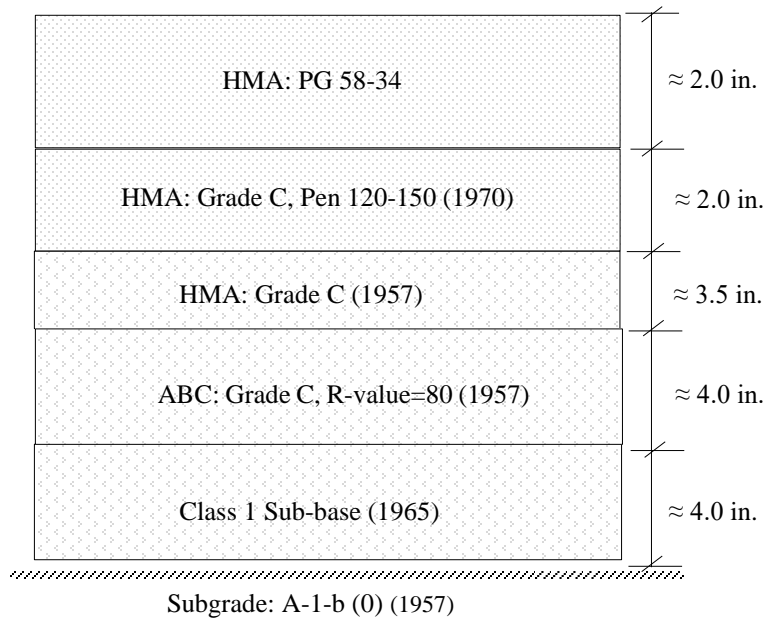


**Figure 40. Cross-section of Pavement Structure at Control Site #10**

## SECTION 4: PERFORMANCE DATA

### General

CDOT subcontracts the collection of pavement management data to a private vendor who drives an automated data collection van over the entire CDOT network. The collected data are reported in tenth-of-mile (tenth-mile) increments and include surface roughness (IRI), permanent deformation (rutting), and fatigue cracking. Collection of the rutting data is accomplished using a five-sensor rut bar that measures the pavement's permanent deformation to the hundredth of an inch. The IRI data is collected with an inertia profile consisting of laser sensors, accelerometer, and distance transducer. The van is also equipped with digital cameras; one camera is positioned for a windshield view, and four cameras (one over each wheel) to view the pavement. The cameras take photos/videos of the pavement showing the type, amount, length, and severity of the cracking. The data collected is recorded and sent to the vendor's data reduction office where it is viewed and rated. The raw data is given to CDOT in tenth-mile intervals. Thus, IRI is reported as the average inches/mile over a tenth-mile section. Bottom-up fatigue cracking is reported as the total square feet in a tenth-mile and is defined by CDOT as a series of small, jagged, interconnecting cracks caused by failure of the asphalt concrete surface under repeated traffic loading. Top-down longitudinal cracking is reported as the total linear feet in a tenth-mile and is defined by CDOT as cracking that is parallel to the pavement centerline. CDOT's practice is to combine top-down longitudinal cracking with bottom-up fatigue cracking, and refer as fatigue cracking. While some top-down longitudinal cracking may be due to construction issues such as joint segregation, mix segregation at the gear box, or other locations of the paving process, CDOT includes all top-down longitudinal cracking into the fatigue distress. Therefore, for the purpose of the study, both top-down longitudinal cracking and bottom-up fatigue cracking will be referred to as fatigue cracking. Transverse cracks are reported in two different ways, first as a numerical count such as 1, 2, or 3 per tenth-mile, the second is by linear feet per tenth-mile. Transverse cracks are defined by CDOT as cracking that is perpendicular to the pavement centerline. For the purpose of this project, the following definitions apply:

- Whole Project – The entire length of the CIR project as stated in Section 3, Selected Test Sites
- Control Site – The entire length of the control project as stated in Section 3, Selected Control Sites
- Test Site – 1000 feet section within the whole project where samples were collected as stated in Section 3, Selected Test Sites

The average performance of each whole project, control site, and test site have been compared and summarized below.

### Site #1 SH 9 Fairplay to Alma

*Fatigue Cracking:* Fatigue cracking at the test site has no measurable cracking 9 years after construction, Figure 41. The control site has greater amount of cracking with a maximum value of 145 square feet per tenth-mile. The whole project and the test site have fatigue cracking averages of 57 and 4 square feet per tenth-mile respectively, these averages are less than one percent of the pavement lane and considered negligible. Figure 41 also shows the amount of fatigue cracking is not expected to increase rapidly over time for CIR pavement.

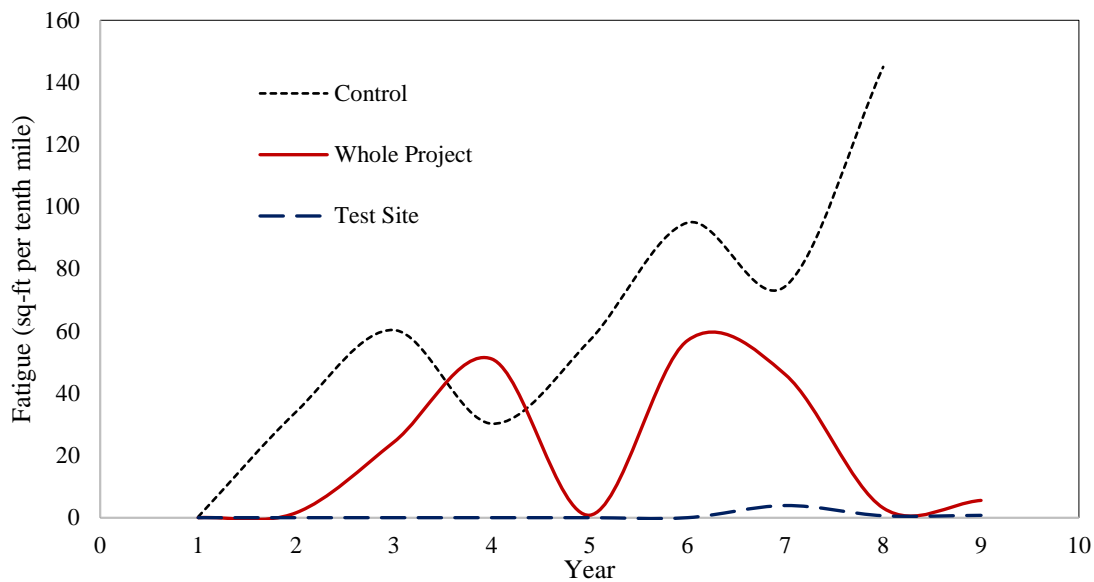


**Figure 41. Fatigue Cracking at Site #1 SH 9 Fairplay to Alma Showing Amount of Cracking at the Control Site, Test Site, and Whole Project**

*Rutting:* The amount of rutting at the whole project, control site, and test site are very similar as depicted in Figure 42. Nine years after construction, rutting at the control site increased from 0.01 to 0.19 inches, at the whole project it increased from 0.04 to 0.18 inches, and at the test site it increased from 0.04 to 0.17 inches. Thus, the rutting measured at the test section versus the whole project is slightly less than the control project and shown a very slight benefit to using CIR. Figure 42 indicates that rutting is expected to grow with age, however will not exceed the terminal threshold value (used by PMED) of 0.5 inches for several years.

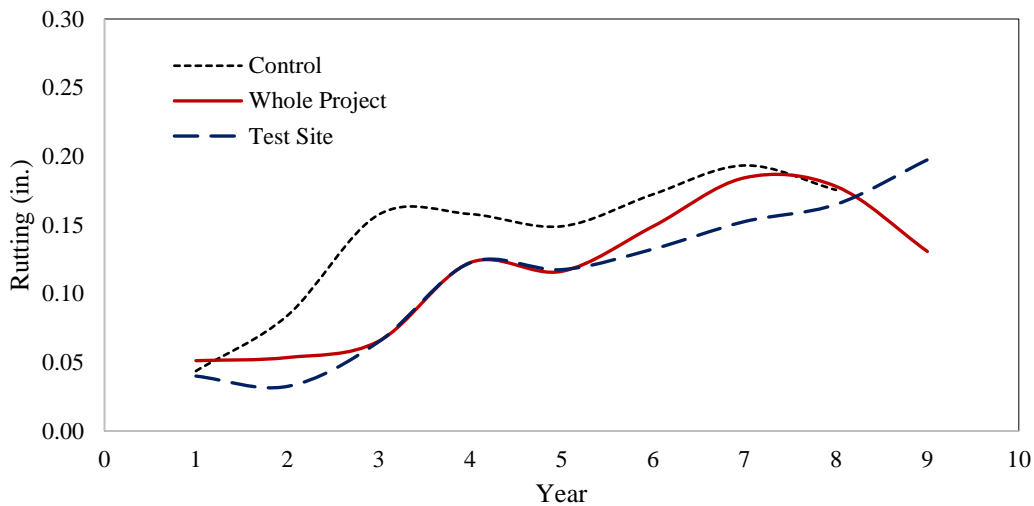


**Figure 42. Rutting at Site #1 SH 9 Fairplay to Alma Showing Amount of Rutting at the Control Site, Test Site, and Whole Project**

*Transverse Cracking:* Nine years after construction, the transverse cracking at the test site and whole project is greater than the cracking at the control site, Figure 43. The control project has a maximum of eight cracks (each 12 feet long) per tenth-mile, while each of the whole project and the test site has a maximum of 11 cracks per tenth-mile. The data shows the difference between the whole project and test site is negligible and that the project that used CIR performed poorer than conventional HMA. Transverse cracking is expected to increase over time, but will unlikely reach the terminal threshold value (used by PMED) of 1,500 feet per mile for several years.

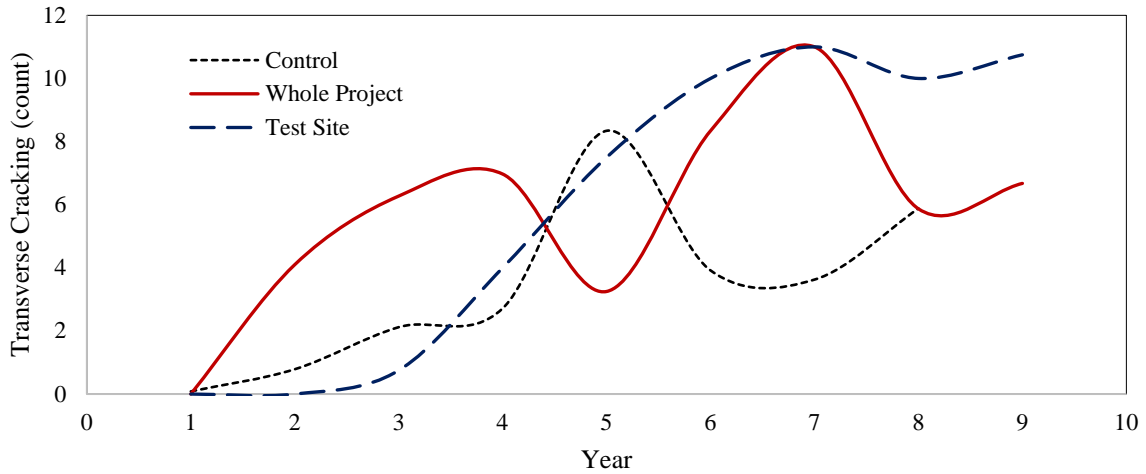


**Figure 43. Transverse Cracking at Site #1 SH 9 Fairplay to Alma Showing Amount of Cracking at the Control Site, Test Site, and Whole Project**

IRI: The IRI at the test site and whole project is less than that measured at the control site, Figure 44. Since the construction of the project nine years ago, the control site’s IRI ranged from 75 to 89 inches per mile. The whole project’s IRI was more consistent and ranged from 67 to 70 inches per mile, and the test site ranged from 58 to 67 inches per mile. Data shows the control site performed poorer than the test site and whole project and indicated the use of CIR may reduce a roadway’s IRI. The graph indicated IRI will not significantly increase over time and will unlikely meet the terminal threshold value PMED used of 200 inches per mile.

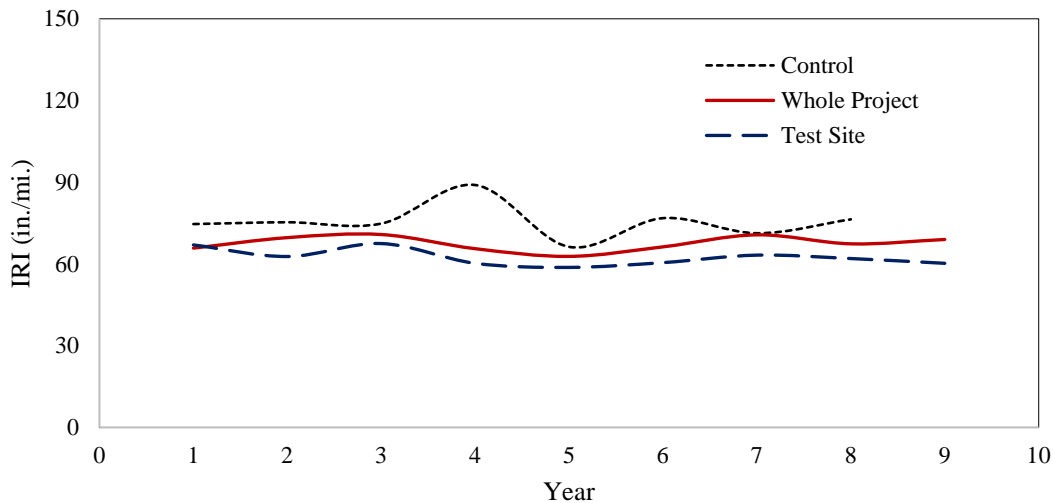


**Figure 44. IRI at Site #1 SH 9 Fairplay to Alma Showing Amount of IRI at the Control Site, Test Site, and Whole Project**

## Site #2 SH 9 Hoosier Pass (Northbound)

*Fatigue Cracking:* Similar to SH 9 Fairplay to Alma site, fatigue cracking at the test site of SH 9 Hoosier Pass (Northbound) has no measurable cracking 8 years after construction, Figure 45. The whole project has greater amount cracking with a maximum value of 190 square feet per tenth-mile compared to 74 square feet per tenth-mile at the control site. However, the whole project average fatigue cracking is less than one percent of the pavement lane and considered negligible. Figure 45 also shows the amount of fatigue cracking is not expected to increase rapidly over time.

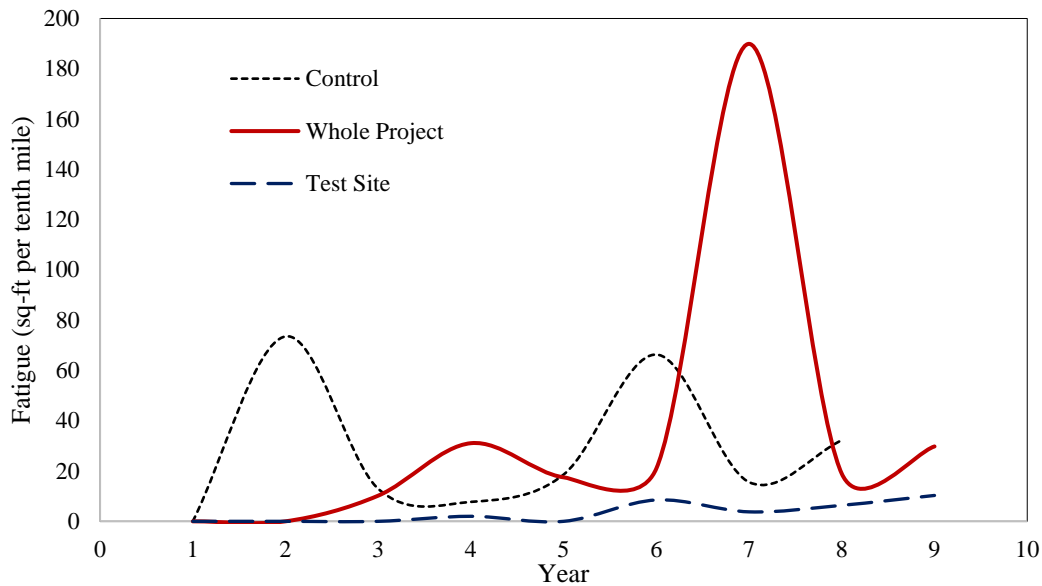


**Figure 45. Fatigue Cracking at Site #2 SH 9 Hoosier Pass (Northbound) Showing Amount of Cracking at the Control Site, Test Site, and Whole Project**

*Rutting:* The amount of rutting at the whole project, control site, and test site are very similar, Figure 46. Eight years after construction rutting at the control site increased from 0.01 to 0.24 inches, at the whole project it increased from 0.06 to 0.33 inches, and at the test site, it increased from 0.07 to 0.24 inches. Thus, the rutting measured at the whole project is slightly more than the control project. Figure 46 indicates that rutting is expected to grow with age, however will not exceed the terminal threshold value (used by PMED) of 0.5 inches for several years.

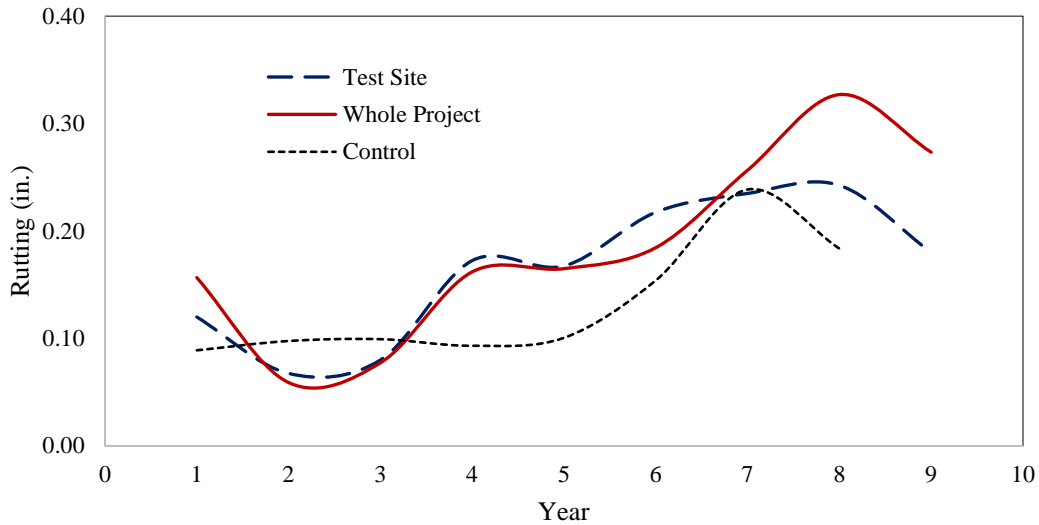


**Figure 46. Rutting at Site #2 SH 9 Hoosier Pass (Northbound) Showing Amount of Rutting at the Control Site, Test Site, and Whole Project**

*Transverse Cracking:* Nine years after construction, the transverse cracking at the test site and whole project is much smaller than the cracking at the control site, Figure 47. The control project has a maximum of 24 cracks (each 12 feet long) per tenth-mile, while the whole project and the test site each has a maximum of 8 cracks per tenth-mile, and shows the benefit of using CIR. Transverse cracking is expected to increase over time, but will unlikely meet the terminal threshold value (used by PMED) of 1,500 feet per mile for several years.

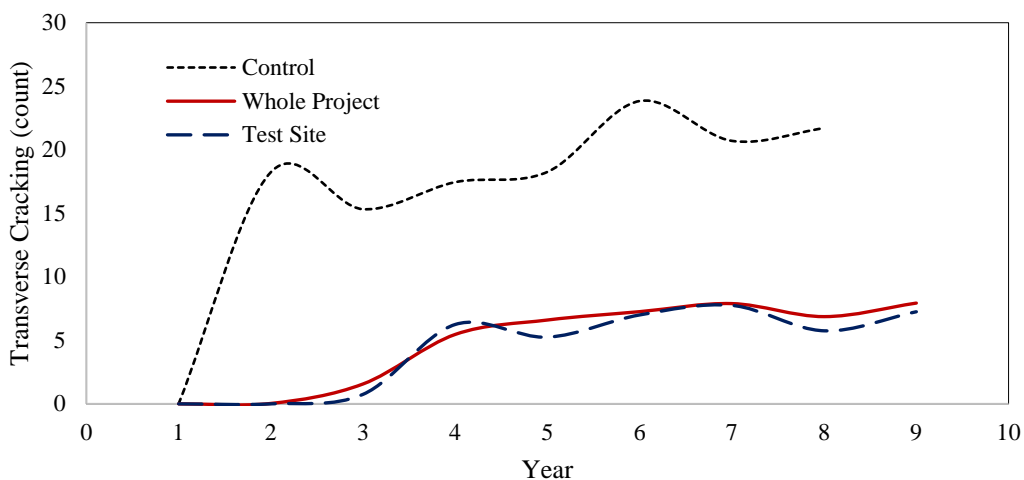


**Figure 47. Transverse Cracking at Site #2 SH 9 Hoosier Pass (Northbound) Showing Amount of Cracking at the Control Site, Test Site, and Whole Project**

IRI: The IRI at the test site and whole project is more than that measured at the control site, Figure 48. Since the construction of the project nine years ago, the control site's IRI ranged from 66 to 113 inches per mile. The whole project's IRI was more consistent and ranged from 92 to 124 inches per mile, and the test site ranged from 84 to 122 inches per mile. Data shows the control site performed better than the test site and whole project. The graph indicated IRI will not significantly increase over time and will unlikely meet the terminal threshold value PMED used of 200 inches per mile.

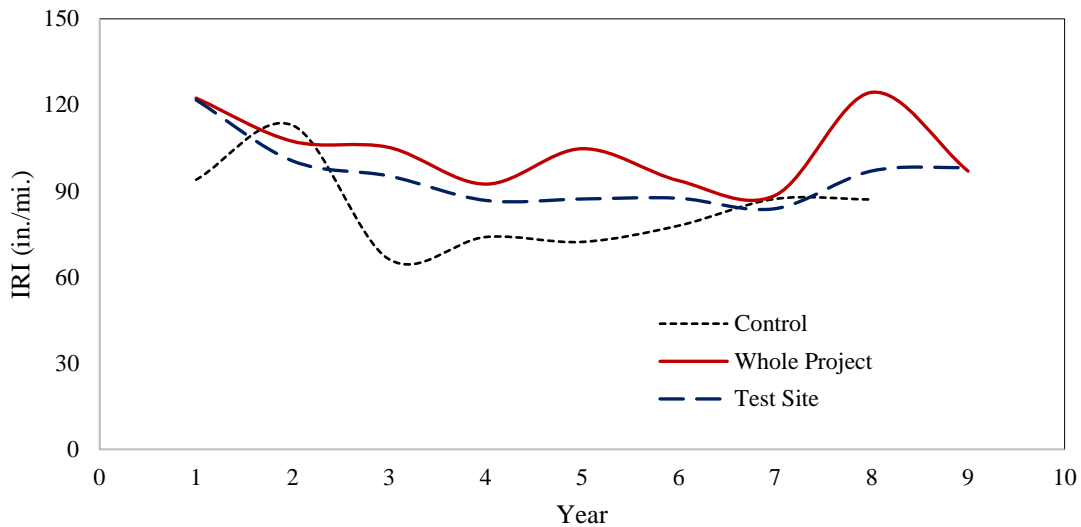


**Figure 48. IRI at Site #2 SH 9 Hoosier Pass (Northbound) Showing Amount of IRI at the Control Site, Test Site, and Whole Project**

### Site #3 SH 86 East of Franktown

*Fatigue Cracking:* Fatigue cracking at the test site has no measurable cracking 9 years after construction, Figure 49. The whole project and control site has similar cracking with a maximum value of 39 square feet per tenth-mile. The whole project has an average fatigue cracking of 42 square feet per tenth-mile, which is less than one percent of the pavement lane and considered negligible. Figure 49 also shows the amount of fatigue cracking is not expected to increase rapidly over time.

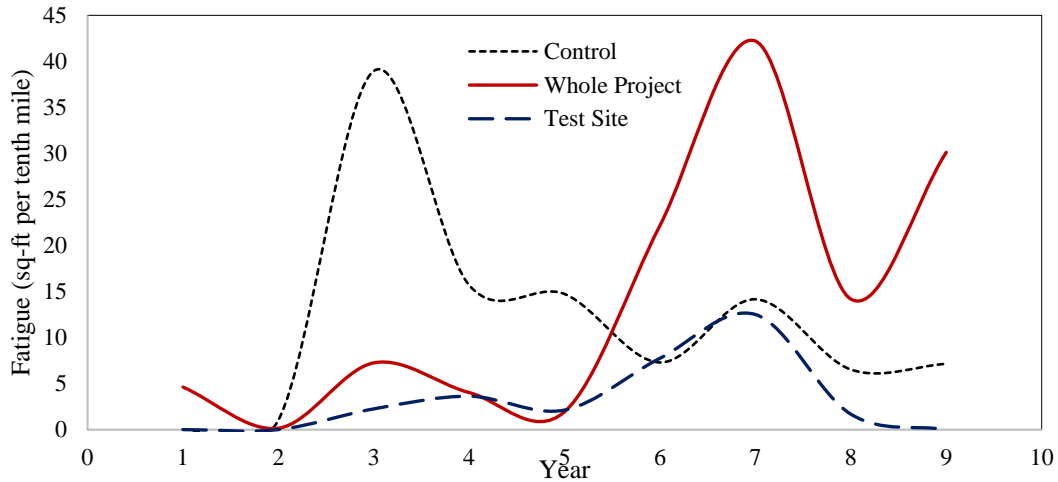


**Figure 49. Fatigue Cracking at Site #3 SH 86 East of Franktown Showing Amount of Cracking at the Control Site, Test Site, and Whole Project**

*Rutting:* The amount of rutting at the whole project, control site, and test site are very similar as shown in Figure 50. Nine years after construction rutting at the control site increased from 0.06 to 0.17 inches, at the whole project it increased from 0.06 to 0.16 inches, and at the test site, it increased from 0.05 to 0.14 inches. Thus, the rutting measured at the test section versus the whole project is slightly less than the control project showing a benefit to using CIR. Figure 50 indicates that rutting is expected to grow with age but will not exceed the terminal threshold value (used by PMED) of 0.5 inches for several years.

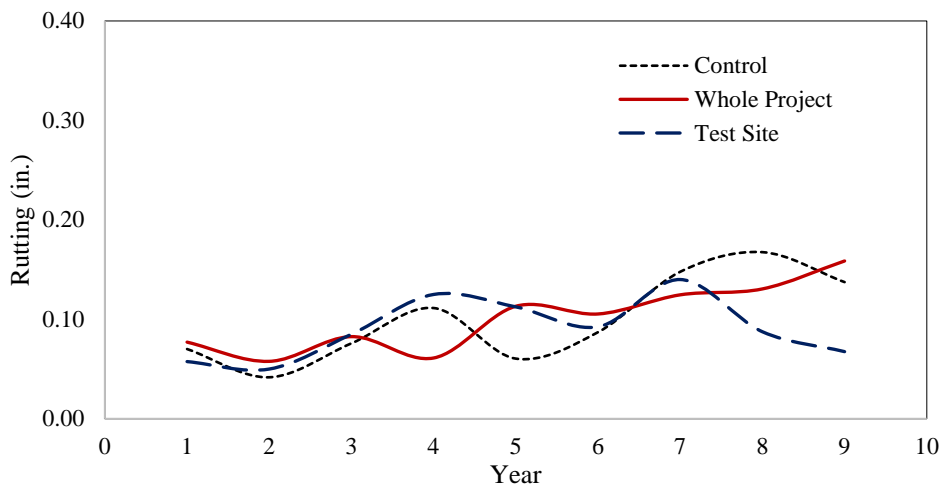


**Figure 50. Rutting at Site #3 SH 86 East of Franktown Showing Amount of Rutting at the Control Site, Test Site, and Whole Project**

*Transverse Cracking:* Nine years after construction, the transverse cracking at the test site and whole project is smaller than the cracking at the control site, Figure 51. The control project has a maximum of seven cracks (each 12 feet long) per tenth-mile, while the whole project and the test site have maximum values of two and three cracks per tenth-mile respectively. Transverse cracking is expected to increase over time, but will unlikely meet the terminal threshold value (used by PMED) of 1,500 feet per mile for several years.

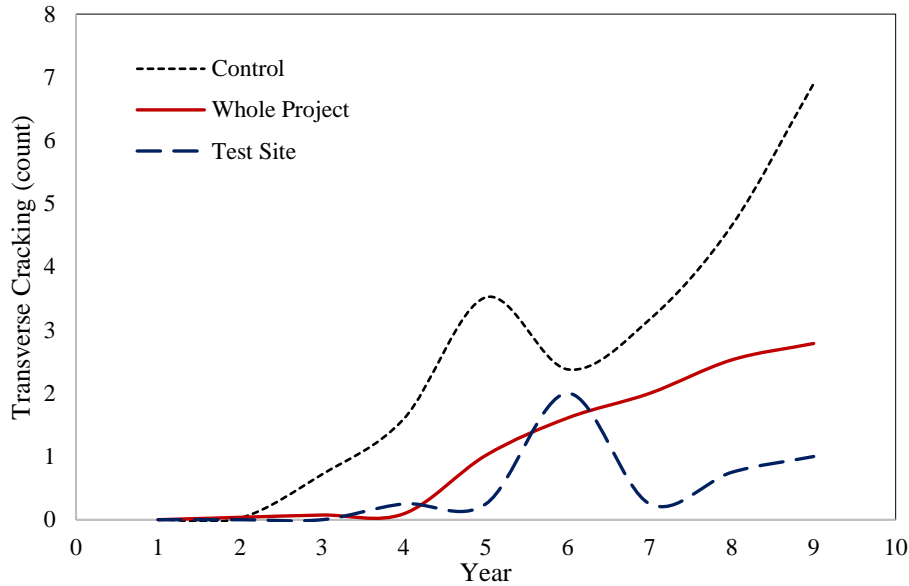


**Figure 51. Transverse Cracking at Site #3 SH 86 East of Franktown Showing Amount of Cracking at the Control Site, Test Site, and Whole Project**

IRI: The IRI at the test site and whole project is more than that measured at the control site as shown in Figure 52. Since the construction of the project nine years ago, the control site’s IRI ranged from 58 to 63 inches per mile. The whole project’s IRI was more consistent and ranged from 60 to 84 inches per mile, and the test site ranged from 52 to 101 inches per mile. Data shows the control site performed better than the test site and whole project and indicated the use of CIR may reduce a roadway’s IRI. The graph indicated IRI will not significantly increase over time and will unlikely meet the terminal threshold value PMED used of 200 inches per mile.

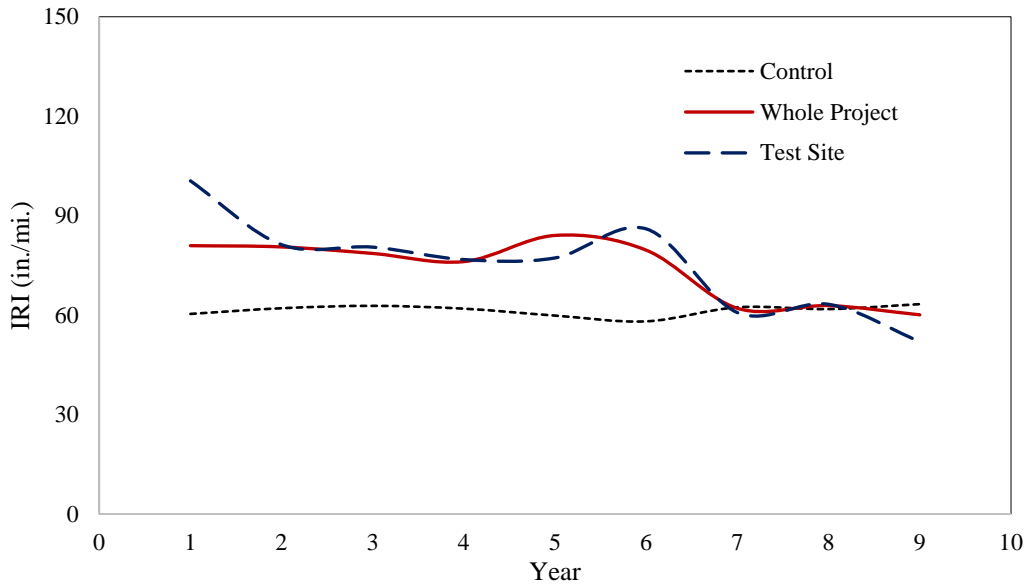


**Figure 52. IRI at Site #3 SH 86 East of Franktown Showing Amount of IRI at the Control Site, Test Site, and Whole Project**

#### **Site #4 SH 86 Kiowa (Eastbound)**

*Fatigue Cracking:* Fatigue cracking at the test site and whole project has no measurable cracking 5 years after construction as shown in Figure 53. The test site and whole project have similar cracking with maximum values of 2 and 12 square feet per tenth-mile respectively. The control site has an average fatigue cracking of 67 square feet per tenth-mile, which is much higher than the test site and whole project. Figure 53 also shows the amount of fatigue cracking is not expected to increase rapidly over time.

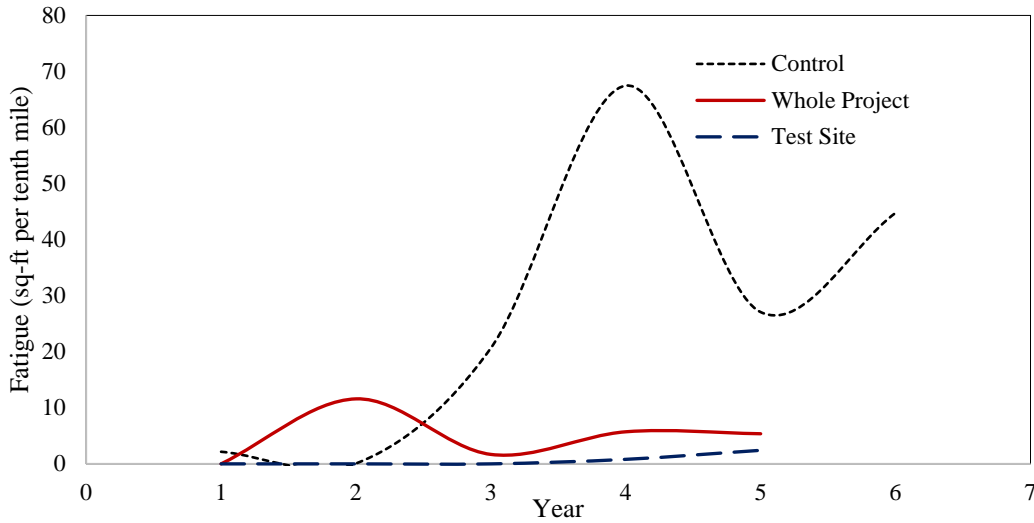


**Figure 53. Fatigue Cracking at Site #4 SH 86 Kiowa (Eastbound) Showing Amount of Cracking at the Control Site, Test Site, and Whole Project**

*Rutting:* The amount of rutting at the whole project, control site, and test site are very similar as shown in Figure 54. Nine years after construction rutting, at the control site increased from 0.08 to 0.14 inches, at the whole project it increased from 0.06 to 0.14 inches, and at the test site, it increased from 0.06 to 0.18 inches. Thus, the rutting measured at the test section is slightly more than the control project. Figure 54 indicates that rutting is expected to grow with age but will not exceed the terminal threshold value (used by PMED) of 0.5 inches for several years.

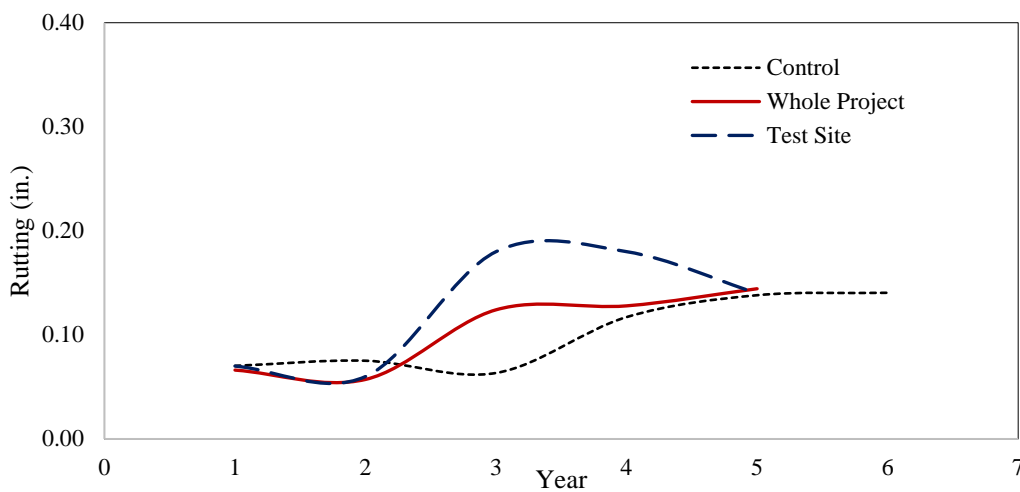


**Figure 54. Rutting at Site #4 SH 86 Kiowa (Eastbound) Showing Amount of Rutting at the Control Site, Test Site, and Whole Project**

*Transverse Cracking:* Nine years after construction, the transverse cracking at the test site and whole project is less than the cracking at the control site as shown in Figure 55. The control project has a maximum of five cracks (each 12 feet long) per tenth-mile, while the whole project and the test site each has a maximum of one crack per tenth-mile. The data show that the difference between the whole project and test site is negligible and the project that used CIR performed better than conventional HMA. Transverse cracking is expected to increase over time, but will unlikely meet the terminal threshold value (used by PMED) of 1,500 feet per mile for several years.

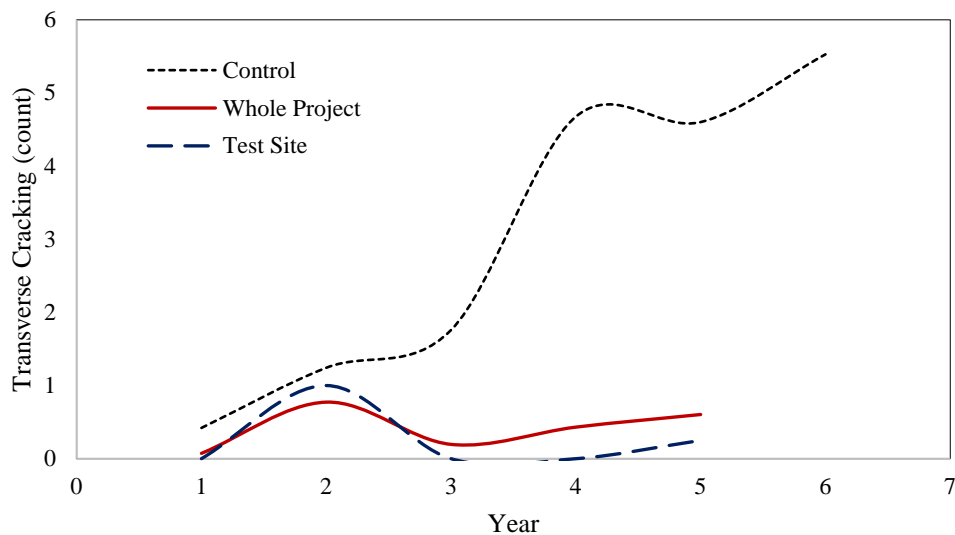


**Figure 55. Transverse Cracking at Site #4 SH 86 Kiowa (Eastbound) Showing Amount of Cracking at the Control Site, Test Site, and Whole Project**

IRI: The IRI at the test site and control site has 76 inch per mile of IRI, after 5 years of construction as shown in Figure 56. The whole project has IRI of 85 inches per mile, which is more than that of test site and control site. Thus, the whole CIR site indicated that the use of CIR may cause an increase in the roadway’s IRI. The graph indicates that IRI will not significantly increase over time and will unlikely reach the terminal threshold value of 200 inches per mile used on the PMED.

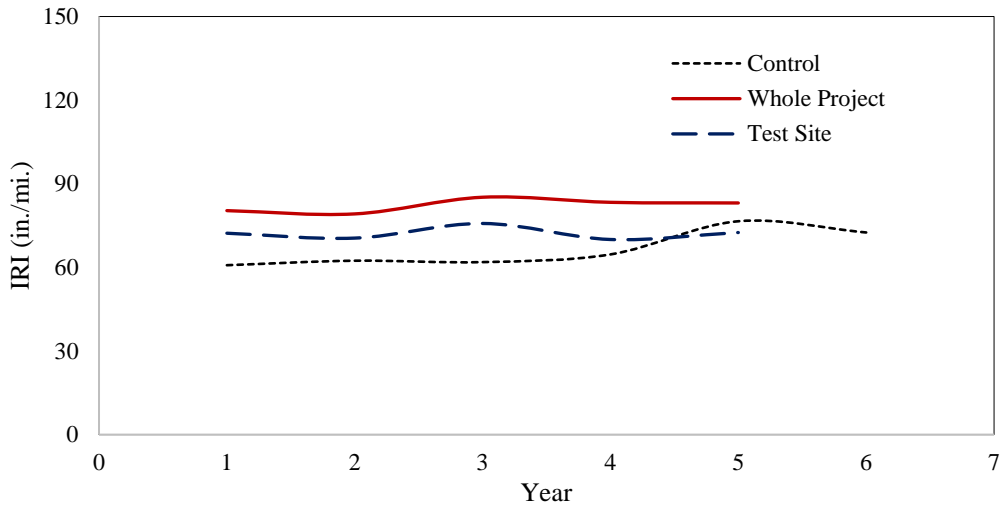


**Figure 56. IRI at Site #4 SH 86 Kiowa (Eastbound) Showing Amount of IRI at the Control Site, Test Site, and Whole Project**

**Site #5 I-25 South of Colorado City to Cedarwood**

*Fatigue Cracking:* Fatigue cracking at the test site and whole project have good amount of fatigue cracking 8 years after construction as shown in Figure 57. The test site and whole project have similar cracking with maximum values of 2887 and 1889 square feet per tenth-mile, respectively. The control site has an average fatigue cracking of 240 square feet per tenth-mile. Figure 57 also shows that the amount of fatigue cracking is expected to increase rapidly over time.

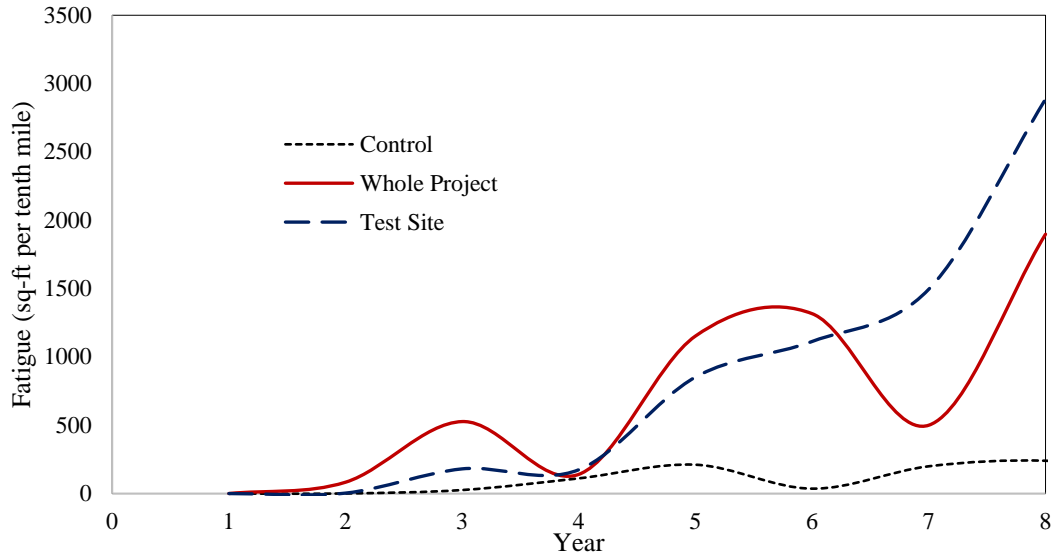


**Figure 57. Fatigue Cracking at Site #5 I-25 South of Colorado City to Cedarwood Showing Amount of Cracking at the Control Site, Test Site, and Whole Project**

*Rutting:* The amount of rutting at the whole project, control site, and test site are very similar as shown in Figure 58. Eight years after construction rutting at the control site increased from 0.06 to 0.22 inches, at the whole project it increased from 0.04 to 0.23 inches, and at the test site, it increased from 0.04 to 0.19 inches. Thus, the rutting measured at whole project is slightly more than that of test site or control site. Figure 58 indicates that rutting is expected to grow with age but will not exceed the terminal threshold value (used by PMED) of 0.5 inches for several years.

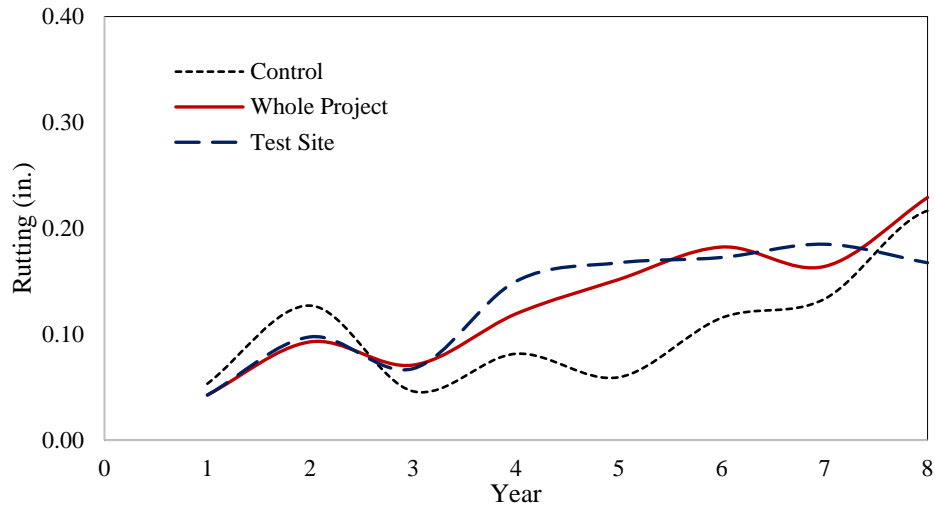


**Figure 58. Rutting at Site #5 I-25 South of Colorado City to Cedarwood Showing Amount of Rutting at the Control Site, Test Site, and Whole Project**

*Transverse Cracking:* Eight years after construction, the transverse cracking at the test site and whole project is greater than the cracking at the control site as shown in Figure 59. The control site has a maximum of 18 cracks (each 12 feet long) per tenth-mile, while the whole project and the test site have maximum values of 44 and 55 cracks per tenth-mile, respectively.

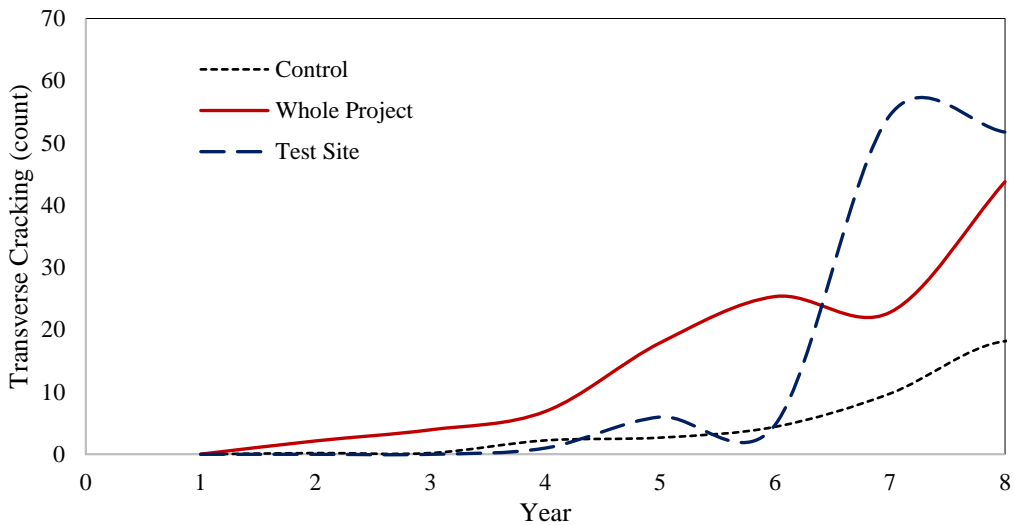


**Figure 59. Transverse Cracking at Site #5 I-25 South of Colorado City to Cedarwood Showing Amount of Cracking at the Control Site, Test Site, and Whole Project**

IRI: Eight years after construction, the IRI at the test site and control site is less than that measured at the whole project as shown in Figure 60. The IRI values at the control site ranged from 47 to 54 inches per mile. The whole project's IRI values ranged from 56 to 80 inches per mile, and the test site ranged from 44 to 49 inches per mile. The field data show that the whole project performed poorer than the test site and control site. They also indicated that the use of CIR may cause an increase in the roadway's IRI. The graph indicates that the IRI will not significantly increase over time and will unlikely reach the terminal threshold value PMED used of 200 inches per mile.

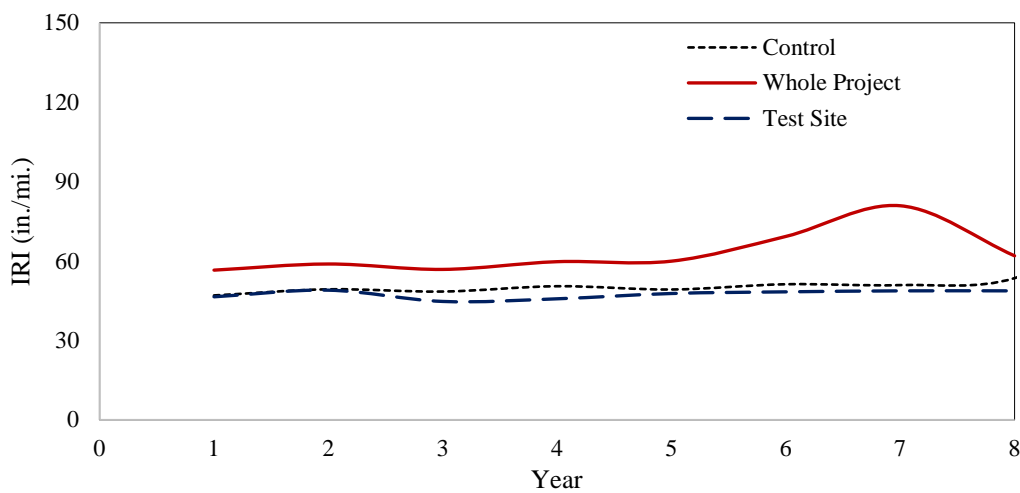


**Figure 60. IRI at Site #5 I-25 South of Colorado City to Cedarwood Showing Amount of IRI at the Control Site, Test Site, and Whole Project**

### Site #6 SH 50 Cerro Summit Paving

*Fatigue Cracking:* Ten years after construction, the fatigue cracking values for the test site and whole project are greater than for the control site as shown in Figure 61. The test site and whole project have maximum values of 163 and 431 square feet per tenth-mile, respectively. The control site has a maximum fatigue cracking of 25 square feet per tenth-mile, which is less than that of the test site and whole project.

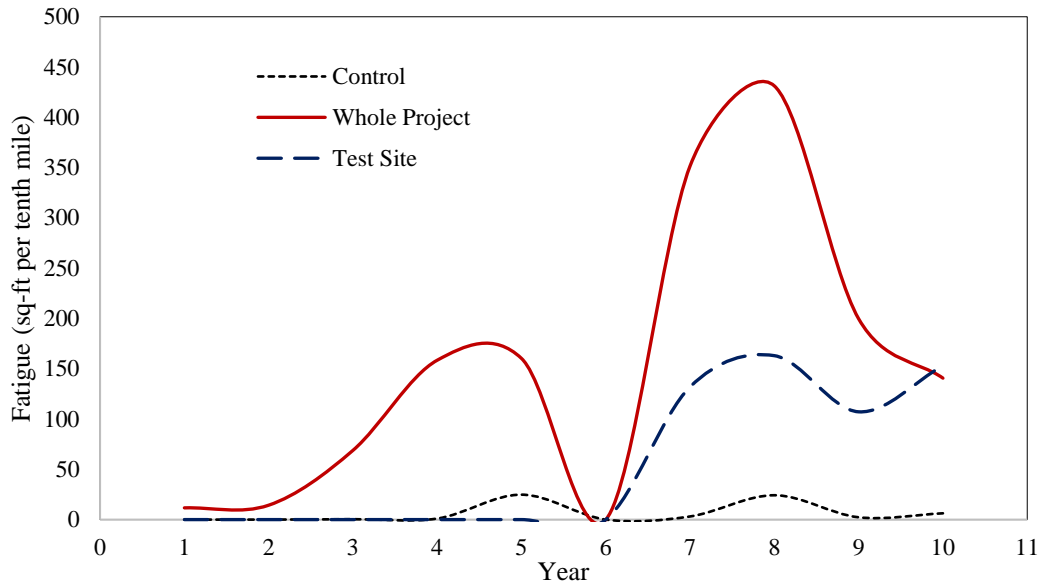


**Figure 61. Fatigue Cracking at Site #6 SH 50 Cerro Summit Paving Showing Amount of Cracking at the Control Site, Test Site, and Whole Project**

*Rutting:* The maximum amount of rutting at the whole project, control site, and test site are 0.24, 0.22, and 0.19 inches, respectively as shown in Figure 62. Thus, the rutting measured at the whole project is more than the others. Figure 62 also indicates that rutting is expected to grow with age but will not exceed the terminal threshold value (used by PMED) of 0.5 inches for several years.

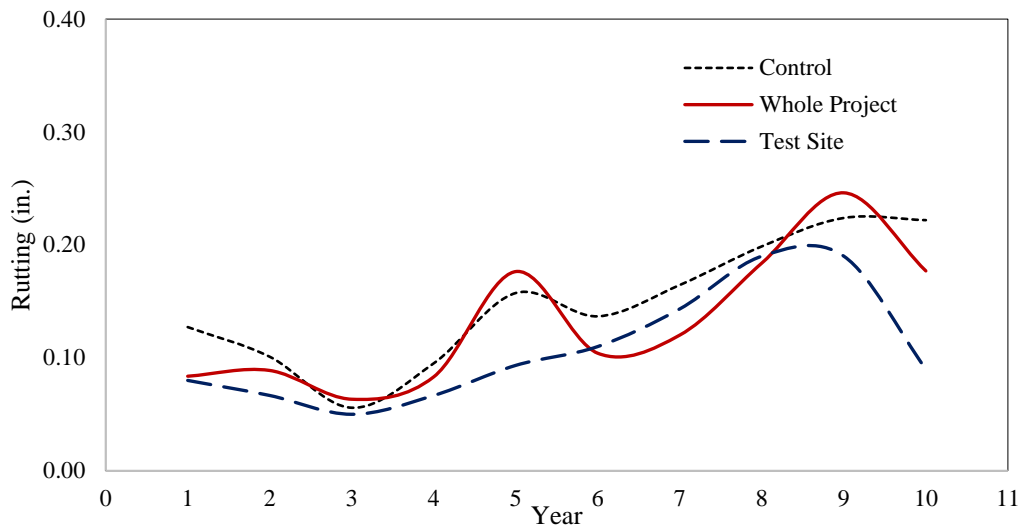


**Figure 62. Rutting at Site #6 SH 50 Cerro Summit Paving Showing Amount of Rutting at the Control Site, Test Site, and Whole Project**

*Transverse Cracking:* Ten years after construction, the transverse cracking at the test site and whole project is greater than the cracking at the control site as shown in Figure 63. The control site has a maximum of two cracks (each 12 feet long) per tenth-mile, while the whole project and the test site each has a maximum of seven cracks per tenth-mile. The data show that the difference between the whole project and test site is negligible, and that the project that used CIR performed poorer than conventional HMA.

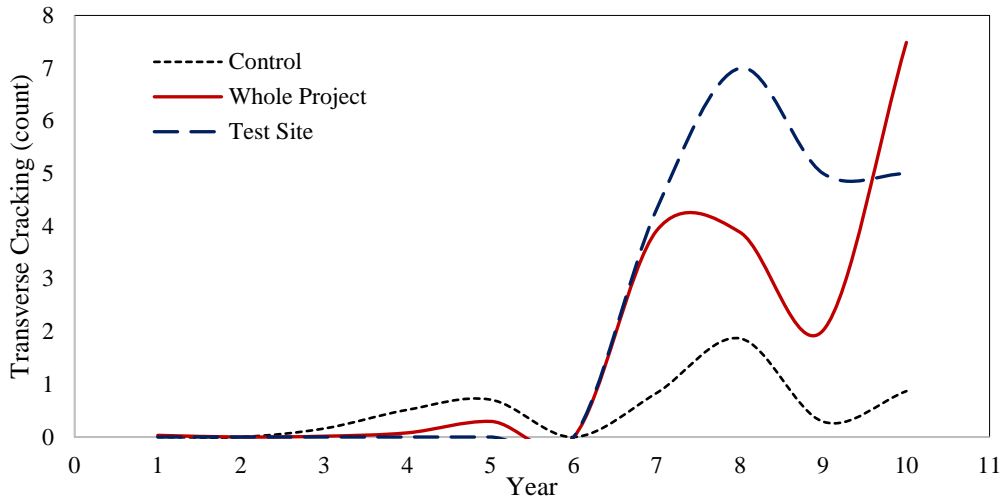


**Figure 63. Transverse Cracking at Site #6 SH 50 Cerro Summit Paving Showing Amount of Cracking at the Control Site, Test Site, and Whole Project**

IRI: The IRI at the test site and whole project is more than that measured at the control site as shown in Figure 64. Since the construction of the project ten years ago, the control site's IRI ranged from 73 to 81 inches per mile. The whole project's IRI ranged from 73 to 95 inches per mile, and the test site ranged from 68 to 95 inches per mile. The field data show that the control site performed better than the test site and whole project and indicate that the use of CIR may cause an increase in the roadway's IRI.

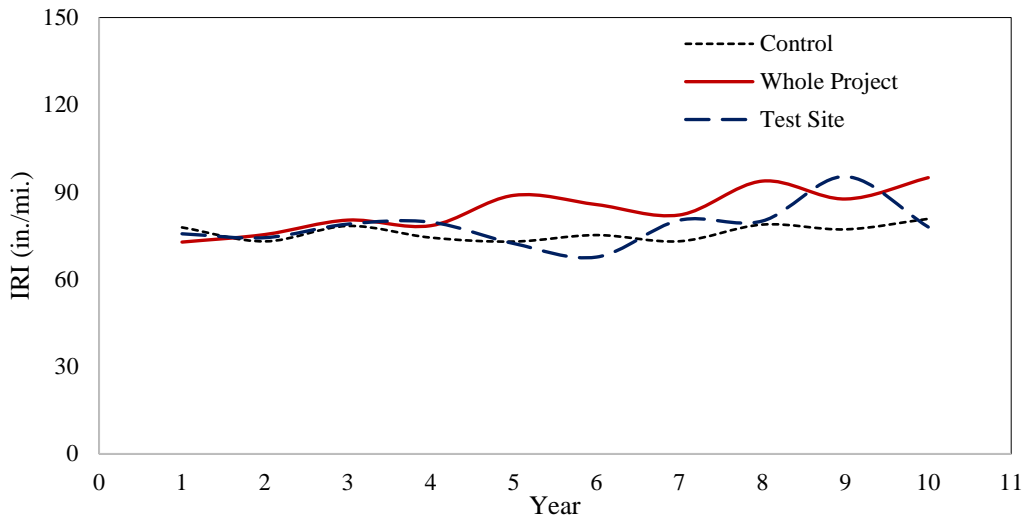


**Figure 64. IRI at Site #6 SH 50 Cerro Summit Paving Showing Amount of IRI at the Control Site, Test Site, and Whole Project**

### **Site #7 I-70 West of Mack**

*Fatigue Cracking:* The test site has only 151 square feet per tenth-mile of cracking 10 years after construction as shown in Figure 65. The whole project has cracking with a maximum value of 811 square feet per tenth-mile. However, the control site has cracking of with a maximum of 539 square feet per tenth-mile, which is in between the test site and whole project. Thus, it can be said that the whole project produced higher amount of cracking compared to the control site. Figure 65 also shows the amount of fatigue cracking is not expected to increase rapidly over time.

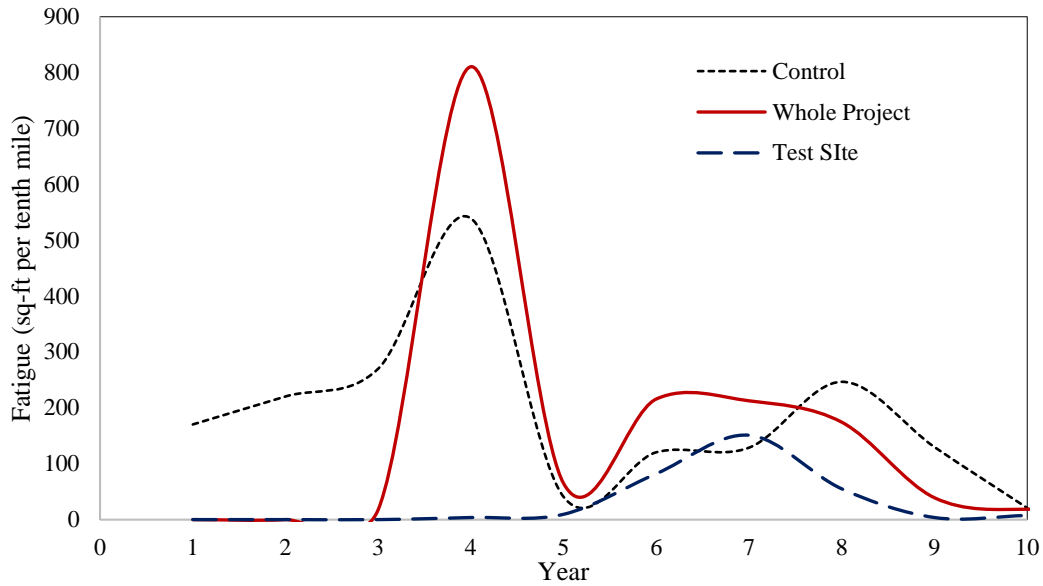


**Figure 65. Fatigue Cracking at Site #7 I-70 West of Mack Showing Amount of Cracking at the Control Site, Test Site, and Whole Project**

*Rutting:* The amount of rutting at the test site and whole project are smaller than the control site as shown in Figure 66. Ten years after construction, rutting at the control site increased from 0.2 to 0.35 inches, at the whole project it increased from 0.07 to 0.24 inches, and at the test site, it increased from 0.07 to 0.20 inches. Thus, the rutting measured at the test section and the whole project is slightly less than at the control project and shown a very slight benefit to using CIR. Figure 66 indicates that rutting is expected to grow with age but will not exceed the terminal threshold value (used by PMED) of 0.5 inches for several years.

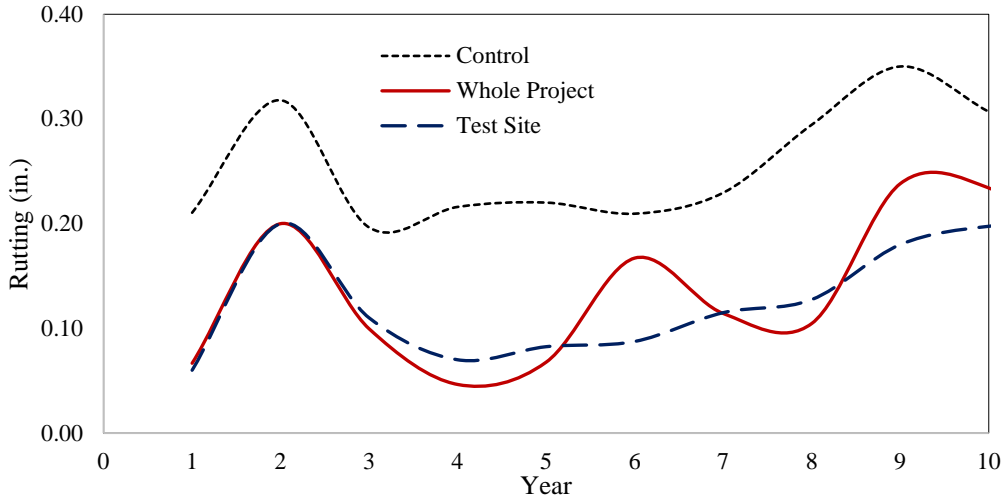


**Figure 66. Rutting at Site #7 I-70 West of Mack Showing Amount of Rutting at the Control Site, Test Site, and Whole Project**

*Transverse Cracking:* Ten years after construction, the transverse cracking at the test site and whole project are greater than the cracking at the control site, Figure 67. The control project has a maximum of six cracks (each 12 feet long) per tenth-mile, while the whole project and the test site each has a maximum of 18, and 12 cracks per tenth-mile, respectively. Transverse cracking is expected to increase over time but will unlikely meet the terminal threshold value (used by PMED) of 1,500 feet per mile for several years.

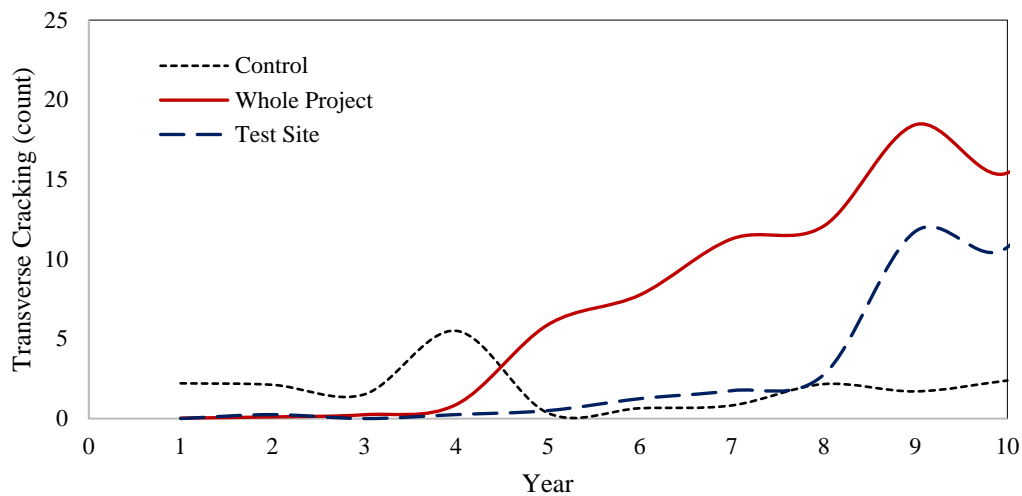


**Figure 67. Transverse Cracking at Site #7 I-70 West of Mack Showing Amount of Cracking at the Control Site, Test Site, and Whole Project**

IRI: The IRI at the whole project is more than that measured at the control site and the test site as shown in Figure 68. Since the construction of the project ten years ago, the control site's IRI values range from 63 to 70 inches per mile. The whole project's IRI values ranged from 48 to 77 inches per mile, and the test site ranged from 43 to 51 inches per mile. The field data show that the control site performed better than the whole project and indicate that the use of CIR may cause an increase in the roadway's IRI. The graph indicates that the IRI will not significantly increase over time and will unlikely reach the terminal threshold value PMED used of 200 inches per mile.

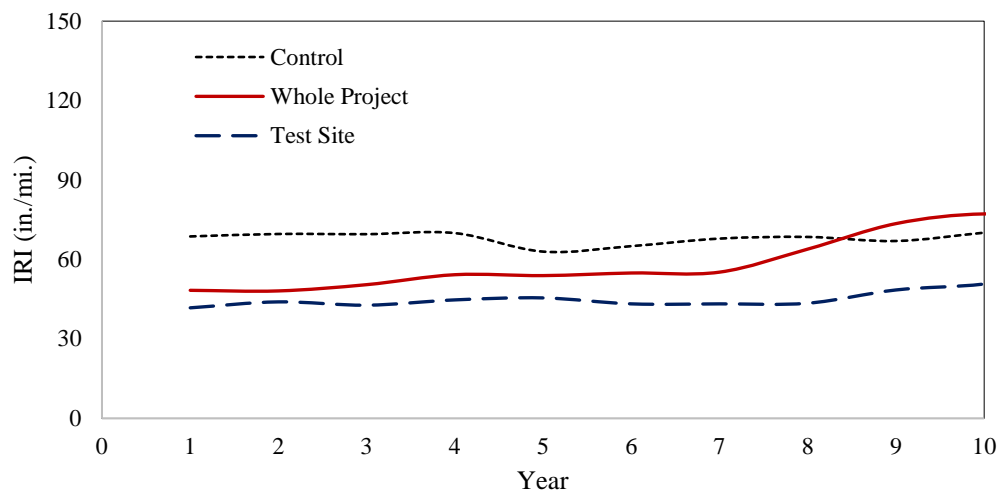


**Figure 68. IRI at Site #7 I-70 West of Mack Showing Amount of IRI at the Control Site, Test Site, and Whole Project**

### Site #8 I-70 Fruita to Clifton

*Fatigue Cracking:* The test site and whole project have more fatigue cracking than the control site 10 years after construction as shown in Figure 69. The test site and the whole project have cracking with maximum values of 1357, and 1569 square feet per tenth-mile, respectively. The control site has a maximum fatigue cracking value of 794 square feet per tenth-mile, which is less than the test site and whole project. Figure 69 also shows the amount of fatigue cracking is not expected to increase rapidly over time.

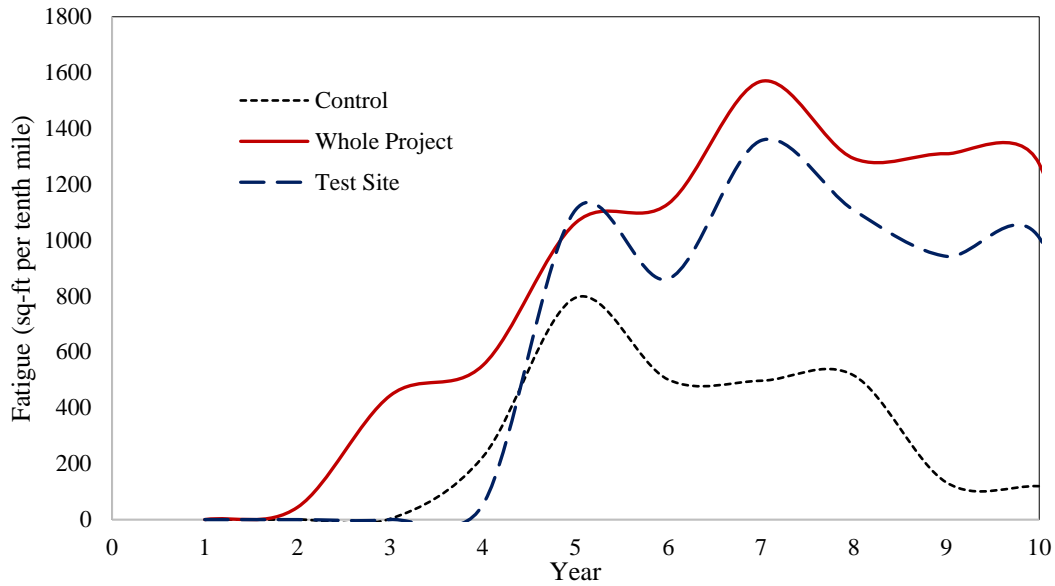


**Figure 69. Fatigue Cracking at Site #8 I-70 Fruita to Clifton Showing Amount of Cracking at the Control Site, Test Site, and Whole Project**

*Rutting:* The amount of rutting at the test site and whole project are less than the control site, Figure 70. Ten years after construction rutting at the control site increased from 0.05 to 0.25 inches, at the whole project it increased from 0.06 to 0.17 inches, and at the test site, it increased from 0.05 to 0.20 inches. Thus, the rutting measured at the test site and whole project is slightly less than the control project and shown a very slight benefit to using CIR. Figure 70 indicates that rutting is expected to grow with age, however will not exceed the terminal threshold value (used by PMED) of 0.5 inches for several years.

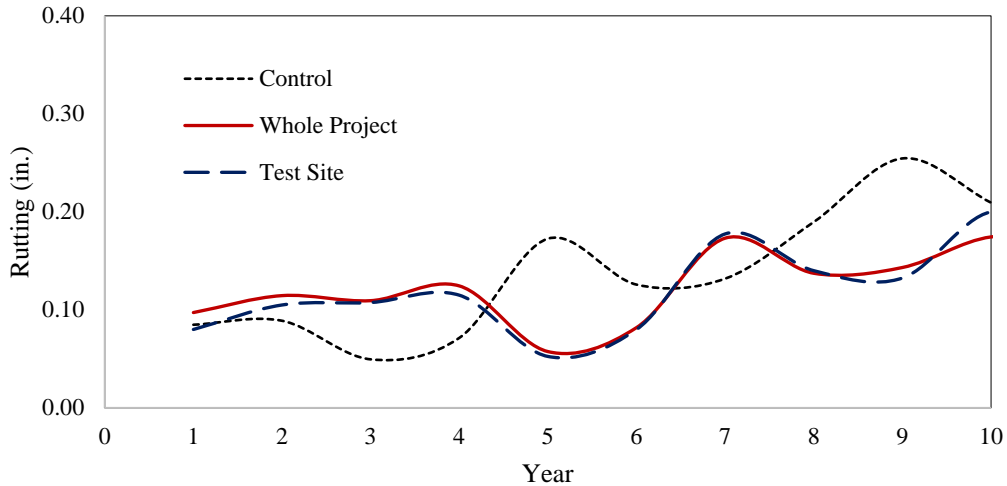


**Figure 70. Rutting at Site #8 I-70 Fruita to Clifton Showing Amount of Rutting at the Control Site, Test Site, and Whole Project**

*Transverse Cracking:* Ten years after construction, the transverse cracking at the test site and whole project is greater than the cracking at the control site as shown in Figure 71. The control project has a maximum of 11 cracks (each 12 feet long) per tenth-mile, while the whole project and the test site have maximum values of 135, and 97 cracks per tenth-mile, respectively. Transverse cracking is expected to increase over time but will unlikely reach the terminal threshold value (used by PMED) of 1,500 feet per mile for several years.

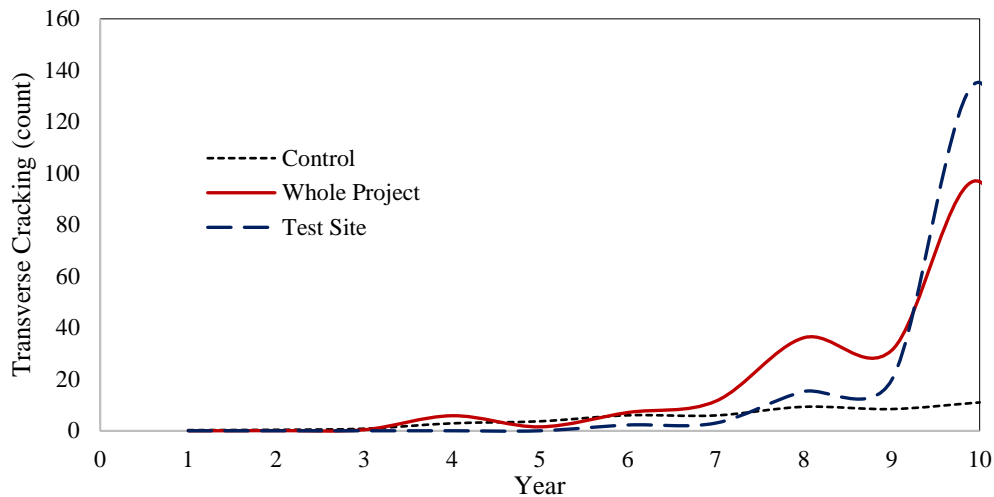


**Figure 71. Transverse Cracking at Site #8 I-70 Fruita to Clifton Showing Amount of Cracking at the Control Site, Test Site, and Whole Project**

IRI: The IRI values at the test site and whole project are less than that measured at the control site as shown in Figure 72. Since the construction of the project ten years ago, the control site's IRI values ranged from 66 to 84 inches per mile. The whole project's IRI values ranged from 50 to 82 inches per mile and the test site ranged from 39 to 55 inches per mile. The field data show that the control site performed poorer than the test site and whole project indicating that the use of CIR may reduce a roadway's IRI. The graph indicates that IRI will not significantly increase over time and will unlikely reach the terminal threshold value PMED used of 200 inches per mile.

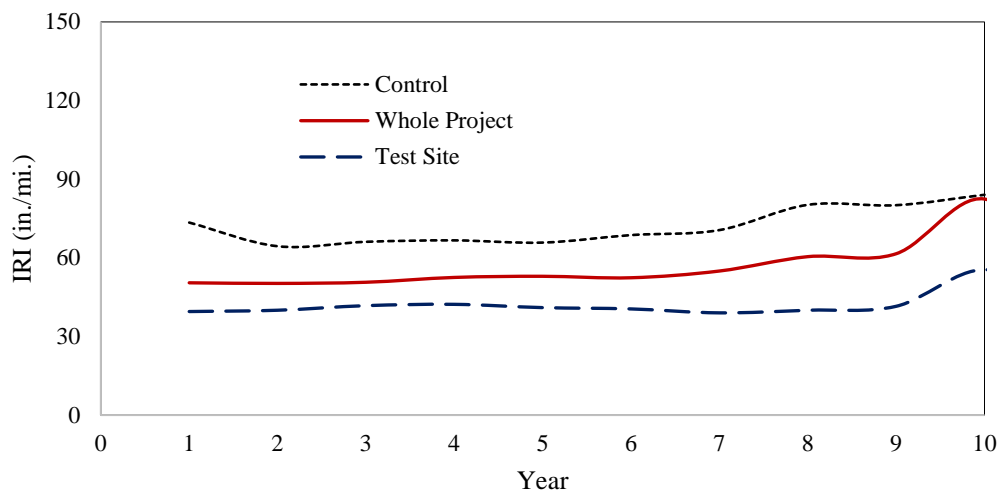


**Figure 72. IRI at Site #8 I-70 Fruita to Clifton Showing Amount of IRI at the Control Site, Test Site, and Whole Project**

**Site #9 SH 92 Delta (Eastbound)**

*Fatigue Cracking:* The test site has no measurable fatigue cracking 11 years after construction as shown in Figure 73. The whole project has cracking with a maximum value of 788 square feet per tenth-mile compared to 681 square feet per tenth-mile for the control site. The whole project has more cracking than the control site. Figure 73 also shows that the amount of fatigue cracking is not expected to increase rapidly over time.

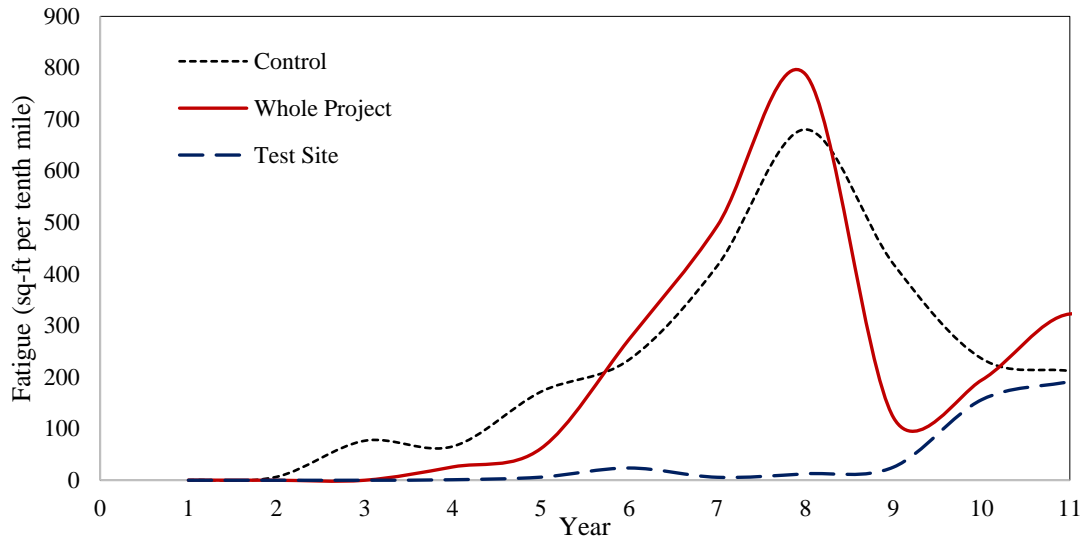


**Figure 73. Fatigue Cracking at Site #9 SH 92 Delta (Eastbound) Showing Amount of Cracking at the Control Site, Test Site, and Whole Project**

*Rutting:* The amounts of rutting at the test site and whole project are higher than at the control site as shown in Figure 74. Eleven years after construction, rutting at the control site increased from 0.05 to 0.18 inches, at the whole project it increased from 0.13 to 0.25 inches, and at the test site, it increased from 0.12 to 0.29 inches. Thus, the rutting values measured at the test site and whole project are slightly higher than at the control site and slightly no benefit to using CIR. Figure 74 indicates that rutting is expected to grow with age but will not exceed the terminal threshold value (used by PMED) of 0.5 inches for several years.

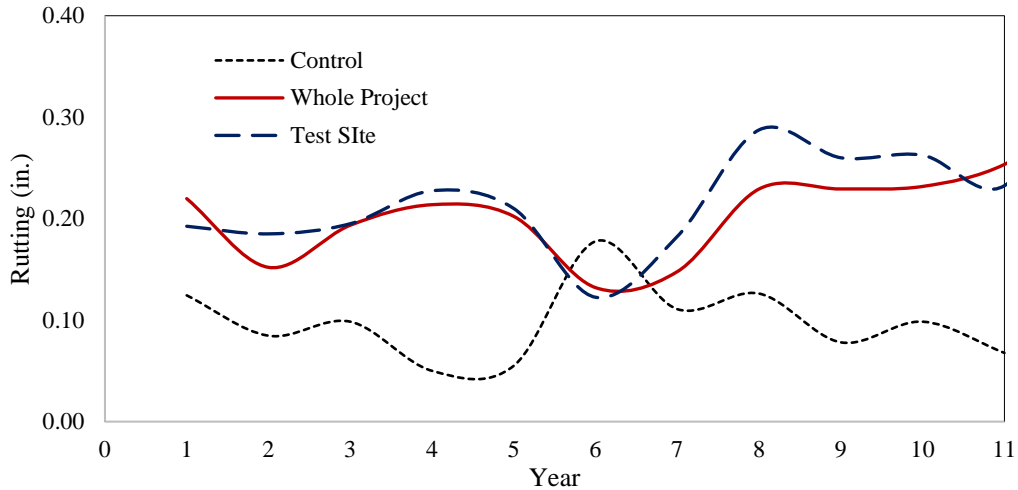


**Figure 74. Rutting at Site #9 SH 92 Delta (Eastbound) Showing Amount of Rutting at the Control Site, Test Site, and Whole Project**

*Transverse Cracking:* Eleven years after construction, the transverse cracking at the test site and whole project is smaller than the cracking at the control site as shown in Figure 75. The control project has a maximum of 24 cracks (each 12 feet long) per tenth-mile while the whole project and the test site have maximum values of 5 and 2 cracks per tenth-mile, respectively. The filed data show that the difference between the whole project and test site is negligible and that the project that used CIR performed better than conventional HMA. Transverse cracking is expected to increase over time but will unlikely meet the terminal threshold value (used by PMED) of 1,500 feet per mile for several years.

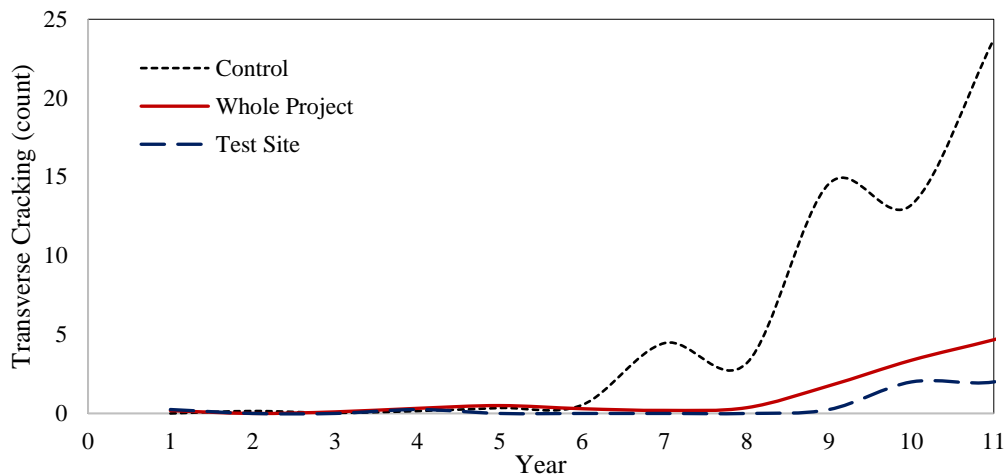


**Figure 75. Transverse Cracking at Site #9 SH 92 Delta (Eastbound) Showing Amount of Cracking at the Control Site, Test Site, and Whole Project**

IRI: The IRI values at the test site and whole project are less than that measured at the control site as shown in Figure 76. Since the construction of the project 11 years ago, the control site's IRI values ranged from 63 to 86 inches per mile. The whole project's IRI values ranged from 49 to 61 inches per mile, and the test site ranged from 39 to 53 inches per mile. The data show that the control site performed poorer than the test site and whole project and indicated that the use of CIR may reduce the roadway's IRI. The graph indicated IRI will not significantly increase over time and will unlikely reach the terminal threshold value PMED used of 200 inches per mile.

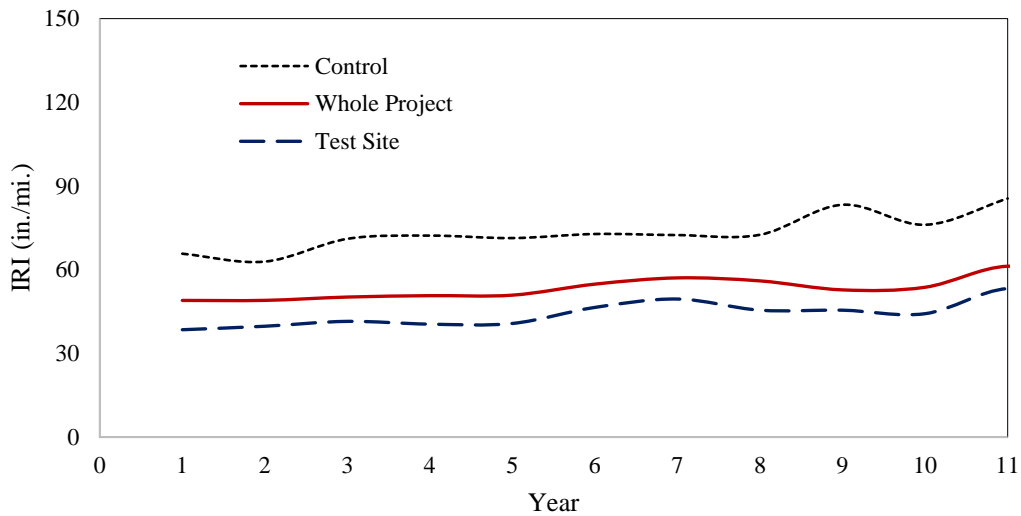


**Figure 76. IRI at Site #9 SH 92 Delta (Eastbound) Showing Amount of IRI at the Control Site, Test Site, and Whole Project**

### Site #10 SH 133 North of Hotchkiss

*Fatigue Cracking:* The test site and whole project have no measurable cracking 8 years after construction as shown in Figure 77. The whole project and test site have similar cracking with maximum values of 18, and 12 square feet per tenth-mile, respectively. The control site has fatigue cracking with a maximum value of 281 square feet per tenth-mile, which is more than that of test site and whole project. Figure 77 also shows that the amount of fatigue cracking is not expected to increase rapidly over time.

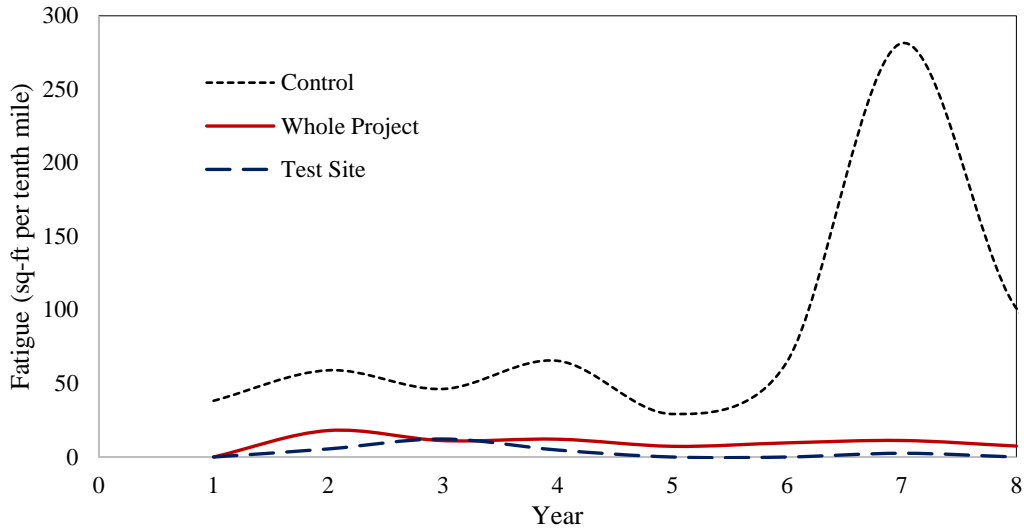


**Figure 77. Fatigue Cracking at Site #10 SH 133 North of Hotchkiss Showing Amount of Cracking at the Control Site, Test Site, and Whole Project**

*Rutting:* The amount of rutting at the test site and whole project are slightly larger than at the control site as shown in Figure 78. During eight years after construction, rutting at the control site increased from 0.06 to 0.16 inches, at the whole project, it increased from 0.07 to 0.24 inches, and at the test site, it increased from 0.05 to 0.21 inches. Thus, the rutting measured at the test section versus the whole project is slightly more than at the control project and slightly shows a no benefit to using CIR. Figure 78 indicates that rutting is expected to grow with age but will not exceed the terminal threshold value (used by PMED) of 0.5 inches for several years.

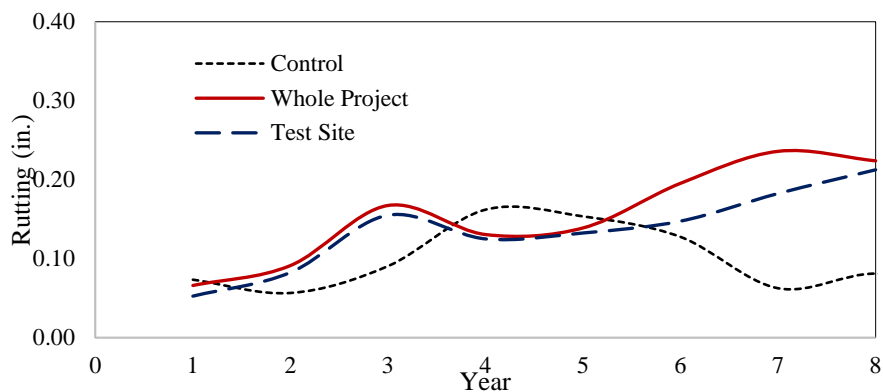


**Figure 78. Rutting at Site #10 SH 133 North of Hotchkiss Showing Amount of Rutting at the Control Site, Test Site, and Whole Project**

*Transverse Cracking:* Eight years after construction, the transverse cracking at the test site and whole project is smaller than the cracking at the control site as shown in Figure 79. The control project has a maximum of 27 cracks (each 12 feet long) per tenth-mile, while the whole project and the test site have a maximum value of one crack per tenth-mile each. The data show that the difference between the whole project and test site is negligible and the project that used CIR performed better than conventional HMA. Transverse cracking is expected to increase over time but will unlikely reach the terminal threshold value (used by PMED) of 1,500 feet per mile for several years.

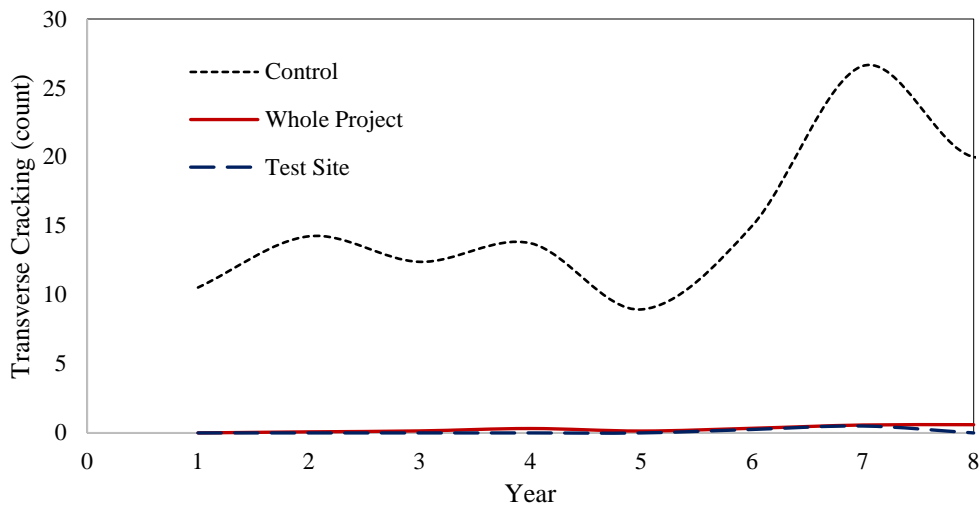


**Figure 79. Transverse Cracking at Site #10 SH 133 North of Hotchkiss Showing Amount of Cracking at the Control Site, Test Site, and Whole Project**

IRI: The IRI values at the test site and whole project are less than that measured at the control site as shown in Figure 80. Since the construction of the project eight years ago, the control site’s IRI values ranged from 81 to 104 inches per mile. The whole project’s IRI values ranged from 67 to 78 inches per mile, and the test site IRI values ranged from 69 to 75 inches per mile. The data show that the control site performed poorer than the test site and whole project and indicated the use of CIR may reduce the roadway’s IRI. The graph indicated that IRI will not significantly increase over time and will unlikely reach the terminal threshold value PMED used of 200 inches per mile.

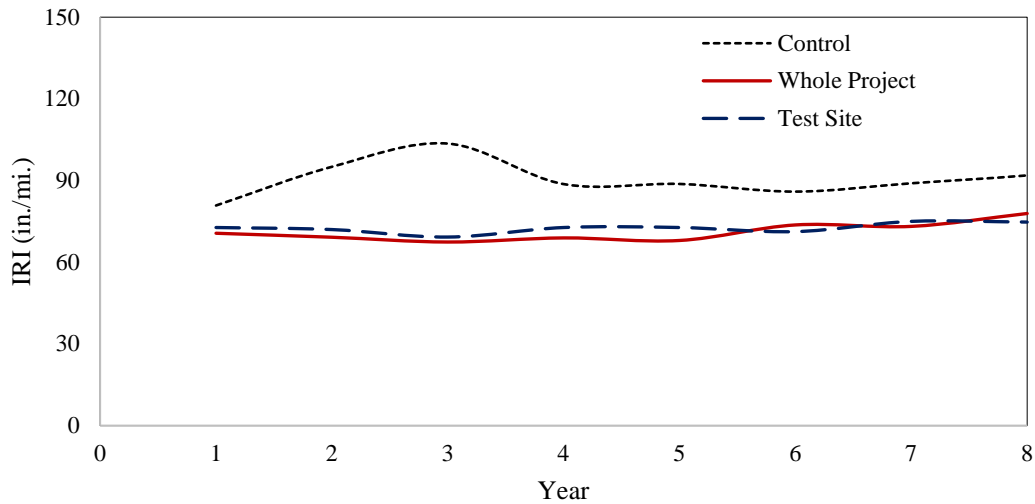


**Figure 80. IRI at Site #10 SH 133 North of Hotchkiss Showing Amount of IRI at the Control Site, Test Site, and Whole Project**

## Pavement Performance Summary

Field performance data for fatigue cracking, rutting, transverse cracking, and IRI were collected from 10 selected sites using CIR and 10 control sites constructed using conventional HMA. Two types of comparisons were made, first, with the CDOT recommended threshold values of performance criteria for rehabilitation of flexible pavement projects obtained from the CDOT 2017 Pavement Design Manual (13), and second, with the distresses of the control sites. Table 2 summarizes the maximum distress data collected from 10 selected sites using CIR and 10 control sites using conventional HMA. Table 3 lists the recommended threshold values of performance criteria for rehabilitation of flexible pavement projects. First, IRI, Rutting and Transverse Cracking did not exceed the threshold values during the service period. For fatigue cracking, CIR exceeds the threshold value at Site #5, and Site #8 after 8-10 years of service. All these locations are from Interstates (I-25 and I-70). Most distress data for interstates are within the threshold values. Due to high volume of traffic, CIR may not be an appropriate option for interstates.

**Table 2. Measured Maximum Distresses**

Project	No. of Years of Data*	Location	IRI (in./mi.)	Rutting (in.)	Fatigue Cracking (sq-ft/0.1 mi)	Transverse Cracking
Site #1: SH 9 from Fairplay to Alma	9	Test Site	67	0.17	4	11
		Whole Project	71	0.18	57	11
		Control Site	89	0.19	145	8
Site #2: SH 9 Hoosier Pass (Northbound)	9	Test Site	122	0.24	13	8
		Whole Project	124	0.33	190	8
		Control Site	113	0.24	74	24
Site #3: SH 86 East of Franktown	9	Test Site	101	0.14	13	2
		Whole Project	84	0.16	42	3
		Control Site	63	0.17	39	7
Site #4: SH 86 Kiowa (Eastbound)	5	Test Site	76	0.18	2	1
		Whole Project	85	0.14	12	1
		Control Site	77	0.14	67	5
Site #5: I-25 South of Colorado City to Cedarwood	8	Test Site	49	0.19	2,887	55
		Whole Project	80	0.23	1,898	44
		Control Site	54	0.22	240	18
Site #6: SH 50 Cerro Summit Paving	10	Test Site	95	0.19	163	7
		Whole Project	95	0.24	431	7
		Control Site	81	0.22	25	2
Site #7: I-70 West of Mack	10	Test Site	51	0.20	151	12
		Whole Project	77	0.24	811	18
		Control Site	70	0.35	539	6
Site #8: I-70 Fruita to Clifton	10	Test Site	55	0.20	1,357	135
		Whole Project	82	0.17	1,569	97
		Control Site	84	0.25	794	11
Site #9: SH 92 Delta (Eastbound)	11	Test Site	53	0.29	192	2
		Whole Project	61	0.25	788	5
		Control Site	86	0.18	681	24
Site #10: SH 133 North of Hotchkiss	8	Test Site	75	0.21	12	1
		Whole Project	78	0.24	18	1
		Control Site	104	0.16	281	27

\*Highlighted figures exceed the threshold recommended by CDOT

**Table 3. Recommended Threshold Values of Performance Criteria for Rehabilitation of Flexible Pavement Projects**

Project	IRI (in./mi.)	Rutting (in.)	Total Fatigue Cracking (sq-ft/0.1 mi)	Transverse Cracking (ft./mi.)
Interstate	160	0.55	1400	1,500
Principal Arterial	200	0.65	2350	1,500

The comparison of the measured distresses with the control sites is summarized in Table 4. The larger values of the measured distresses at the Test Site and Whole Project were considered the distresses of CIR at that pavement. Table 4 shows CIR performed better at three sites, similar at one site and worse at six sites compared to the control projects for fatigue cracking. Results of rutting shows CIR performed better at four sites, similar at two sites and worse at four sites compared to the control site. For transverse cracking, CIR performed better at five sites, and worse at five sites compared to the control projects. CIR performed better at four sites, and worse at six sites compared to the control projects for IRI. Considering all these results, it can be said that measured distresses of CIR rehabilitation techniques are similar to conventional pavements.

**Table 4. CIR Performance Compared to Conventional Pavement**

<b>Performances</b>	<b>Locations Favoring the CIR</b>	<b>Neutral Locations</b>	<b>Locations against the CIR</b>
Fatigue Cracking	Sites #1, #4, #10	Site #3	Sites #2, #5, #6, #7, #8, #9
Rutting	Sites #1, #3, #7, #8	Sites #5, #6	Sites #2, #4, #9, #10
Transverse Cracking	Sites #2, #3, #4, #9, #10	-	Sites #1, #5, #6, #7, #8
IRI	Sites #1, #8, #9, #10	-	Sites #2, #3, #4, #5, #6, #7

This page is left intentionally blank

## SECTION 5: MATERIALS COLLECTION AND TESTING

### Background

Laboratory testing was conducted on the collected asphalt cores, base, and subgrade from the ten fore-mentioned sites. The testing parameters and the responsible parties are listed in Table 5.

**Table 5. Test Protocols for Measuring Material Properties**

<b>Design Type</b>	<b>Measured Property</b>	<b>Recommended Test Protocol and/or Data Source</b>	<b>Responsible Party for Testing</b>
Cold in-Place Recycling	Dynamic modulus	AASHTO TP 62 (cores)	CDOT
Base-Course	Classification	CP 31 and 32 AASHTO T 89/T 90	Contractor
	Maximum dry density	AASHTO T 180	Contractor
	Optimum moisture content	AASHTO T 180	Contractor
	Resilient modulus	AASHTO T 307	Contractor
	R-value	AASHTO T 190	Contractor
Subgrade	Classification	CP 23 and 31 AASHTO T 89/T 90	Contractor
	Maximum dry density	AASHTO T 99	Contractor
	Optimum moisture content	AASHTO T 99	Contractor
	Resilient modulus	AASHTO T 307	Contractor
	R-value	AASHTO T 190	Contractor

### Materials Collection

Ten asphalt cores were collected from each site. Coring layout, coring operation, and cored samples from a test site are shown in Figures 81-83.

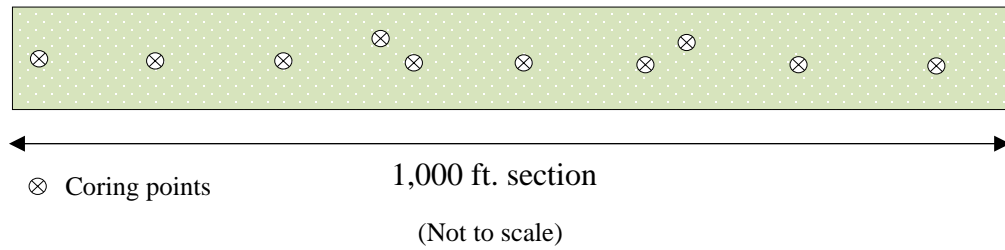


**Figure 81. Approximate Coring Locations at Each Site**



**Figure 82. Coring Operation at SH 86 Kiowa East**



**Figure 83. Cored Asphalt Samples from the SH 86 Kiowa East**

Samples collected had the following characteristics: (1) CIR cores were bound materials, (2) layer separation between the CIR and underlying HMA bonding was common, and (3) the bottom layer

(old asphalt layer) had deteriorated. Since the CIR layer was a bound material, it was possible to conduct dynamic modulus tests.

## Characterization of CIR

The collected field samples were tested by CDOT or Ground Engineering as indicated in Table 2.

The following tests were performed:

### *Dynamic Modulus ( $E^*$ ) Testing*

The  $E^*$  testing on collected field cores was conducted by CDOT following the AASHTO TP 62 test protocol using the Asphalt Mixture Performance Tester (AMPT) testing device. The procedure is described below:

- a) Label each 6-inch core and identify the cold-in-place layer using construction data and by visually inspecting each core.
- b) Cut a 50-mm diameter core horizontally out of the cold-in-place layer as shown in Figure 84.
- c) Trim the cores to 110-mm in height.
- d) Record the exact measurements of each 110-mm specimen.
- e) Attach the gauge points for an AMPT instrumentation.
- f) Run the Dynamic Modulus test on each specimen at 4 °C, 20 °C, and 35 °C at 0.1 Hz, 1 Hz, and 10 Hz each.

The AMPT test setup is shown in Figure 85.



**Figure 84. AMPT Sample Preparation and Test Setup**

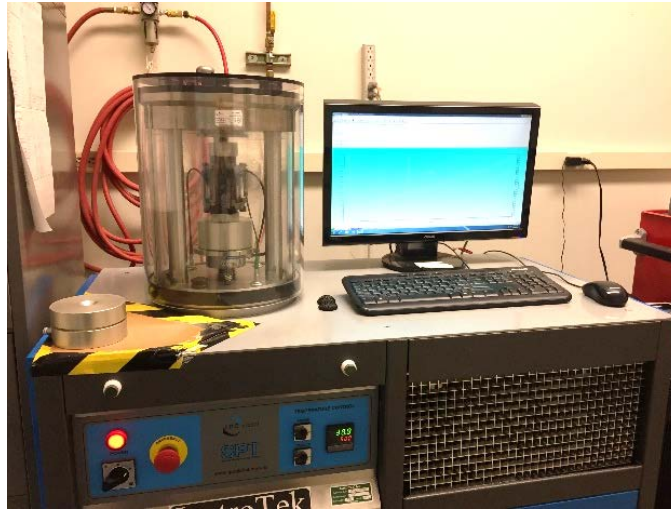


**Figure 85. AMPT Test Setup**

*Resilient Modulus Testing*

Resilient modulus testing was conducted by Ground Engineering in accordance to the AASHTO T 307 test standard. A repeated axial cyclic stress of fixed magnitude was applied to a cylindrical sample. During testing, the sample was subjected to a dynamic cyclic stress and a static confining pressure by means of a pressure chamber. The total recoverable axial deformation of the sample was measured and used to calculate the  $M_R$  value as shown in equation shown below.

$$M_R = \frac{S_{cyclic}}{\epsilon_r}$$

where  $S_{cyclic}$  is the applied cyclic axial stress and  $\epsilon_r$  is the resilient axial deformation. The resilient modulus sample preparation and testing setup are shown in Figure 86 and Figure 87 respectively.



(a) Compacted 150 mm diameter sample



(b) Test-ready sample

**Figure 86. Resilient Modulus Sample Preparation**

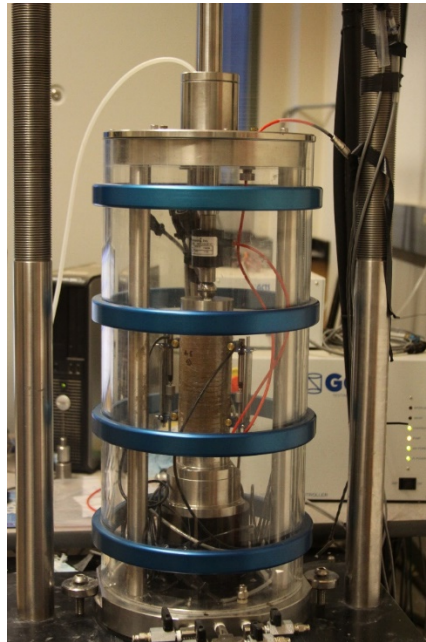


**Figure 87. Resilient Modulus Test Setup on a Soil Sample**

*Classification of Base and Subgrade Courses*

Classifications of the base and subgrade courses were determined by Ground Engineering in accordance with the CP 31, CP 32 and AASHTO T 89/T 90 testing standards. These tests determine the liquid and plastic limits of the base and subgrade courses. These values are used to classify the soil using AASHTO's classification system. The liquid limit is calculated by mixing the soil sample in water until thoroughly mixed and the desired water content is achieved. That mixture is then placed in to the liquid-limit-device cup and leveled out. A grooving tool is used to score a groove into the soil mixture, and then the knob on the liquid limit tool is rotated to lift and drop the cup. The number of drops needed to close the groove in the soil is recorded. This procedure is repeated until the moisture content needed to close the soil's groove in 25 drops is determined and is reported as the liquid limit. Plastic limit is the amount of moisture a soil can absorb before it loses its plasticity. A portion of the soil from the liquid limit test is shaped into an ellipsoidal-shaped mass, and rolled on a glass plate with fingers or the palm of the hand. When the diameter of the soil reaches 1/8 inch, the soil roll is broken up into pieces and rolled again until the soil can no longer be shaped and begins to crumble. The moisture content of the crumbling sample is the plastic limit of the soil.

### *Maximum Dry Density and Optimum Moisture Content Testing for Base Course*

Maximum dry density and optimum moisture content of the base course were determined by the Ground Engineering according to the AASHTO T 180 standard test which is commonly referred to as the modified proctor test. A sample of soil is placed into a 6-inch diameter mold, and compacted with a 10-pound hammer falling 18 inches in five lifts, each lift being hammered 25 times. The weight of the soil, divided by the volume results in the density of the soil. The soil is dried using an oven and weighed. The difference in mass loss over the dry mass is the moisture content.

### *R-Value (California Bearing Ratio) Testing*

R-Value testing was performed by Ground Engineering following the AASHTO T 190 testing protocol. The R-Value test measures the material's resistance to deformation due to a ratio of vertical pressure being applied and transmitted to lateral pressure. A stabilometer is used to apply a vertical load to the sample and measures the lateral pressure exerted through the sample under the compression. The R-Value is the ratio of axial pressure to the vertical pressure applied.

### *Maximum Dry Density and Optimum Moisture Content Testing for Subgrade Course*

Subgrade course tests for maximum dry density and optimum moisture content were performed by Ground Engineering according to the AASHTO T 99 testing standards. This test is commonly referred to as the Standard Proctor test. A sample of soil is placed, in three lifts, into a 6-inch diameter mold, and compacted with a 5.5-pound hammer falling 12 inches, each lift being hammered 25 times. The weight of the soil in the mold, divided by the volume of the mold results in the density of the soil. The soil is then dried in an oven and weighed.

## **SECTION 6: SUMMARY OF RESULTS AND DISCUSSION**

### **General**

This section discusses the field performance, and laboratory testing results. The laboratory testing includes dynamic modulus on cored CIR samples, resilient modulus on base/subgrade, classification of base/subgrade, names the tests.

### **Dynamic Modulus Test Results**

Dynamic modulus testing was conducted by the CDOT laboratory on the field CIR cores. The dynamic modulus test results for each site is listed below.

#### *Site #1 SH 9 From Fairplay to Alma*

Two CIR cores were tested for this site. The sample-wise modulus and the average modulus are listed in Table 6. Figure 88 shows the dynamic moduli variation with the reduced frequency of both samples.

**Table 6. Dynamic Moduli of Two Samples from SH 9 from Fairplay to Alma**

<b>Temperature</b>	<b>Frequency</b>	<b>Sample 1</b>	<b>Sample 2</b>	<b>Average</b>
<b>°F</b>	<b>Hz</b>	<b>psi</b>	<b>psi</b>	<b>psi</b>
14	25	1,286,600	1,530,800	1,408,700
14	10	1,210,600	1,447,500	1,329,050
14	5	1,152,800	1,383,300	1,268,050
14	1	1,018,800	1,231,100	1,124,950
14	0.5	961,400	1,164,800	1,063,100
14	0.1	830,700	1,010,700	920,700
40	25	843,800	1,036,700	940,250
40	10	771,200	949,600	860,400
40	5	717,700	884,500	801,100
40	1	598,900	737,800	668,350
40	0.5	550,500	677,200	613,850
40	0.1	445,700	544,500	495,100
70	25	445,300	552,700	499,000
70	10	390,800	482,500	436,650
70	5	352,300	432,500	392,400
70	1	272,000	327,900	299,950
70	0.5	241,400	288,000	264,700
70	0.1	179,500	207,600	193,550
100	25	200,500	239,700	220,100
100	10	168,300	197,500	182,900
100	5	146,500	169,100	157,800
100	1	104,200	114,700	109,450
100	0.5	89,100	95,900	92,500
100	0.1	60,800	61,300	61,050
130	25	79,000	85,400	82,200
130	10	63,400	66,100	64,750
130	5	53,400	54,000	53,700
130	1	35,100	32,700	33,900
130	0.5	29,100	26,000	27,550
130	0.1	18,400	14,800	16,600

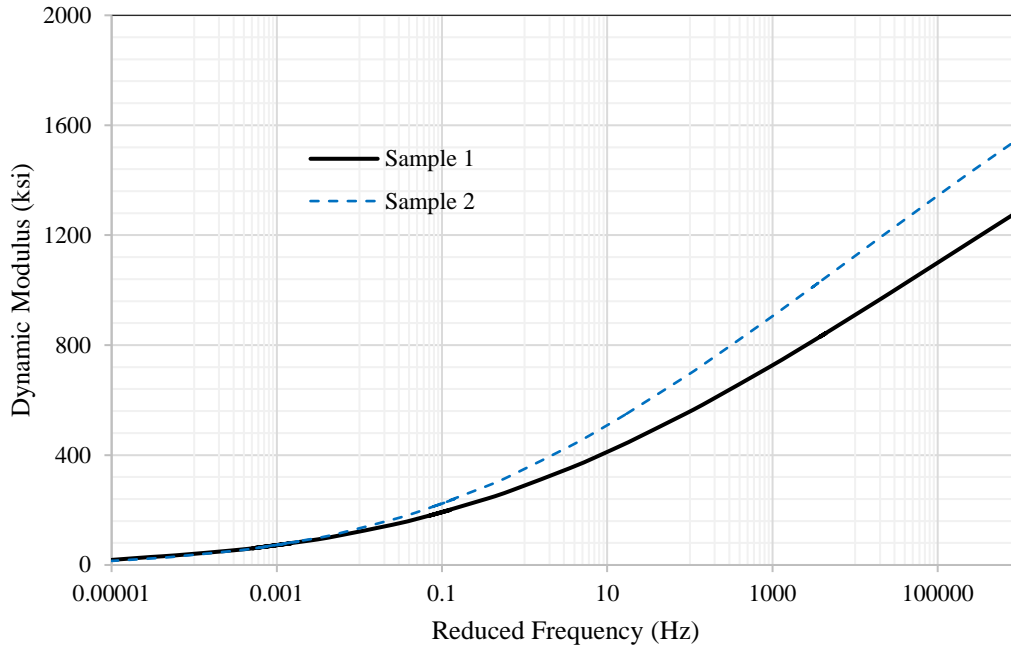


**Figure 88. Dynamic Moduli of Samples from SH 9 From Fairplay to Alma**

*Site #2 Hoosier Pass (Northbound)*

Two CIR cores were tested for this site. The sample-wise modulus and the average modulus are listed in Table 7. Figure 89 also shows the dynamic moduli variation with the reduced frequency of both samples.

**Table 7. Dynamic Moduli of Two Samples from Hoosier Pass (Northbound)**

<b>Temperature</b>	<b>Frequency</b>	<b>Sample 1</b>	<b>Sample 2</b>	<b>Average</b>
<b>°F</b>	<b>Hz</b>	<b>psi</b>	<b>psi</b>	<b>psi</b>
14	25	1,263,100	1,077,530	1,170,315
14	10	1,165,000	998,152	1,081,576
14	5	1,091,100	938,852	1,014,976
14	1	922,400	804,770	863,585
14	0.5	851,800	749,026	800,413
14	0.1	695,400	625,541	660,471
40	25	769,900	696,690	733,295
40	10	682,900	627,398	655,149
40	5	620,000	577,102	598,551
40	1	485,400	468,199	476,800
40	0.5	432,900	424,973	428,937
40	0.1	324,600	333,759	329,179
70	25	364,700	377,210	370,955
70	10	307,400	327,440	317,420
70	5	268,200	292,650	280,425
70	1	191,100	221,396	206,248
70	0.5	163,500	194,749	179,124
70	0.1	111,300	141,821	126,560
100	25	147,100	183,688	165,394
100	10	118,000	153,403	135,702
100	5	99,300	133,066	116,183
100	1	65,000	93,747	79,373
100	0.5	53,800	79,921	66,861
100	0.1	34,000	54,071	44,035
130	25	53,600	82,226	67,913
130	10	41,400	66,135	53,768
130	5	33,900	55,749	44,825
130	1	21,000	36,749	28,874
130	0.5	17,000	30,450	23,725
130	0.1	10,300	19,307	14,804

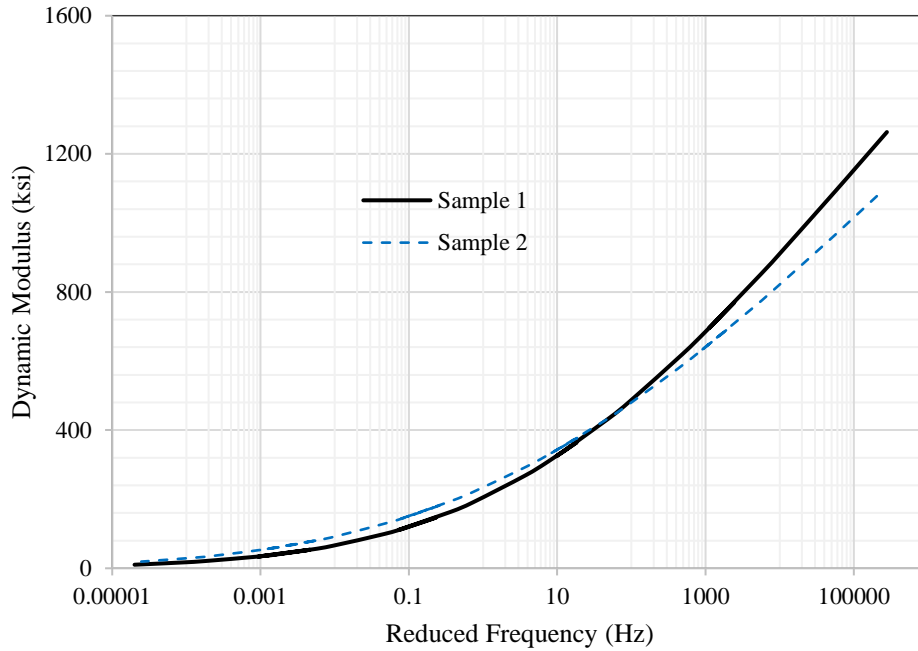


**Figure 89. Dynamic Moduli of Samples from Hoosier Pass (Northbound)**

*Site #3 SH 86 East of Franktown*

Two CIR cores were tested for this site. The sample-wise modulus and the average modulus are listed in Table 8. Figure 90 shows the dynamic moduli variation with the reduced frequency of both samples.

**Table 8. Dynamic Moduli of Two Samples from SH 86 East of Franktown**

<b>Temperature</b>	<b>Frequency</b>	<b>Sample 1</b>	<b>Sample 2</b>	<b>Average</b>
<b>°F</b>	<b>Hz</b>	<b>psi</b>	<b>psi</b>	<b>psi</b>
14	25	1,515,000	1,578,300	1,546,650
14	10	1,431,900	1,529,300	1,480,600
14	5	1,368,200	1,491,800	1,430,000
14	1	1,218,600	1,403,500	1,311,050
14	0.5	1,153,900	1,365,200	1,259,550
14	0.1	1,004,900	1,275,600	1,140,250
40	25	1,063,200	1,106,200	1,084,700
40	10	979,000	1,055,700	1,017,350
40	5	916,300	1,017,700	967,000
40	1	775,400	931,000	853,200
40	0.5	717,300	894,400	805,850
40	0.1	589,800	811,300	700,550
70	25	626,400	651,200	638,800
70	10	557,200	610,100	583,650
70	5	507,500	579,900	543,700
70	1	402,300	513,300	457,800
70	0.5	361,400	486,200	423,800
70	0.1	277,400	426,800	352,100
100	25	328,800	348,900	338,850
100	10	282,200	321,700	301,950
100	5	250,200	302,300	276,250
100	1	186,200	260,700	223,450
100	0.5	162,800	244,300	203,550
100	0.1	117,500	209,500	163,500
130	25	158,600	179,900	169,250
130	10	132,000	164,400	148,200
130	5	114,300	153,400	133,850
130	1	80,800	130,600	105,700
130	0.5	69,300	121,700	95,500
130	0.1	47,900	103,500	75,700

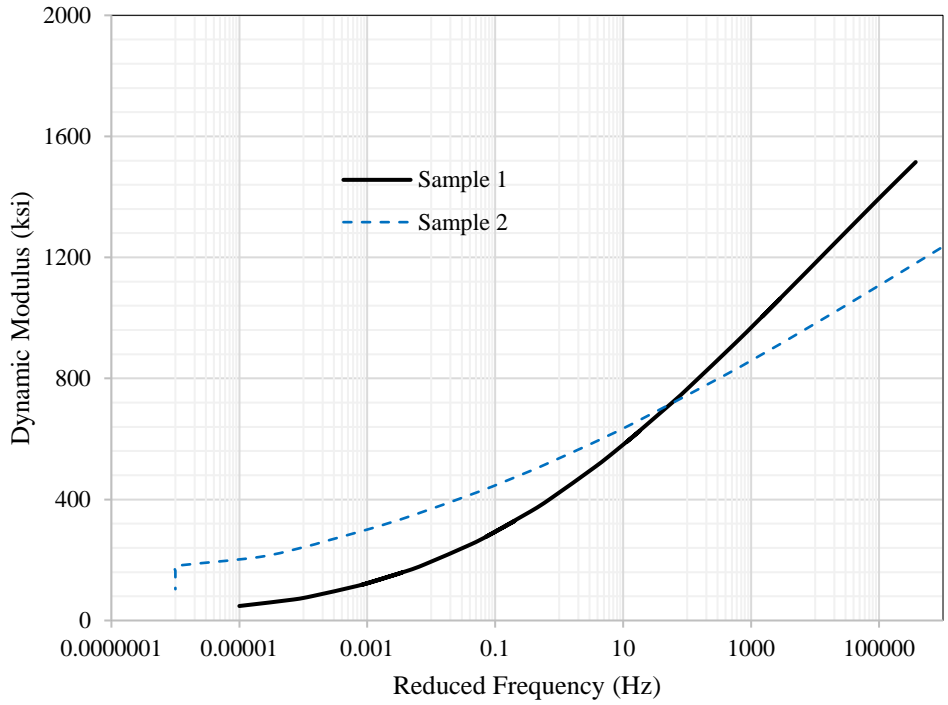


**Figure 90. Dynamic Moduli of Samples from SH 86 East of Franktown**

*Site #4 SH 86 Kiowa (Eastbound)*

Two CIR cores were tested for this site. The sample-wise modulus and the average modulus are listed in Table 9. Figure 91 also shows the dynamic moduli variation with the reduced frequency of both samples.

**Table 9. Dynamic Moduli of Two Samples from Kiowa (Eastbound)**

<b>Temperature</b>	<b>Frequency</b>	<b>Sample 1</b>	<b>Sample 2</b>	<b>Average</b>
<b>°F</b>	<b>Hz</b>	<b>psi</b>	<b>psi</b>	<b>psi</b>
14	25	1,415,312	1,888,359	1,651,836
14	10	1,342,018	1,810,292	1,576,155
14	5	1,286,324	1,749,499	1,517,911
14	1	1,157,026	1,603,335	1,380,181
14	0.5	1,101,707	1,538,597	1,320,152
14	0.1	975,222	1,385,450	1,180,336
40	25	1,027,096	1,379,497	1,203,296
40	10	955,836	1,291,303	1,123,569
40	5	902,902	1,224,549	1,063,725
40	1	784,098	1,070,901	927,499
40	0.5	735,031	1,005,916	870,473
40	0.1	626,874	859,618	743,246
70	25	660,252	838,492	749,372
70	10	600,998	759,805	680,401
70	5	558,188	702,580	630,384
70	1	465,904	578,442	522,173
70	0.5	429,348	529,097	479,223
70	0.1	352,056	424,834	388,445
100	25	401,159	447,971	424,565
100	10	357,965	393,248	375,607
100	5	327,577	355,072	341,325
100	1	264,473	276,999	270,736
100	0.5	240,410	247,786	244,098
100	0.1	191,343	189,526	190,434
130	25	236,868	220,540	228,704
130	10	208,157	189,030	198,593
130	5	188,412	167,821	178,117
130	1	148,657	126,474	137,565
130	0.5	133,955	111,719	122,837
130	0.1	104,796	83,491	94,143

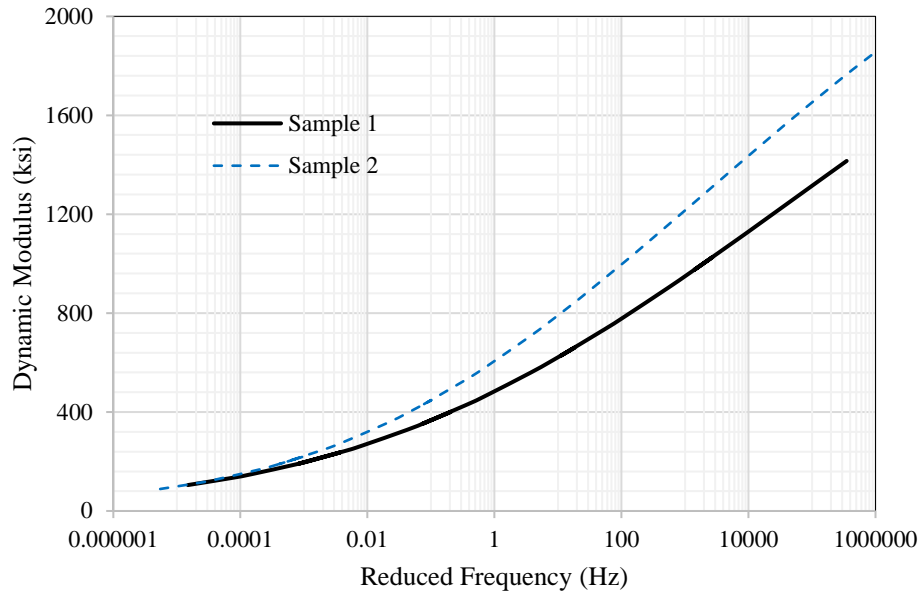


**Figure 91. Dynamic Moduli of Samples from Kiowa (Eastbound)**

*Site #5 I-25 South of Colorado City to Cedarwood*

Two CIR cores were tested for this site. The sample-wise modulus and the average modulus are listed in Table 10. Figure 92 also shows the dynamic moduli variation with the reduced frequency of both samples.

**Table 10. Dynamic Moduli of Two Samples from I-25 South of Colorado City to Cedarwood**

<b>Temperature</b>	<b>Frequency</b>	<b>Sample 1</b>	<b>Sample 2</b>	<b>Average</b>
<b>°F</b>	<b>Hz</b>	<b>psi</b>	<b>psi</b>	<b>psi</b>
14	25	1,814,400	1,718,700	1,766,550
14	10	1,735,300	1,643,300	1,689,300
14	5	1,674,000	1,584,900	1,629,450
14	1	1,527,500	1,445,500	1,486,500
14	0.5	1,463,000	1,384,300	1,423,650
14	0.1	1,311,500	1,240,500	1,276,000
40	25	1,335,500	1,238,700	1,287,100
40	10	1,248,800	1,156,500	1,202,650
40	5	1,183,500	1,094,600	1,139,050
40	1	1,033,600	952,800	993,200
40	0.5	970,400	893,200	931,800
40	0.1	828,800	759,500	794,150
70	25	836,100	743,700	789,900
70	10	759,100	672,000	715,550
70	5	703,000	620,000	661,500
70	1	581,400	507,500	544,450
70	0.5	532,900	462,800	497,850
70	0.1	430,400	368,700	399,550
100	25	471,200	391,700	431,450
100	10	415,800	342,200	379,000
100	5	377,000	307,700	342,350
100	1	297,100	237,200	267,150
100	0.5	267,000	210,900	238,950
100	0.1	206,400	158,600	182,500
130	25	248,800	187,600	218,200
130	10	214,800	159,200	187,000
130	5	191,800	140,100	165,950
130	1	146,400	103,100	124,750
130	0.5	130,000	90,000	110,000
130	0.1	98,300	65,100	81,700

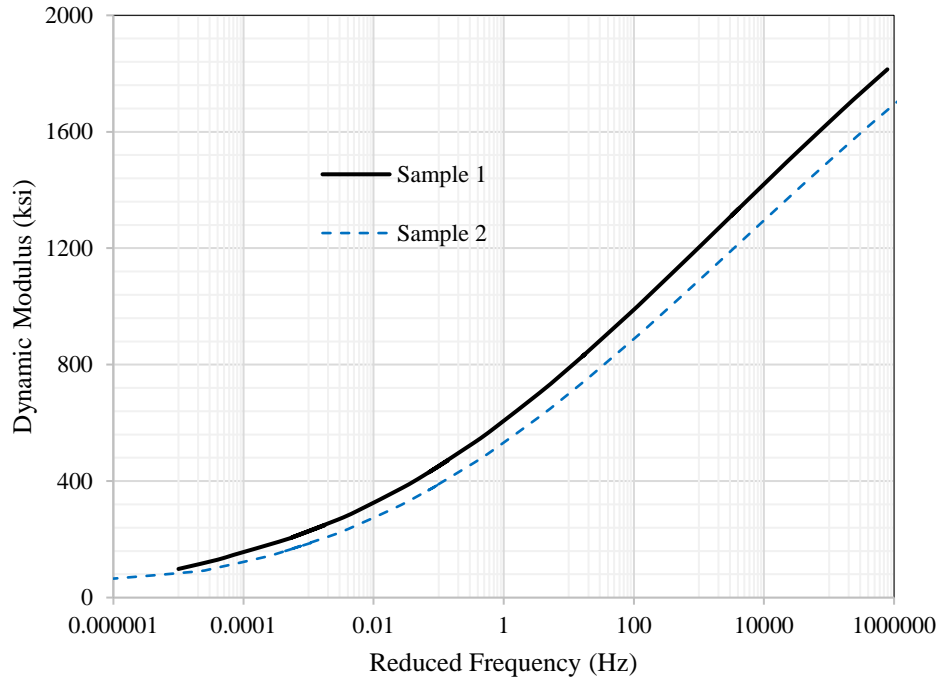


**Figure 92. Dynamic Moduli of Samples from I-25 South of Colorado City to Cedarwood**

*Site #6 Cerro Summit Paving*

Two CIR cores were tested for this site. The sample-wise modulus and the average modulus are listed in Table 11. Figure 93 also shows the dynamic moduli variation with the reduced frequency of both samples.

**Table 11. Dynamic Moduli of Two Samples from Cerro Summit Paving**

<b>Temperature</b>	<b>Frequency</b>	<b>Sample 1</b>	<b>Sample 2</b>	<b>Average</b>
<b>°F</b>	<b>Hz</b>	<b>psi</b>	<b>psi</b>	<b>psi</b>
14	25	1,644,700	1,882,800	1,763,750
14	10	1,560,200	1,789,700	1,674,950
14	5	1,495,300	1,717,200	1,606,250
14	1	1,342,400	1,543,400	1,442,900
14	0.5	1,276,100	1,466,900	1,371,500
14	0.1	1,122,700	1,287,400	1,205,050
40	25	1,174,200	1,333,700	1,253,950
40	10	1,087,500	1,231,500	1,159,500
40	5	1,022,800	1,154,700	1,088,750
40	1	876,800	980,200	928,500
40	0.5	816,300	907,600	861,950
40	0.1	683,200	747,700	715,450
70	25	714,000	771,800	742,900
70	10	641,700	685,800	663,750
70	5	589,800	624,200	607,000
70	1	478,900	493,900	486,400
70	0.5	435,600	443,500	439,550
70	0.1	345,400	340,600	343,000
100	25	396,000	390,400	393,200
100	10	346,400	334,900	340,650
100	5	312,000	297,000	304,500
100	1	242,300	222,000	232,150
100	0.5	216,400	195,000	205,700
100	0.1	165,200	143,000	154,100
130	25	209,100	183,700	196,400
130	10	179,400	153,900	166,650
130	5	159,400	134,400	146,900
130	1	120,500	97,700	109,100
130	0.5	106,600	85,000	95,800
130	0.1	80,100	61,600	70,850

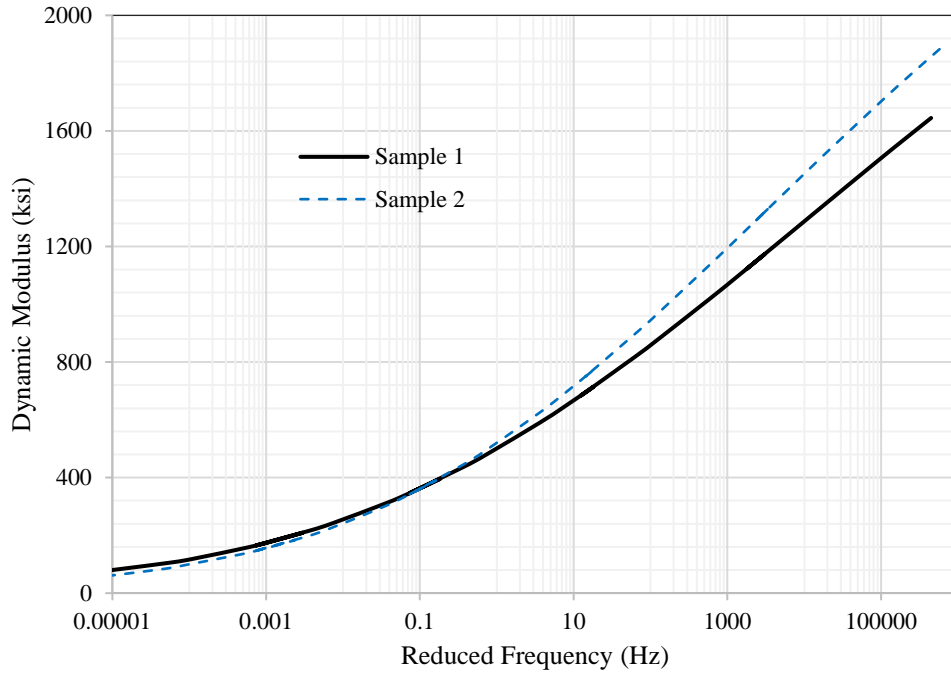


**Figure 93. Dynamic Moduli of Samples from Cerro Summit Paving**

*Site #7 West of Mack*

Two CIR cores were tested for this site. The sample-wise modulus and the average modulus are listed in Table 12. Figure 94 also shows the dynamic moduli variation with the reduced frequency of both samples.

**Table 12. Dynamic Moduli of Two Samples from West of Mack**

<b>Temperature</b>	<b>Frequency</b>	<b>Sample 1</b>	<b>Sample 2</b>	<b>Average</b>
<b>°F</b>	<b>Hz</b>	<b>psi</b>	<b>psi</b>	<b>psi</b>
14	25	2,444,100	2,105,058	2,274,579
14	10	2,376,200	2,034,951	2,205,575
14	5	2,322,000	1,980,134	2,151,067
14	1	2,186,900	1,847,352	2,017,126
14	0.5	2,124,700	1,788,010	1,956,355
14	0.1	1,971,700	1,646,033	1,808,867
40	25	1,994,800	1,670,086	1,832,443
40	10	1,903,600	1,587,535	1,745,567
40	5	1,832,400	1,524,275	1,678,338
40	1	1,660,900	1,375,717	1,518,309
40	0.5	1,584,900	1,311,462	1,448,181
40	0.1	1,405,700	1,163,073	1,284,386
70	25	1,413,200	1,172,331	1,292,766
70	10	1,310,500	1,088,991	1,199,746
70	5	1,233,100	1,026,907	1,130,003
70	1	1,056,500	887,166	971,833
70	0.5	982,600	829,354	905,977
70	0.1	818,600	701,913	760,257
100	25	883,600	754,686	819,143
100	10	792,900	684,250	738,575
100	5	727,300	633,376	680,338
100	1	586,500	523,911	555,205
100	0.5	531,300	480,688	505,994
100	0.1	416,600	389,745	403,173
130	25	496,400	454,806	475,603
130	10	431,900	403,443	417,672
130	5	387,100	367,437	377,269
130	1	296,600	293,144	294,872
130	0.5	263,200	265,034	264,117
130	0.1	197,600	208,227	202,914

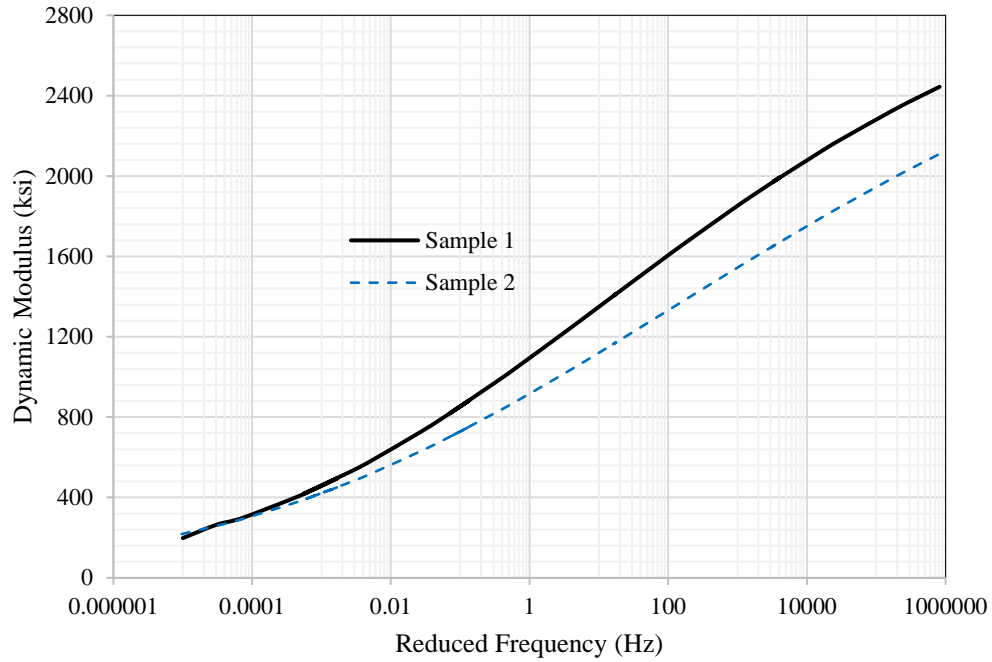


**Figure 94. Dynamic Moduli of Samples from West of Mack**

*Site #8 Fruita to Clifton*

One CIR cores was tested for this site. The sample-wise modulus and the average modulus are listed in Table 13. Figure 95 also shows the dynamic moduli variation with the reduced frequency of the sample tested.

**Table 13. Dynamic Modulus of one Sample from Fruita to Clifton**

<b>Temperature</b>	<b>Frequency</b>	<b>Sample 1</b>
<b>°F</b>	<b>Hz</b>	<b>psi</b>
14	25	1,053,430
14	10	998,131
14	5	956,664
14	1	861,997
14	0.5	822,086
14	0.1	731,889
40	25	690,957
40	10	642,585
40	5	607,031
40	1	528,225
40	0.5	496,007
40	0.1	425,472
70	25	386,563
70	10	351,340
70	5	326,091
70	1	272,121
70	0.5	250,875
70	0.1	206,093
100	25	199,428
100	10	177,252
100	5	161,748
100	1	129,765
100	0.5	117,628
100	0.1	92,948
130	25	97,594
130	10	85,059
130	5	76,494
130	1	59,375
130	0.5	53,087
130	0.1	40,684

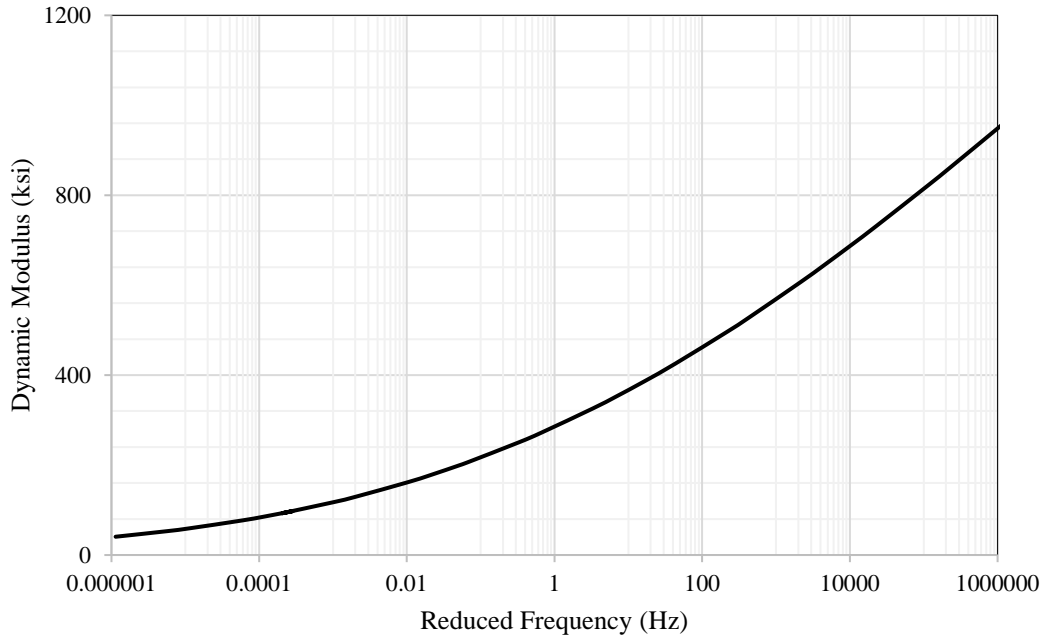


**Figure 95. Dynamic Moduli of One Sample from Fruita to Clifton**

*Site #9 Delta (Eastbound)*

Two CIR cores were tested for this site. The sample-wise modulus and the average modulus are listed in Table 14. Figure 96 also shows the dynamic moduli variation with the reduced frequency of both samples.

**Table 14. Dynamic Moduli of Two Samples from Delta (Eastbound)**

<b>Temperature</b>	<b>Frequency</b>	<b>Sample 1</b>	<b>Sample 2</b>	<b>Average</b>
<b>°F</b>	<b>Hz</b>	<b>psi</b>	<b>psi</b>	<b>psi</b>
14	25	2,422,764	2,545,800	2,484,282
14	10	2,309,485	2,419,000	2,364,242
14	5	2,217,617	2,315,300	2,266,458
14	1	1,985,003	2,049,900	2,017,452
14	0.5	1,877,389	1,926,300	1,901,844
14	0.1	1,614,485	1,623,900	1,619,192
40	25	1,703,961	1,737,600	1,720,781
40	10	1,550,786	1,561,900	1,556,343
40	5	1,433,278	1,427,600	1,430,439
40	1	1,161,382	1,120,500	1,140,941
40	0.5	1,047,450	994,100	1,020,775
40	0.1	798,584	725,200	761,892
70	25	854,706	794,300	824,503
70	10	722,052	653,600	687,826
70	5	629,264	557,600	593,432
70	1	442,452	372,400	407,426
70	0.5	375,019	308,700	341,859
70	0.1	248,221	194,800	221,511
100	25	316,535	259,000	287,768
100	10	249,137	198,600	223,868
100	5	206,346	161,700	184,023
100	1	130,700	99,400	115,050
100	0.5	106,747	80,700	93,724
100	0.1	66,378	50,200	58,289
130	25	100,288	76,800	88,544
130	10	76,513	58,500	67,507
130	5	62,350	47,800	55,075
130	1	39,042	30,800	34,921
130	0.5	32,098	25,800	28,949
130	0.1	20,798	17,700	19,249

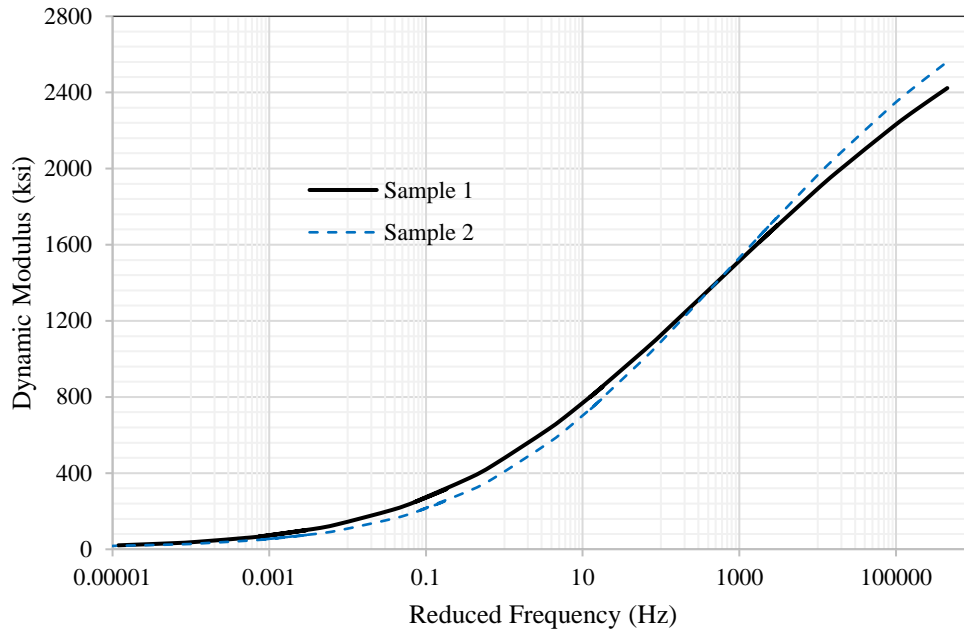


**Figure 96. Dynamic Moduli of Samples from Delta East**

*Site #10 SH 133 North of Hotchkiss*

Two CIR cores were tested for this site. The sample-wise modulus and the average modulus are listed in Table 15. Figure 97 also shows the dynamic moduli variation with the reduced frequency of both samples.

**Table 15. Dynamic Moduli of Two Samples from SH 133 North of Hotchkiss**

<b>Temperature</b>	<b>Frequency</b>	<b>Sample 1</b>	<b>Sample 2</b>	<b>Average</b>
<b>°F</b>	<b>Hz</b>	<b>psi</b>	<b>psi</b>	<b>psi</b>
14	25	1,398,195	2,018,900	1,708,548
14	10	1,320,998	1,948,500	1,634,749
14	5	1,262,359	1,893,500	1,577,929
14	1	1,126,418	1,760,100	1,443,259
14	0.5	1,068,390	1,700,500	1,384,445
14	0.1	936,180	1,558,000	1,247,090
40	25	1,021,210	1,575,300	1,298,255
40	10	946,248	1,492,400	1,219,324
40	5	890,638	1,429,000	1,159,819
40	1	766,192	1,280,500	1,023,346
40	0.5	714,997	1,216,500	965,748
40	0.1	602,738	1,069,400	836,069
70	25	664,177	1,071,400	867,789
70	10	601,520	989,300	795,410
70	5	556,358	928,500	742,429
70	1	459,432	792,700	626,066
70	0.5	421,250	736,900	579,075
70	0.1	341,062	615,300	478,181
100	25	409,807	660,200	535,004
100	10	363,606	593,600	478,603
100	5	331,208	545,900	438,554
100	1	264,312	444,500	354,406
100	0.5	238,977	405,000	321,988
100	0.1	187,719	323,100	255,409
130	25	246,227	378,200	312,213
130	10	215,026	332,300	273,663
130	5	193,659	300,400	247,029
130	1	150,925	235,700	193,312
130	0.5	135,246	211,600	173,423
130	0.1	104,416	163,700	134,058

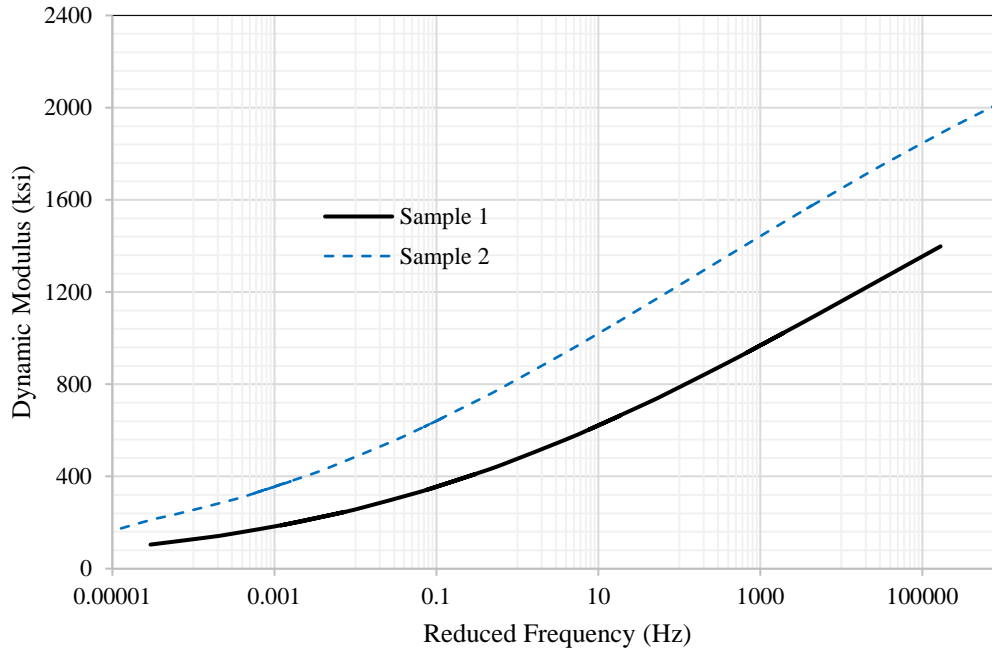


**Figure 97. Dynamic Moduli of Samples from North of Hotchkiss**

## Development of Dynamic Modulus Data for the PMED

Mastersolver was used to determine the master curve of dynamic modulus to be used in the PMED software. The dynamic modulus is determined using the following equation:

$$\log|E^*| = \log(\text{Min}) + \frac{(\log(\text{Max}) - \log(\text{Min}))}{1 + e^{\beta + \gamma \log \omega_r}}$$

where:

$|E^*|$  = dynamic modulus

$\omega_r$  = reduced frequency, Hz

Max = limiting maximum modulus, ksi

Min = limiting minimum modulus, ksi

$\beta$  and  $\gamma$  = fitting parameters

The reduced frequency is computed using the Arrhenius given below:

$$\log(\omega_r) = \log \omega + \frac{\Delta E_a}{19.14714} \left( \frac{1}{T} - \frac{1}{T_r} \right)$$

where:

$\omega_r$  = reduced frequency at the reference temperature

$\omega$  = loading frequency at the test temperature

$T_r$  = reference temperature, °K

$T$  = test temperature, °K

$\Delta E_a$  = activation energy (treated as a fitting parameter)

The combination of the above mentioned two equations gives the following equation:

$$\log|E^*| = \log(\text{Min}) + \frac{(\log(\text{Max}) - \log(\text{Min}))}{1 + e^{\beta + \gamma \left\{ \log \omega + \frac{\Delta E_a}{19.14714} \left( \frac{1}{T} - \frac{1}{T_r} \right) \right\}}}$$

The shift factors for each temperature are given by the following equation:

$$\log[a(T)] = \frac{\Delta E_a}{19.14714} \left( \frac{1}{T} - \frac{1}{T_r} \right)$$

where:

$a(T)$  = shift factor at temperature T

The maximum limiting modulus is estimated from mixture volumetric properties using the Hrisch model shown below and a limiting binder modulus of 1 GPa:

$$|E^*|_{\max} = P_c \left[ 4,200,000 \left( 1 - \frac{VMA}{100} \right) + 435,000 \left( \frac{VMA \times VFA}{10,000} \right) \right] + \frac{1 - P_c}{\left[ \frac{\left( 1 - \frac{VMA}{100} \right)}{4,200,000} + \frac{VFA}{435,000} \right]}$$

where:

$$P_c = \frac{\left( 20 + \frac{435,000 VFA}{VMA} \right)^{0.58}}{650 + \left( \frac{435,000 VFA}{VMA} \right)^{0.58}}$$

$|E^*|_{\max}$  = limiting maximum dynamic modulus, psi

VMA = voids in mineral aggregates, %

VFA = voids filled with asphalt, %

To determine a recommended dynamic modulus for CIR from AMPT (master curve) data, the average raw dynamic moduli, VMA and VFA of all ten sites were combined, the average value calculated, and then fitted using the Mastersolver. The average raw dynamic modulus data are presented in Table 16 presented below:

**Table 16. Average Raw Dynamic Moduli of Ten Sites**

Temperature °C	Frequency Hz	Modulus ksi
4	0.1	752.7
4	1.0	917.7
4	10.0	1,099.6
20	0.1	418.5
20	1.0	511.5
20	10.0	678.1
35	0.01	134.9
35	0.1	180.8
35	1.0	266.3
35	10.0	400.9

The average VMA and VFA are 13.3% and 26.6% respectively. After the execution of the Mastersolver, the final parameters and the fitting parameters are given below. The PMED input modulus is listed in Table 17.

- Max.  $E^*$  (ksi): 3,102.4
- Min.  $E^*$  (ksi): 0.5
- Beta,  $\beta$ : - 1.34372
- Gamma,  $\gamma$ : -0.19225
- $\Delta E_a$ : 241,692
- $R^2 = 0.989$
- $S_e/S_y = 0.07$

**Table 17. Fitted Dynamic Modulus of CIR Material**

No.	Temperature		Frequency (Hz)	Shift Factor	Reduced Frequency	E*	
	°C	°F				ksi	MPa
1	-10.0	14	25	4.90714	2,018,759	1,664.7	11,481.5
2	-10.0	14	10	4.90714	807,503	1,590.4	10,968.9
3	-10.0	14	5	4.90714	403,751	1,533.3	10,575.1
4	-10.0	14	1	4.90714	80,750	1,398.5	9,645.4
5	-10.0	14	0.5	4.90714	40,375	1,339.8	9,240.7
6	-10.0	14	0.1	4.90714	8,075	1,203.2	8,298.6
7	4.4	40	25	2.41207	6,456	1,184.3	8,168.0
8	4.4	40	10	2.41207	2,582	1,107.0	7,635.3
9	4.4	40	5	2.41207	1,291	1,049.2	7,236.1
10	4.4	40	1	2.41207	258	917.6	6,328.9
11	4.4	40	0.5	2.41207	129	862.6	5,949.5
12	4.4	40	0.1	2.41207	25	739.8	5,102.6
13	21.1	70	25	-0.16253	17.19515	710.1	4,897.2
14	21.1	70	10	-0.16253	6.87806	645.1	4,449.3
15	21.1	70	5	-0.16253	3.43903	598.0	4,124.7
16	21.1	70	1	-0.16253	0.68781	496.3	3,422.7
17	21.1	70	0.5	-0.16253	0.34390	455.8	3,143.9
18	21.1	70	0.1	-0.16253	0.06878	370.2	2,553.5
19	37.8	100	25	-2.46117	0.08645	381.7	2,632.5
20	37.8	100	10	-2.46117	0.03458	337.2	2,325.9
21	37.8	100	5	-2.46117	0.01729	306.1	2,111.3
22	37.8	100	1	-2.46117	0.00346	242.1	1,669.5
23	37.8	100	0.5	-2.46117	0.00173	217.9	1,502.7
24	37.8	100	0.1	-2.46117	0.00035	169.1	1,166.3
25	54.4	130	25	-4.52595	0.00074	191.1	1,318.0
26	54.4	130	10	-4.52595	0.00030	165.1	1,138.6
27	54.4	130	5	-4.52595	0.00015	147.4	1,016.7
28	54.4	130	1	-4.52595	0.00003	112.5	776.1
29	54.4	130	0.5	-4.52595	0.00001	99.9	689.0
30	54.4	130	0.1	-4.52595	0.00000	75.4	519.9

The dynamic moduli for all fitted data for all 10 sites have been plotted in Figure 98. The figure also has two conventional [SX(100) PG 64-22 and SX(75) PG 64-22] mixtures’ dynamic moduli for the comparison. Figure 98 shows that at lower reduced frequency (or higher temperature zone), the dynamic moduli of CIR materials are higher than that of the control mixture. At higher reduced frequency (or lower temperature), the dynamic moduli of CIR materials are smaller (roughly 50%) than that of the control mixture. This means CIR is more susceptible to rutting but less susceptible to cracking compared to conventional mixtures. The fitted dynamic moduli (named as ‘Fit’ in Figure 98), lies almost in the middle of the all dynamic moduli range. The fitted dynamic modulus

data can be used by CDOT for future CIR overlay design. As full details of CIR of individual sites are not available, different dynamic moduli values for different CIR mixes cannot be recommended.

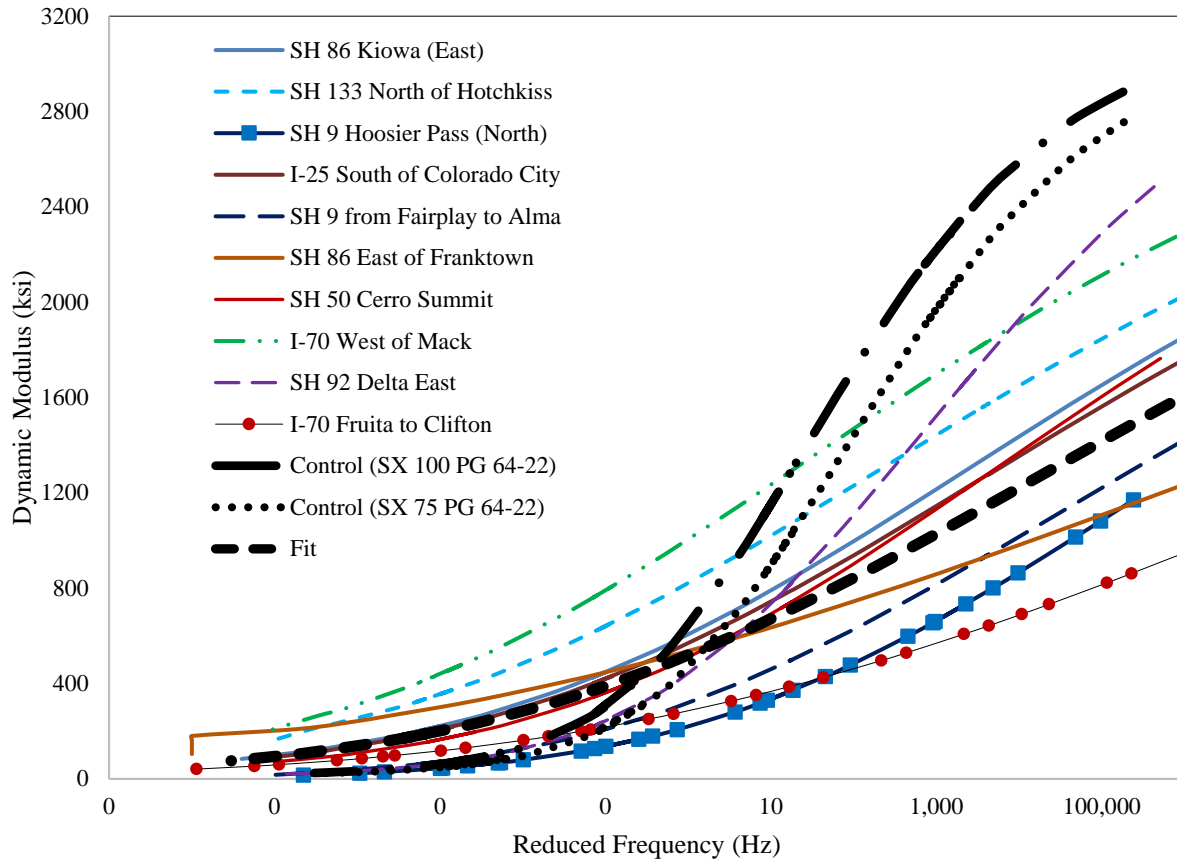


**Figure 98. Dynamic Moduli of all Mixes Including Conventional Mixtures**

## Properties of Base/Subgrade

### *Classification, R-Value and Proctor Results*

The measured properties (classification, R-Value, Proctor results) of base and subgrade of the sites are listed in Table 18. However, some sites, such as SH 9 Hoosier Pass, base and subgrade could not be differentiated and were considered as subgrade.

**Table 18. Test Results Summary for Base/Subgrade**

Site	Type		R-value at 300 psi		OMC (%)		Max. Dry Density (pcf)	
	Subgrade	Base	Subgrade	Base	Sub-grade	Base	Subgrade	Base
SH 9 from Fairplay to Alma	A-2-4	A-2-4	44	-	8.5	-	130	-
SH 9 Hoosier Pass (Northbound)	A-1-b	-	61	-	7.2	-	134	-
SH 86 East of Franktown	A-1-b	-	68	-	8.6	-	128	-
SH 86 Kiowa (Eastbound)	A-2-6	A-2-4	19	66	14	11.4	113	119
I-25 South of Colorado City	A-2-4	-	38	-	7.2	-	132	-
SH 50 Cerro Summit	A-6	-	20	-	15	-	117	-
I-70 West of Mack	A-7-6	-	13	-	21.9	-	101	-
I-70 Fruita to Clifton	A-1-a	-	74	-	6.5	-	138	-
SH 92 Delta	A-1-a	A-1-a	74	79	5.4	5.2	142	142
SH 133 North of Hotchkiss	A-4	A-2-4	28	65	10.3	7.1	123	140

*Resilient Modulus of Base/Subgrade*

**Site #1 SH 9 From Fairplay to Alma.** The base and subgrade materials were blended to determine the resilient modulus which is presented in Table 19 and Figure 99. The resilient modulus increases with cell pressure because as the cell pressure increases, the confinement increases which resists deformation. Consequently, the resilient modulus increases. Thus, the resilient modulus decreases with an increase in deviator stress. A decreasing resilient modulus occurs when a soil has a clayey component and shear deformation occurs upon applying a load.

**Table 19. Resilient Modulus of SH 9 from Fairplay to Alma Subgrade**

Test Sequence	Confining Pressure (psi)	Deviatoric Stress (psi)	Resilient Modulus (ksi)
Conditioning:	6	4	-
1	6	2	37,593
2	6	4	28,092
3	6	6	23,842
4	6	8	21,355
5	6	10	20,358
6	4	2	28,321
7	4	4	19,848
8	4	6	17,893
9	4	8	17,385
10	4	10	17,171
11	2	2	19,755
12	2	4	14,453
13	2	6	13,954
14	2	8	14,356
15	2	10	14,646

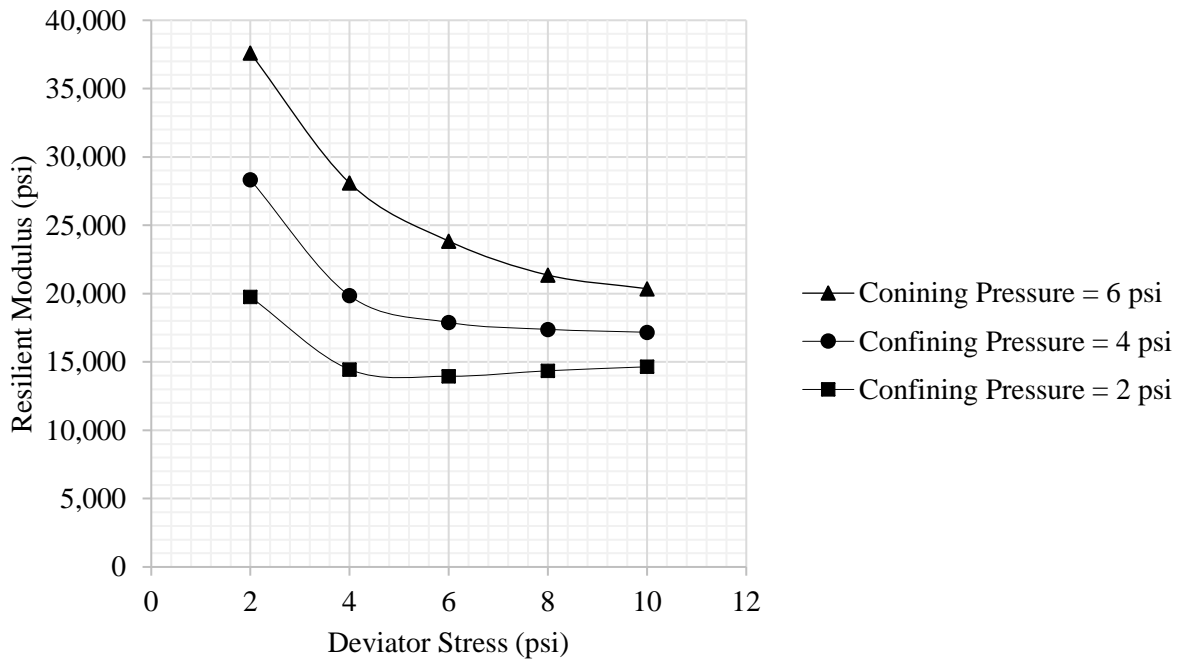


**Figure 99. Resilient Modulus of the Blended Base and Subgrade at SH 9 from Fairplay to Alma Subgrade**

**Site #2 SH 9 Hoosier Pass.** For this site, only subgrade material was found, and the resilient modulus is presented in Table 20 and Figure 100.

**Table 20. Resilient Modulus of SH 9 Hoosier Pass Subgrade**

Test Sequence	Confining Pressure (psi)	Deviatoric Stress (psi)	Resilient Modulus (ksi)
Conditioning:	15	15	-
1	3	3	16,422
2	3	6	15,296
3	3	9	16,204
4	5	5	20,291
5	5	10	21,292
6	5	15	22,302
7	10	10	32,430
8	10	20	32,808
9	10	30	30,591
10	15	10	37,979
11	15	15	37,024
12	15	30	35,775
13	20	15	41,658
14	20	20	41,799
15	20	40	40,610

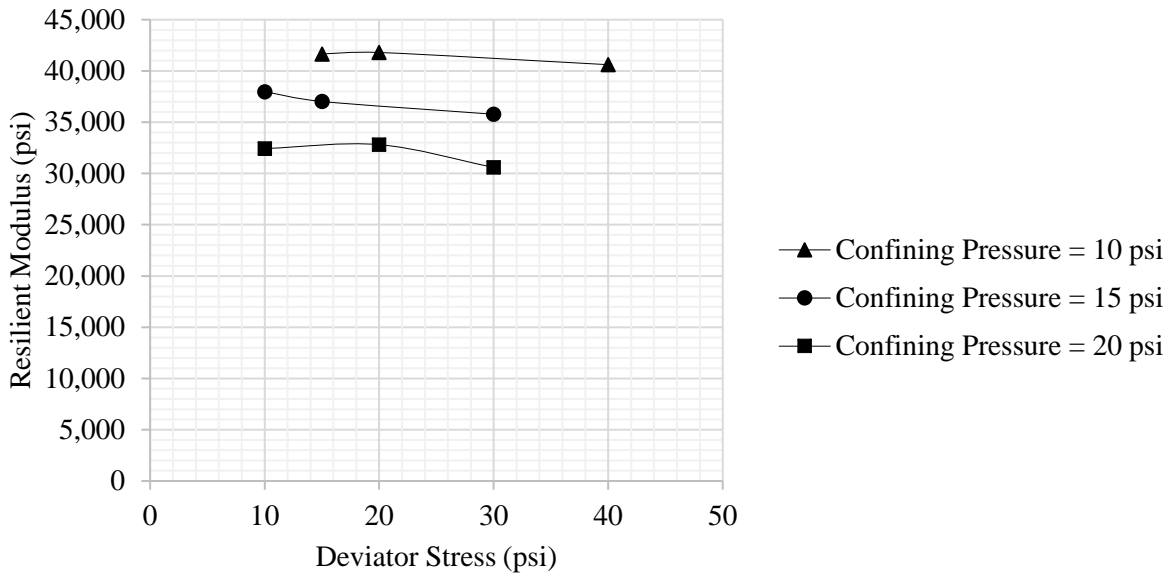


**Figure 100. Resilient Modulus of the Subgrade at SH 9 Hoosier Pass.**

**Site #3 SH 86 East of Franktown.** The resilient modulus of the subgrade of this site is presented in Table 21 and Figure 101.

**Table 21. Resilient Modulus of SH 86 Franktown Subgrade**

Test Sequence	Confining Pressure (psi)	Deviatoric Stress (psi)	Resilient Modulus (ksi)
Conditioning:	15	15	-
1	3	3	23,022
2	3	6	20,525
3	3	9	20,932
4	5	5	23,971
5	5	10	24,191
6	5	15	24,356
7	10	10	31,509
8	10	20	32,533
9	10	30	33,001
10	15	10	37,858
11	15	15	37,834
12	15	30	38,650
13	20	15	43,575
14	20	20	44,391
15	20	40	43,782

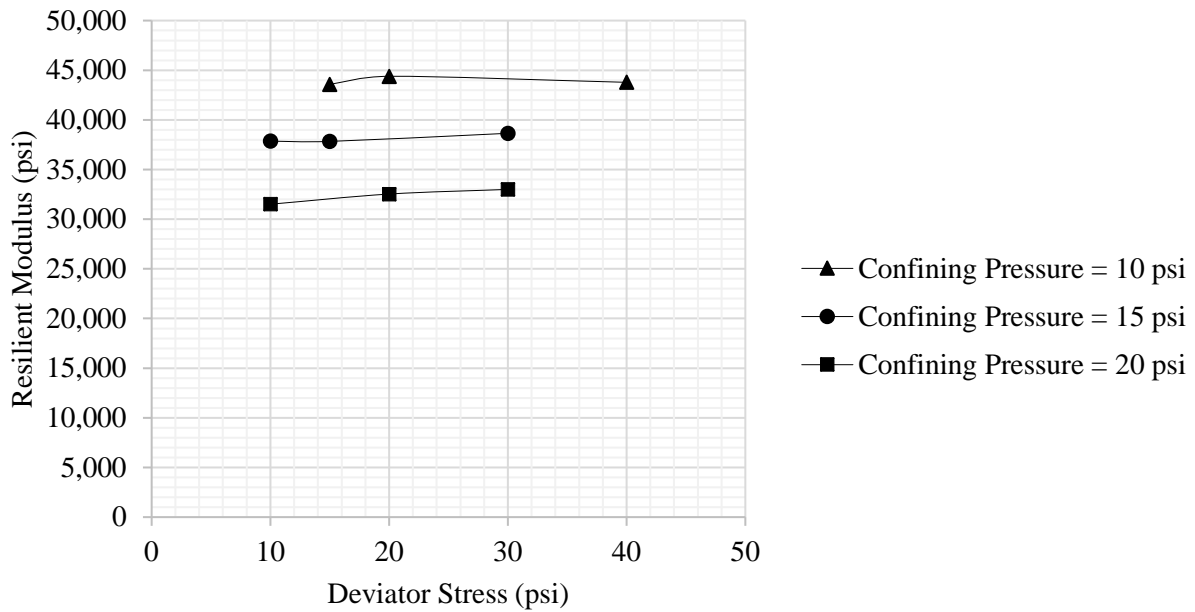


**Figure 101. Resilient Modulus of the Subgrade at SH 86 Franktown.**

**Site #4 SH 86 Kiowa (Eastbound).** The resilient modulus of the subgrade of this site is presented in Table 22 and Figure 102.

**Table 22. Resilient Modulus of SH 86 Kiowa (Eastbound) Subgrade**

Test Sequence	Confining Pressure (psi)	Deviatoric Stress (psi)	Resilient Modulus (ksi)
Conditioning:	6	4	-
1	6	2	21,325
2	6	4	13,893
3	6	6	10,562
4	6	8	8,766
5	6	10	7,991
6	4	2	19,621
7	4	4	12,240
8	4	6	9,977
9	4	8	8,829
10	4	10	7,989
11	2	2	17,581
12	2	4	10,849
13	2	6	8,718
14	2	8	7,808
15	2	10	7,037

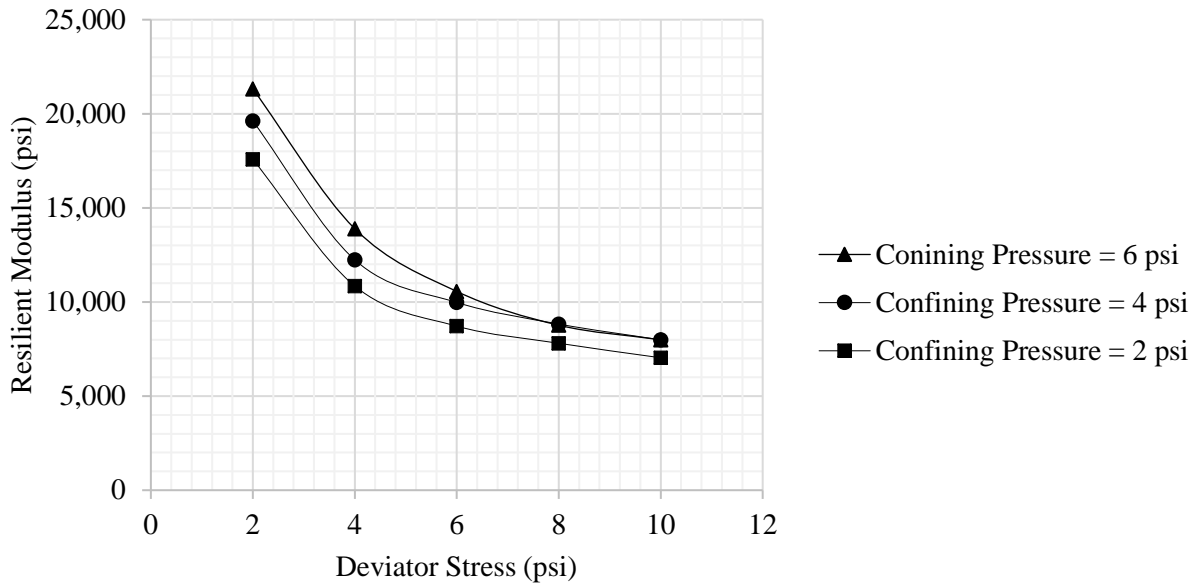


**Figure 102. Resilient Modulus of the Subgrade at SH 86 Kiowa (Eastbound).**

**Site #5 I-25 South of Colorado City.** The resilient modulus of the subgrade of this site is presented in Table 23 and Figure 103.

**Table 23. Resilient Modulus of I-25 South of Colorado City Subgrade**

Test Sequence	Confining Pressure (psi)	Deviatoric Stress (psi)	Resilient Modulus (ksi)
Conditioning:	6	4	-
1	6	2	57,090
2	6	4	48,379
3	6	6	42,875
4	6	8	40,532
5	6	10	38,734
6	4	2	43,125
7	4	4	34,604
8	4	6	32,113
9	4	8	31,422
10	4	10	31,385
11	2	2	23,172
12	2	4	20,491
13	2	6	20,784
14	2	8	21,816
15	2	10	23,140

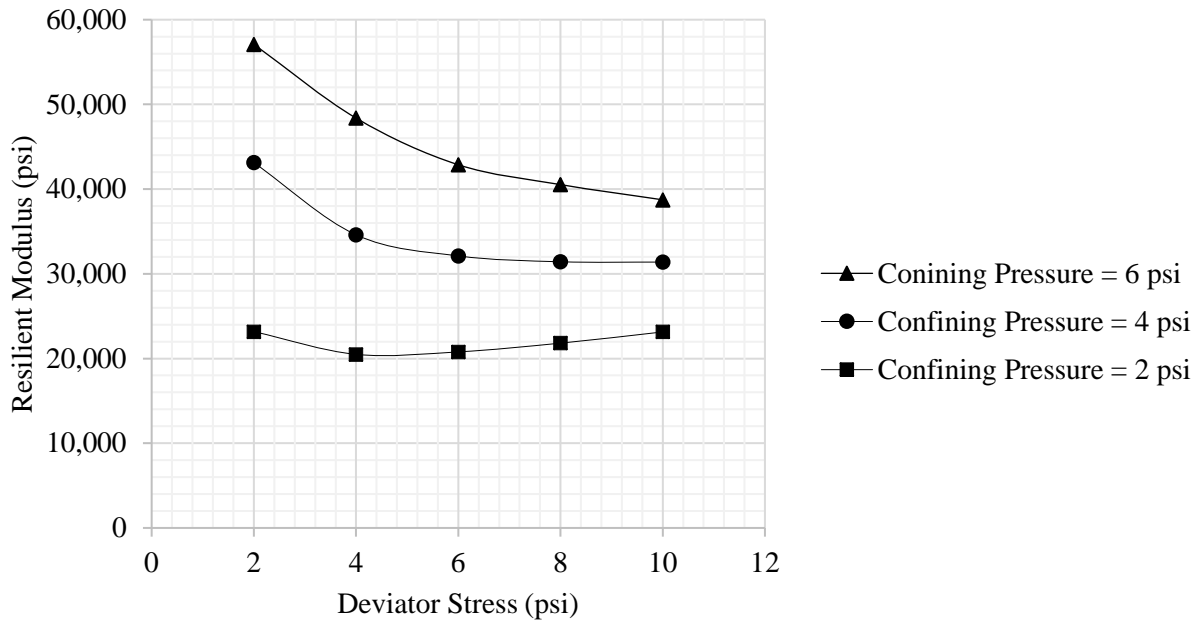


**Figure 103. Resilient Modulus of the Subgrade at I-25 South of Colorado City.**

**Site #6 SH 50 Cerro Summit.** The resilient modulus of the subgrade of this site is presented in Table 24 and Figure 104.

**Table 24. Resilient Modulus of SH 50 Cerro Summit Subgrade**

Test Sequence	Confining Pressure (psi)	Deviatoric Stress (psi)	Resilient Modulus (ksi)
Conditioning:	6	4	-
1	6	2	33,037
2	6	4	25,651
3	6	6	21,874
4	6	8	19,692
5	6	10	17,960
6	4	2	28,100
7	4	4	21,998
8	4	6	19,841
9	4	8	18,353
10	4	10	17,151
11	2	2	25,156
12	2	4	19,207
13	2	6	17,359
14	2	8	16,355
15	2	10	15,515

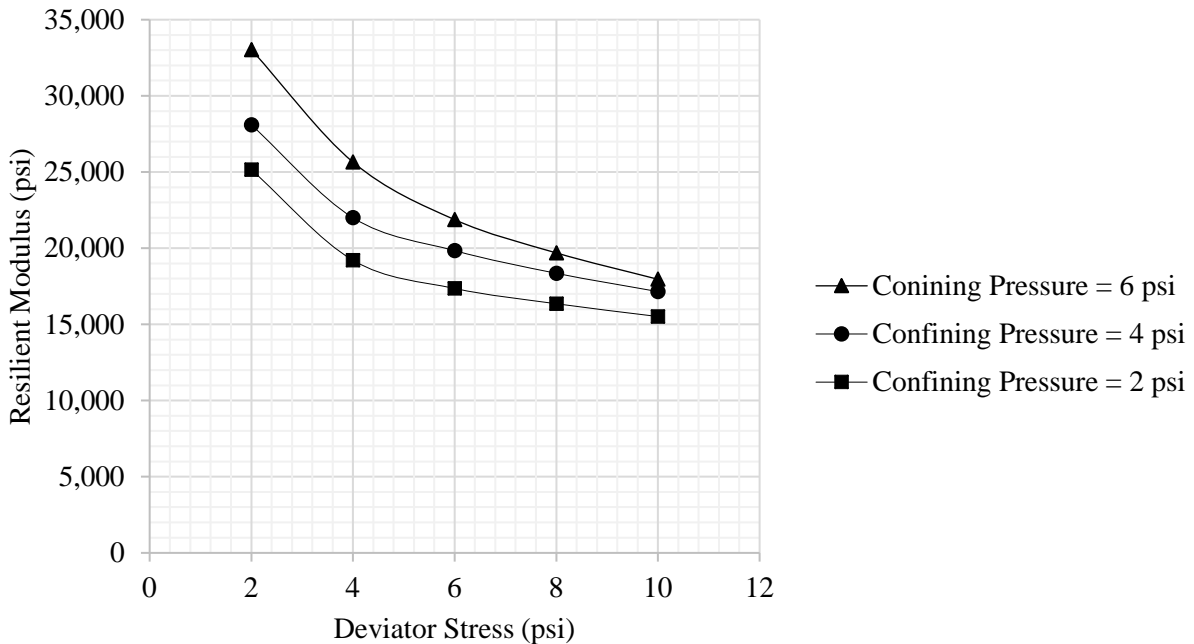


**Figure 104. Resilient Modulus of the Subgrade.**

**Site #7 I-70 West of Mack.** The resilient modulus of the subgrade of this site is presented in Table 25 and Figure 105.

**Table 25. Resilient Modulus of I-70 West of Mack Subgrade**

Test Sequence	Confining Pressure (psi)	Deviatoric Stress (psi)	Resilient Modulus (ksi)
Conditioning:	6	4	-
1	6	2	30,056
2	6	4	24,364
3	6	6	21,257
4	6	8	19,502
5	6	10	18,354
6	4	2	27,258
7	4	4	20,624
8	4	6	18,847
9	4	8	17,952
10	4	10	17,203
11	2	2	22,600
12	2	4	17,906
13	2	6	16,118
14	2	8	15,374
15	2	10	15,046

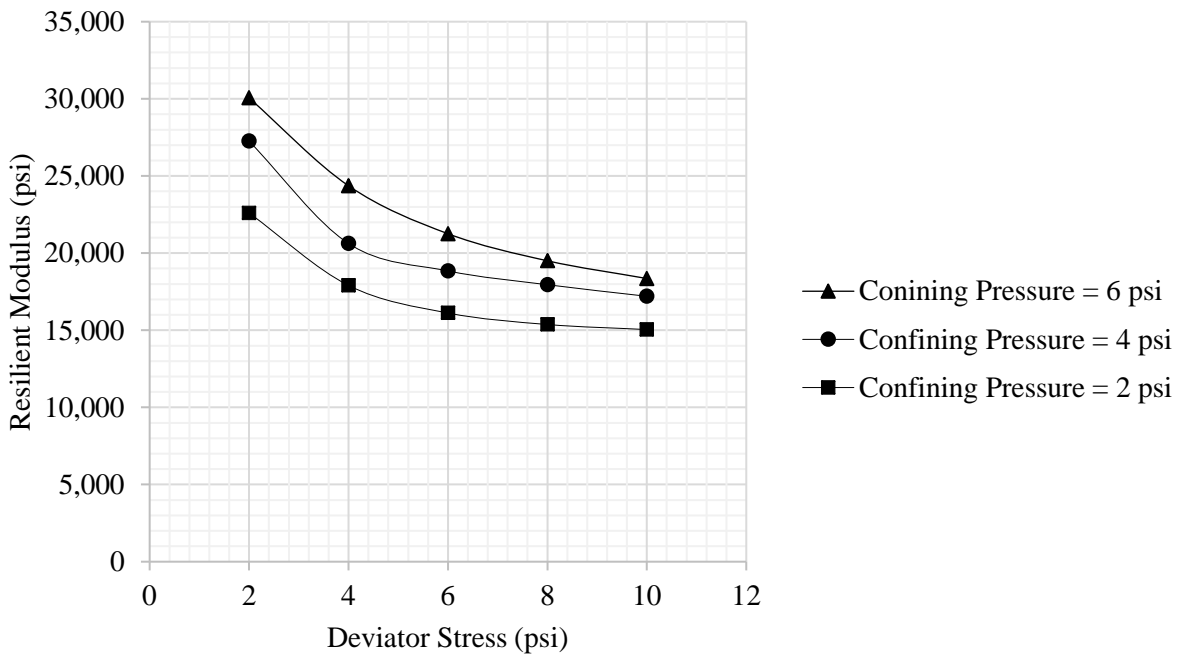


**Figure 105. Resilient Modulus of the Subgrade at I-70 West of Mack.**

**Site #8 I-70 Fruita to Clifton.** The resilient modulus of the subgrade of this site is presented in Table 26 and Figure 106.

**Table 26. Resilient Modulus of I-70 Fruita to Clifton Subgrade**

Test Sequence	Confining Pressure (psi)	Deviatoric Stress (psi)	Resilient Modulus (ksi)
Conditioning:	15	15	-
1	3	3	37,028
2	3	6	30,948
3	3	9	29,871
4	5	5	36,912
5	5	10	33,696
6	5	15	36,322
7	10	10	43,570
8	10	20	45,589
9	10	30	48,632
10	15	10	51,352
11	15	15	52,522
12	15	30	57,828
13	20	15	61,097
14	20	20	63,924
15	20	40	68,029

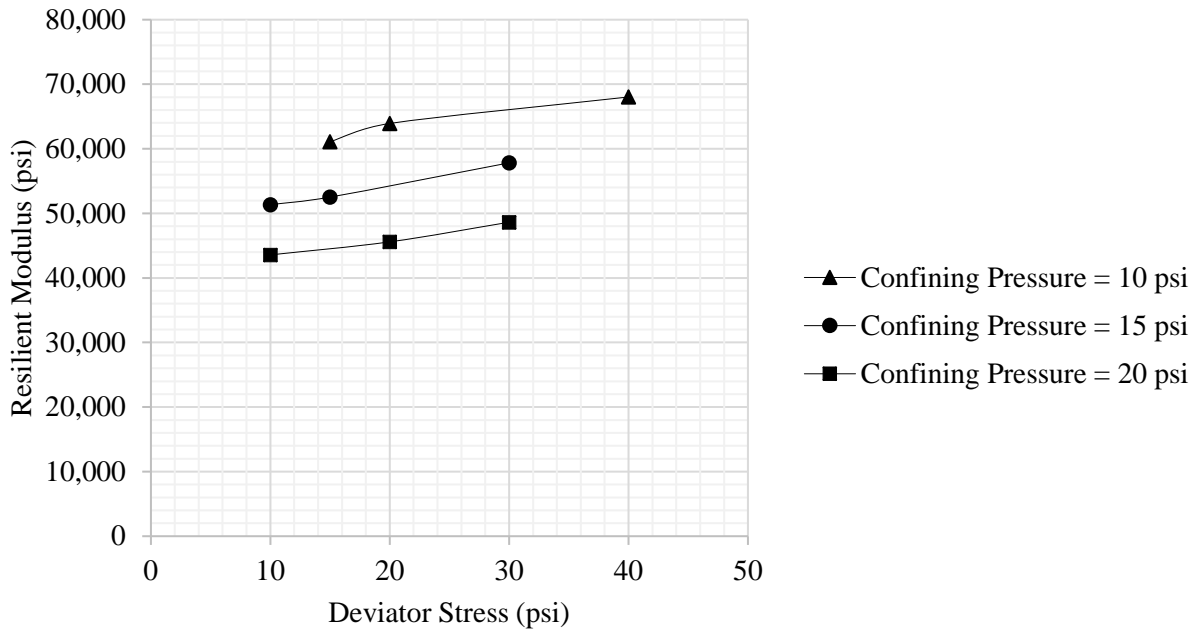


**Figure 106. Resilient Modulus of the Subgrade at I-70 Fruita to Clifton.**

**Site #9 SH 92 Delta East.** For this site, the base and subgrade materials could be separated, and the resilient moduli were determined separately. The resilient modulus of the subgrade of this site is presented in Table 27 and Figure 107.

**Table 27. Resilient Modulus of SH 92 Delta (Eastbound) Subgrade**

Test Sequence	Confining Pressure (psi)	Deviatoric Stress (psi)	Resilient Modulus (ksi)
Conditioning:	15	15	-
1	3	3	16,222
2	3	6	16,868
3	3	9	18,764
4	5	5	19,745
5	5	10	22,374
6	5	15	22,686
7	10	10	30,107
8	10	20	30,785
9	10	30	28,415
10	15	10	34,569
11	15	15	34,180
12	15	30	34,893
13	20	15	40,880
14	20	20	41,724
15	20	40	43,445

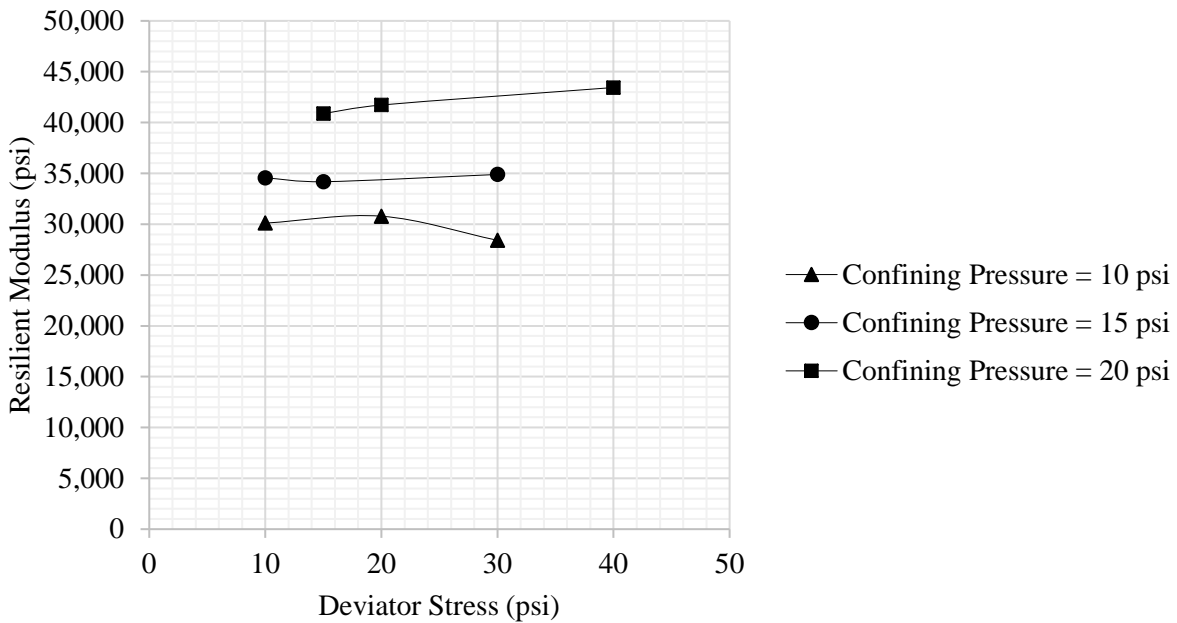


**Figure 107. Resilient Modulus of the Subgrade at SH 92 Delta (Eastbound)**

The resilient modulus of the base of this site is presented in Table 28 and Figure 108.

**Table 28. Resilient Modulus of SH 92 Delta (Eastbound) Base**

Test Sequence	Confining Pressure (psi)	Deviatoric Stress (psi)	Resilient Modulus (ksi)
Conditioning:	15	15	-
1	3	3	26,194
2	3	6	23,718
3	3	9	24,135
4	5	5	28,483
5	5	10	27,659
6	5	15	29,939
7	10	10	36,872
8	10	20	40,097
9	10	30	43,377
10	15	10	46,567
11	15	15	46,944
12	15	30	51,038
13	20	15	54,949
14	20	20	55,552
15	20	40	60,464

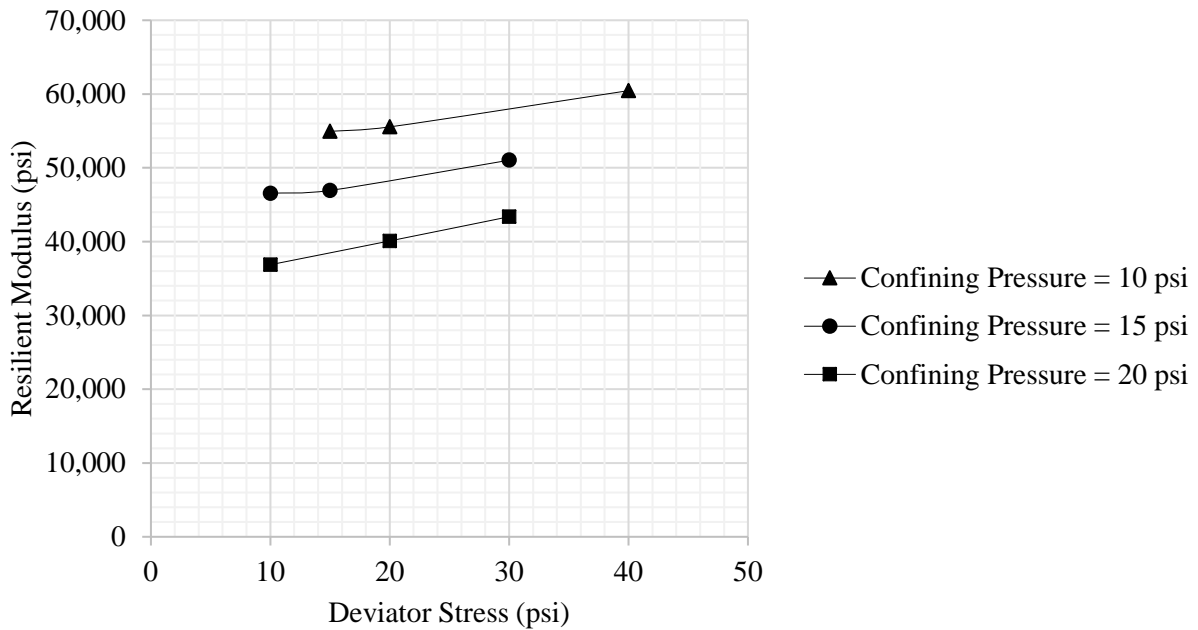


**Figure 108. Resilient Modulus of the Base at SH 92 Delta (Eastbound)**

**Site #10 SH 133 Hotchkiss.** For this site, the base and subgrade materials could be separated, and the resilient moduli were determined separately. The resilient modulus of subgrade is presented in Table 29 and Figure 109.

**Table 29. Resilient Modulus of SH 133 Hotchkiss Subgrade**

Test Sequence	Confining Pressure (psi)	Deviatoric Stress (psi)	Resilient Modulus (ksi)
Conditioning:	6	4	-
1	6	2	64,007
2	6	4	49,013
3	6	6	45,117
4	6	8	42,777
5	6	10	41,854
6	4	2	47,436
7	4	4	37,204
8	4	6	35,021
9	4	8	35,464
10	4	10	36,835
11	2	2	36,894
12	2	4	27,587
13	2	6	27,559
14	2	8	28,621
15	2	10	30,494

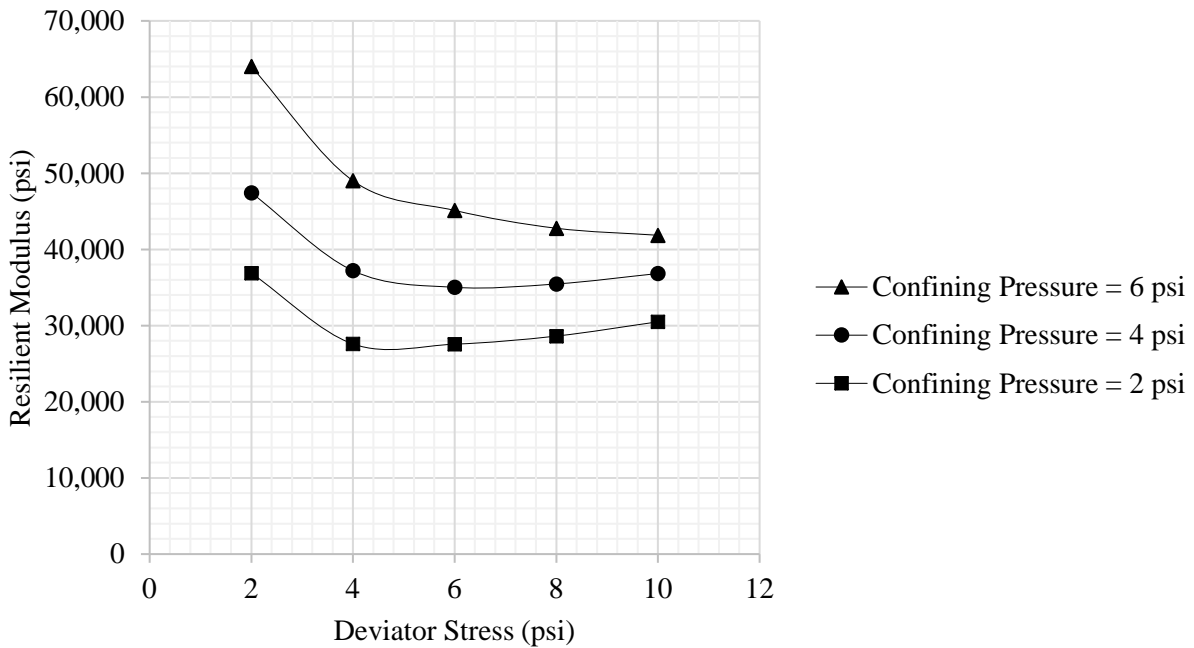


**Figure 109. Resilient Modulus of the Subgrade at SH 133 Hotchkiss.**

The resilient modulus of the base of this site is presented in Table 30 and Figure 110.

**Table 30. Resilient Modulus of SH 133 Hotchkiss Base**

Test Sequence	Confining Pressure (psi)	Deviatoric Stress (psi)	Resilient Modulus (ksi)
Conditioning:	15	15	-
1	3	3	52,617
2	3	6	44,534
3	3	9	41,191
4	5	5	50,758
5	5	10	45,659
6	5	15	44,254
7	10	10	56,617
8	10	20	52,456
9	10	30	49,703
10	15	10	62,751
11	15	15	59,635
12	15	30	58,471
13	20	15	67,769
14	20	20	66,236
15	20	40	63,990

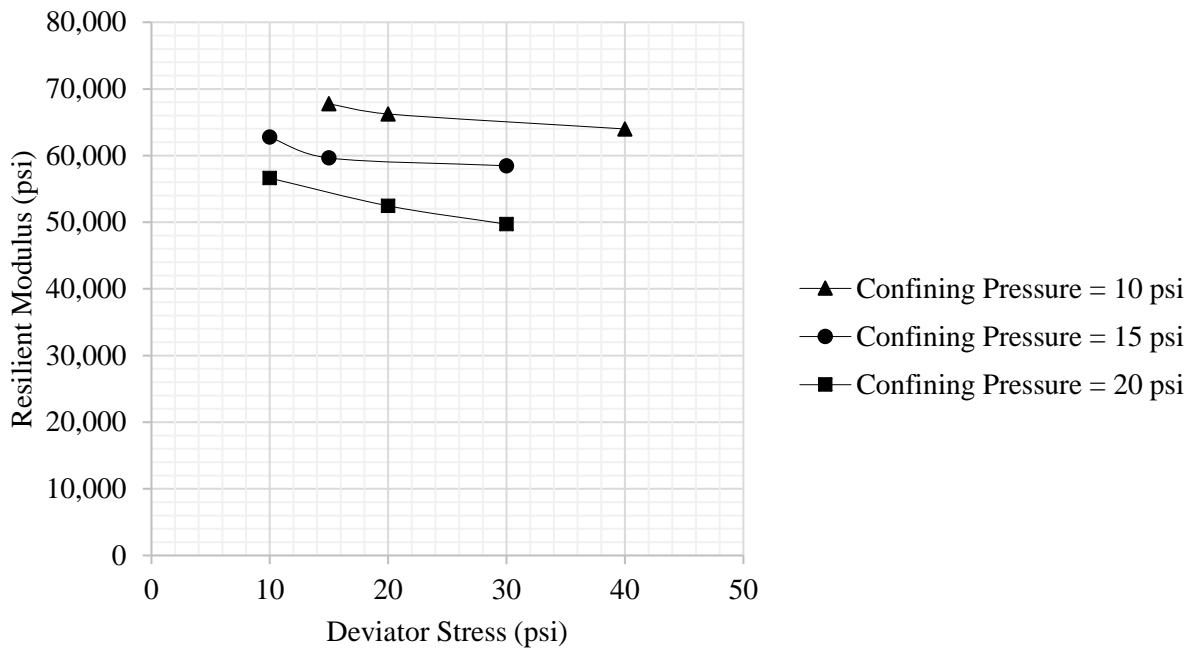


**Figure 110. Resilient Modulus of the Base at SH 133 Hotchkiss.**

## SECTION 7: PMED SOFTWARE ANALYSIS

### General

Pavement Mechanistic-Empirical Design (PMED) software in conjunction with laboratory data from the test sites for the following analysis was conducted. The purpose of the analysis was to determine how the CDOT-calibrated PMED outputs compare to the measured distress data. It is important to mention that the current PMED software considers CIR layer an unbound layer and the inputs of the CIR layers are similar to an aggregate base layer. However, while field coring it was found that CIR is a bound asphalt layer. Therefore, the PMED analysis was conducted using CIR as a bound material/layer. The CDOT-calibrated overlay design template (AC over AC, 2018 version) was used for analysis. The input data were taken from the laboratory test results, the CDOT 2017 Pavement Design Manual (13), and the mix design datasheet. For some sites (Sites #1, #2, #3 and #8), limited input data was available and PMED analysis using the CIR layers were not possible. Due to the limited data, a different analysis was conducted using the CIR layer as HMA SX (75) PG 58-28 material. This also allowed us to examine whether CIR material behaves similar to the HMA SX (75) PG 58-28 material or not.

### PMED Analysis

The most recent version of the PMED software (version 2.2.6) was used in this analysis. All analysis used a 90% reliability. Three predicted distresses (IRI, total rutting, and fatigue cracking) were compared with the measured distresses. The following terminology is used in the figures in the this section to show the results.

- Measured – Test Site: The measured distress data at the 1,000-ft segment of the test site.
- Measured – Whole Project: The measured distress data from the whole CIR project.
- PMED – 90% Reliability: The PMED output at 90% reliability using the CIR input.
- PMED – Mean: The PMED mean output using CIR material.
- PMED – HMA (PG 58 – 28) – 90% Reliability: The PMED output at 90% reliability using

CIR as HMA SX 75 PG 58-28 material.

- PMED – HMA (PG 58 – 28) – Mean: The PMED mean output using the CIR as HMA SX (75) PG 58-28 material.

*Site #1 SH 9 from Fairplay to Alma*

The PMED analysis using the CIR material was not possible for this site. Figure 111 shows the PMED-90% Reliability using the HMA SX (75) PG 58-28 are slightly higher than the measured IRI values. The PMED-Mean IRI values using the HMA SX (75) PG 58-28 are closer to the measured IRI values especially after 4 years versus the PMED-90% Reliability.

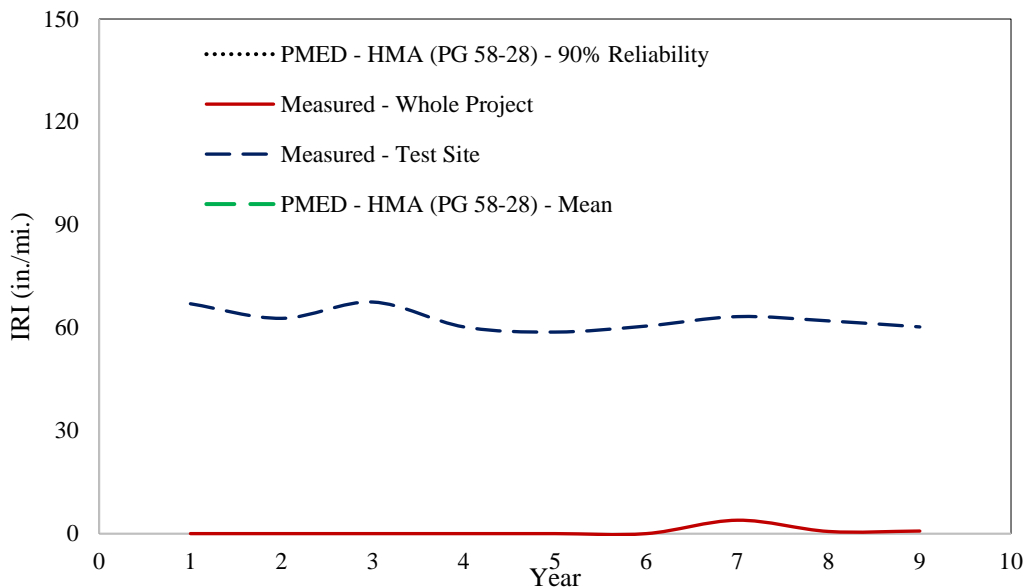


**Figure 111. IRI at SH 9 from Fairplay to Alma Showing Amount of Measured and PMED Predicted IRI**

The measured total rutting values are in good agreement with the PMED-predicted mean rutting values using the HMA SX(75) PG 58-28 compared to the PMED-predicted IRI at 90% reliability, Figure 112. The PMED-predicted rutting values at 90% reliability using the HMA SX (75) PG 58-28 are higher than the measured rutting values.

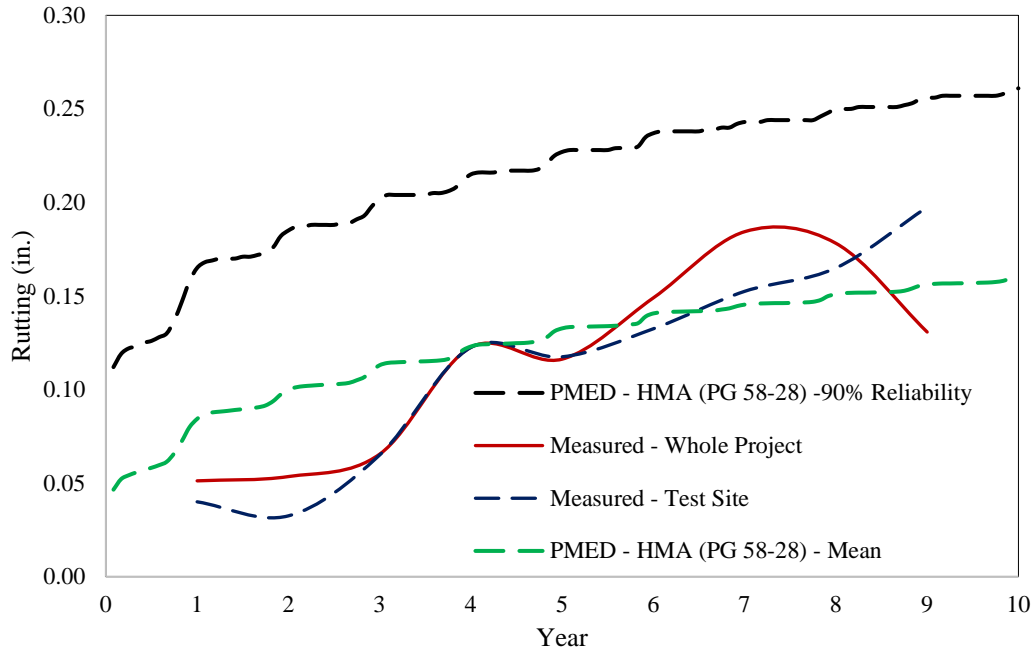


**Figure 112. Total Rutting at SH 9 from Fairplay to Alma Showing Amount of Measured and PMED Predicted Rutting**

The measured fatigue cracking values on the whole project of SH 9 From Fairplay to Alma site are much higher than the PMED-predicted fatigue cracking values using the HMA SX (75) PG 58-28, Figure 113. The PMED-predicted fatigue cracking values by HMA SX (75) PG 58-28 mix at mean level is very small (close to zero), while at 90% reliability, it produces about 9.5 square feet per tenth-mile, which is due to the reliability.

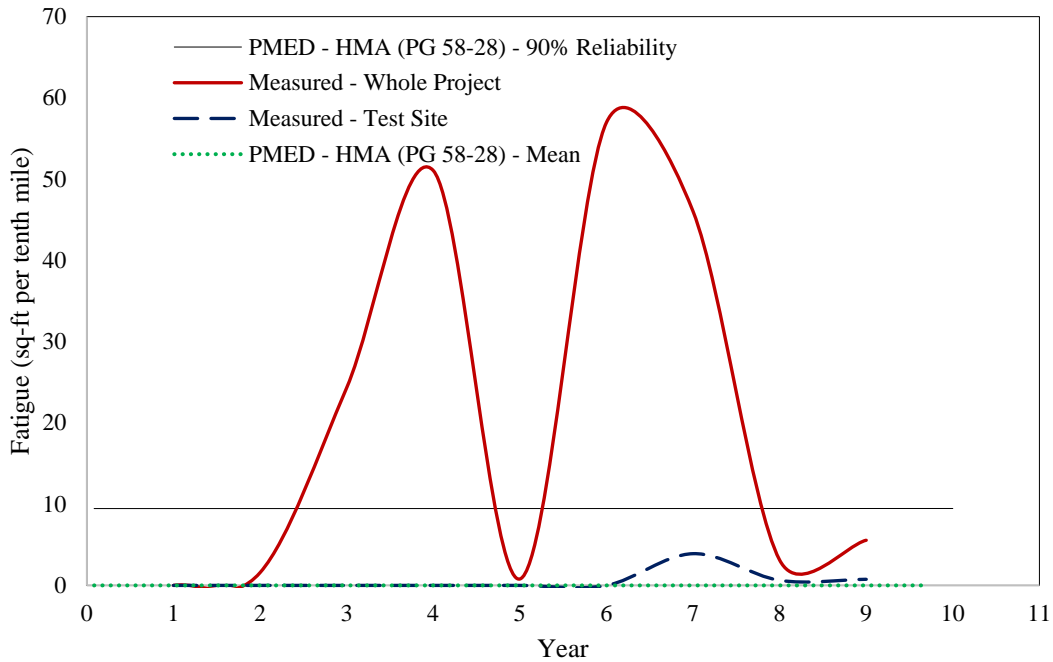


**Figure 113. Fatigue Cracking at SH 9 from Fairplay to Alma Showing Amount of Measured and PMED Predicted Cracking**

*Site #2 SH 9 Hoosier Pass (Northbound)*

The measured and the PMED-predicted IRI of Hoosier Pass (Northbound) are presented in Figure 114 below. It shows the PMED-predicted IRI values at 90% reliability and the PMED-predicted mean IRI values using the HMA SX (75) PG 58-28 are lower than the measured IRI values. However, both the predicted and the measured IRI values tend to converge with time especially after 7 years.

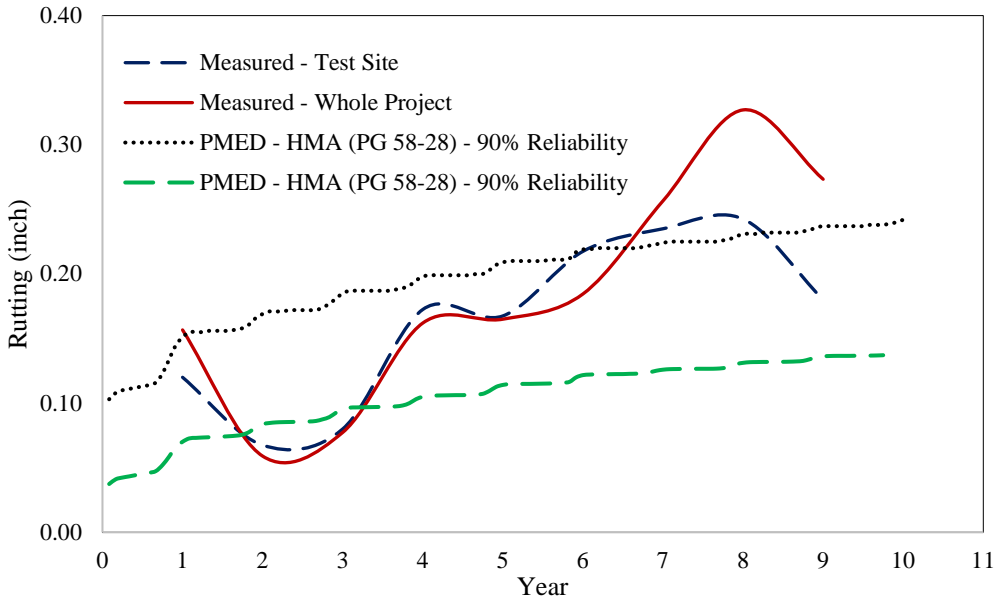


**Figure 114. IRI at Hoosier Pass (Northbound) Showing Amount of Measured and PMED Predicted IRI**

The measured and the PMED-predicted total rutting of Hoosier Pass (Northbound) are presented in Figure 115 below. The measured total rutting values are in good agreement with the PMED-predicted rutting values at 90% reliability using the HMA SX (75) PG 58-28 compared to the PMED-predicted mean rutting value. The PMED-predicted mean rutting values using the HMA SX (75) PG 58-28 are lower than the measured rutting values.

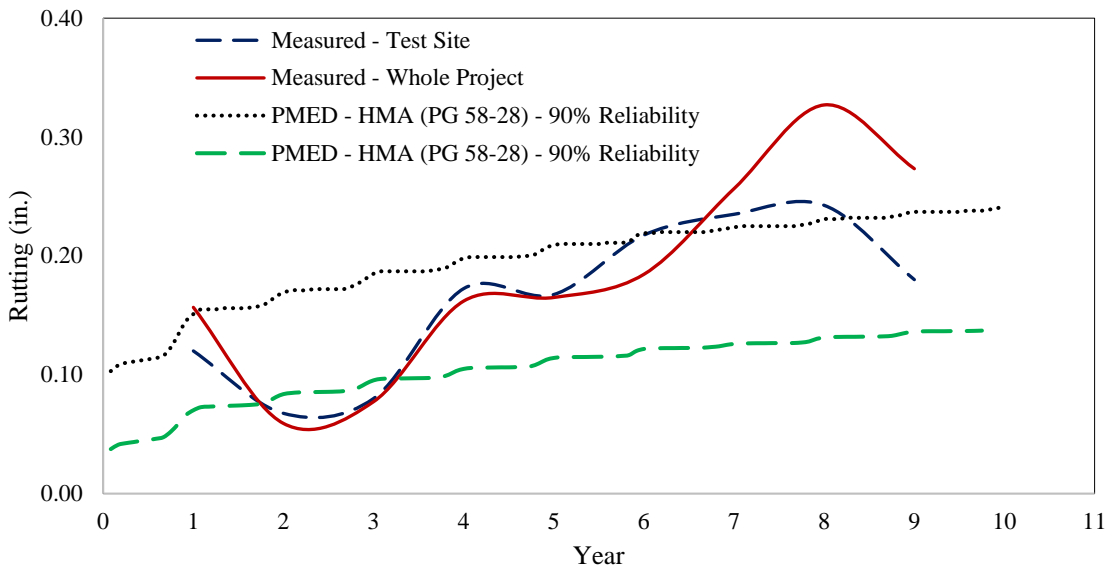


**Figure 115. Total Rutting at Hoosier Pass (Northbound) Showing Amount of Measured and PMED Predicted Rutting**

The measured fatigue cracking values on the whole project of SH 9 Hoosier Pass (Northbound) site are much higher than the PMED-predicted fatigue cracking values using the HMA SX (75) PG 58-28, Figure 116. The PMED-predicted fatigue cracking values by HMA SX (75) PG 58-28 mix at mean level is very small (close to zero), while at 90% reliability, it produces about 9.5 square feet per tenth-mile, which is due to the reliability.

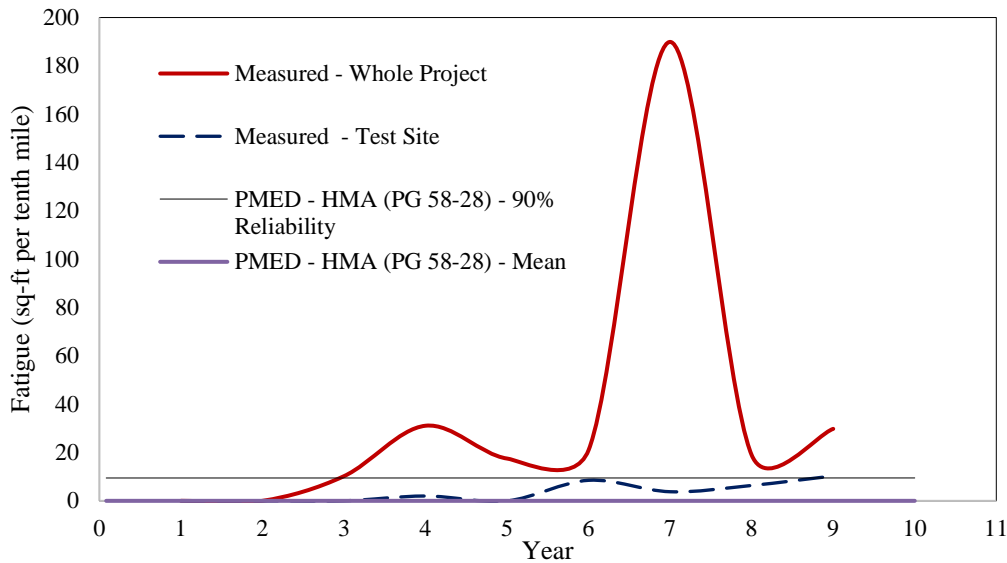


**Figure 116. Fatigue Cracking at Hoosier Pass (Northbound) Showing Amount of Measured and PMED Predicted Cracking**

*Site #3 SH 86 East of Franktown*

The measured and the PMED-predicted IRI of SH 86 East of Franktown are presented in Figure 117 below. It shows the PMED-predicted IRI values both at mean level and at 90% reliability using the HMA SX (75) PG 58-28 are in good agreement with the measured IRI values.

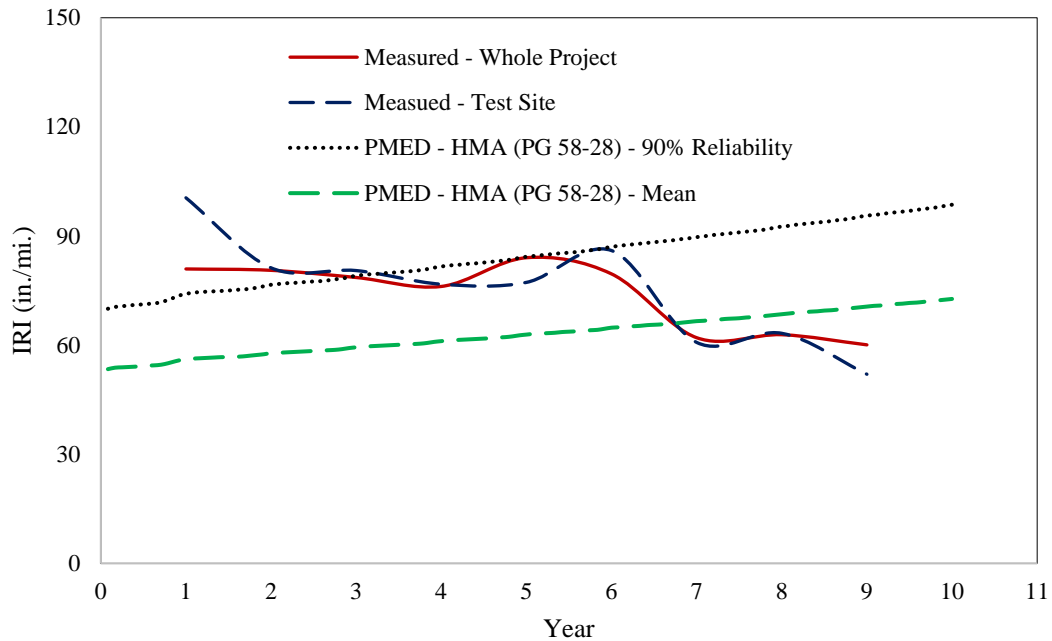


**Figure 117. IRI at SH 86 East of Franktown Showing Amount of Measured and PMED Predicted IRI**

The measured and the PMED-predicted total rutting of SH 86 East of Franktown are presented in Figure 118 below. The measured total rutting values are in good agreement with the PMED-predicted mean rutting values using the HMA SX (75) PG 58-28. The PMED-predicted rutting values at 90% reliability using the HMA SX (75) PG 58-28 are much higher than the measured rutting values.

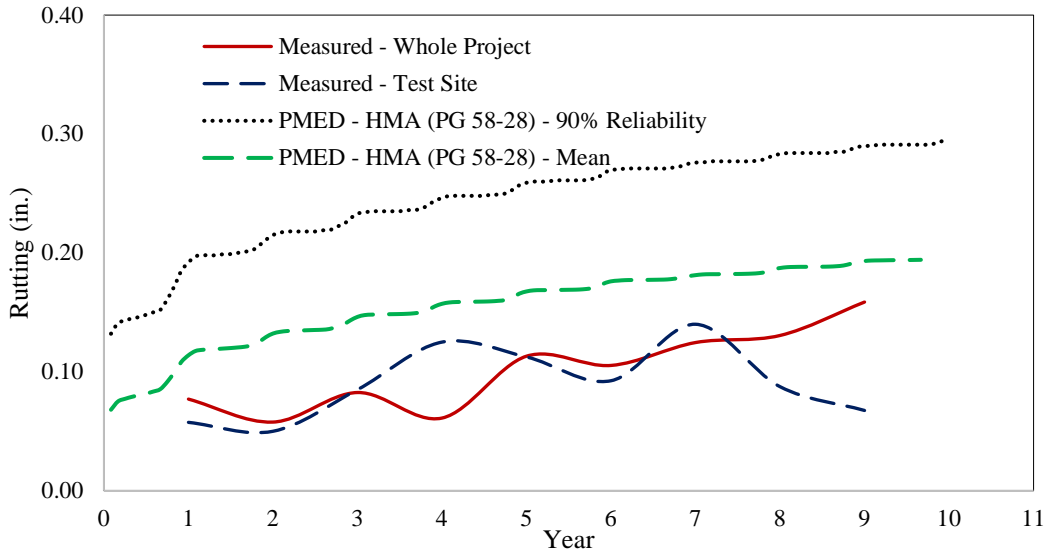


**Figure 118. Total Rutting at SH 86 East of Franktown Showing Amount of Measured and PMED Predicted Rutting**

The measured fatigue cracking values on the whole project of SH 86 East of Franktown site are much higher than the PMED-predicted fatigue cracking values using the HMA SX (75) PG 58-28, Figure 119. The PMED-predicted fatigue cracking values by HMA SX (75) PG 58-28 mix at mean level is very small (close to zero), while at 90% reliability, it produces about 9.5 square feet per tenth-mile, which is due to the reliability.

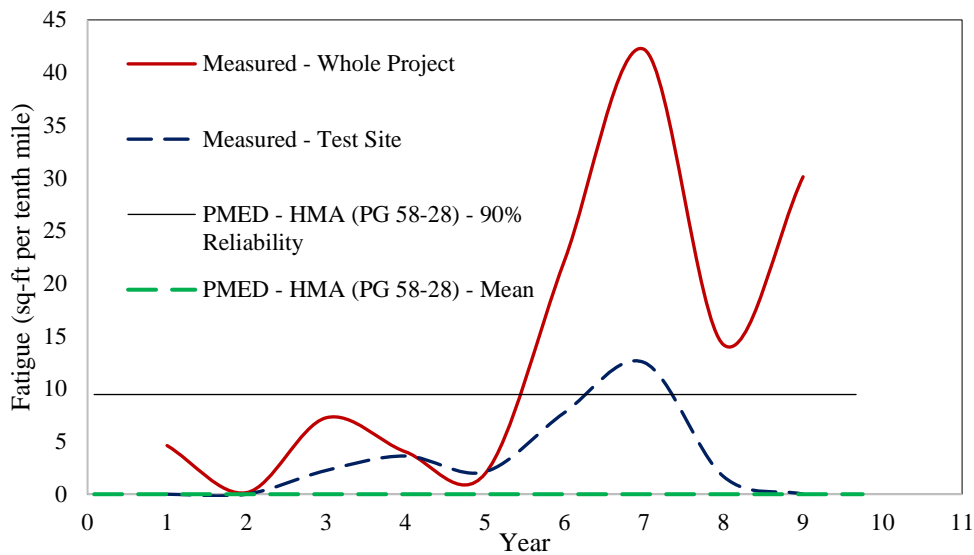


**Figure 119. Fatigue Cracking at SH 86 East of Franktown Showing Amount of Measured and PMED Predicted Cracking**

Site #4 SH 86 Kiowa (Eastbound)

The measured and the PMED-predicted IRI of SH 86 Kiowa (Eastbound) are presented in Figure 120 below. The first observation from this figure is that the PMED-outputs using the CIR and the HMA SX (75) PG 58-28 are almost the same. It also shows the PMED-predicted IRI values using both the CIR and the HMA SX (75) PG 58-28 at 90% reliability are in good agreement with the measured IRI values. The PMED-predicted mean IRI values using both the CIR and the HMA SX (75) PG 58-28 are lower than the measured IRI values.

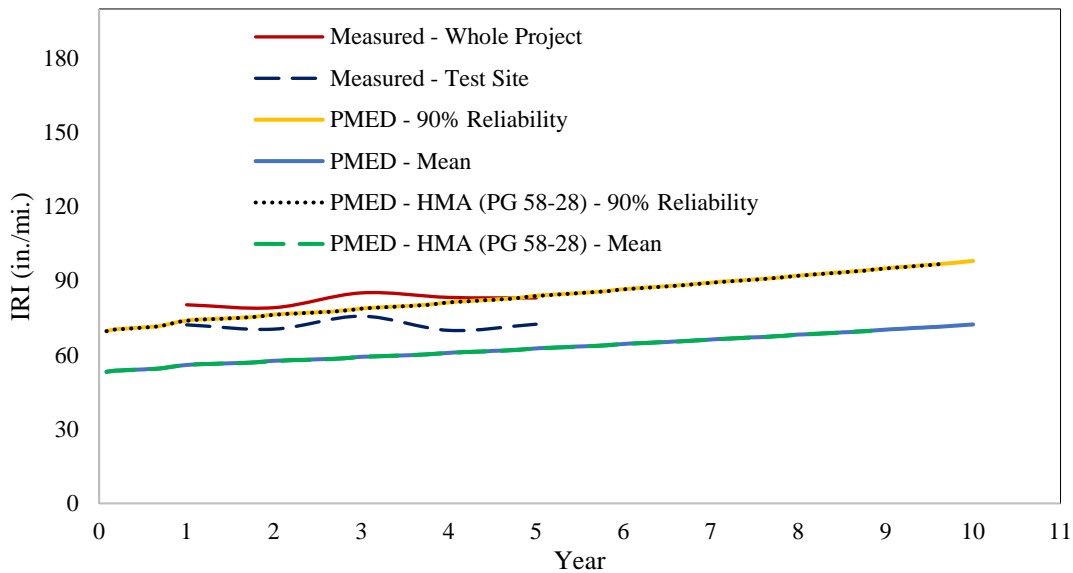


**Figure 120. IRI at SH 86 Kiowa (Eastbound) Showing Amount of Measured and PMED Predicted IRI**

The measured and the PMED-predicted total rutting of SH 86 Kiowa (Eastbound) are presented in Figure 121 below. The PMED-outputs using the CIR and the HMA SX (75) PG 58-28 are almost the same. The measured total rutting values are in good agreement with the PMED-predicted mean rutting values compared to the PMED-predicted IRI. The PMED-predicted rutting values at 90% reliability are higher than the measured rutting values.

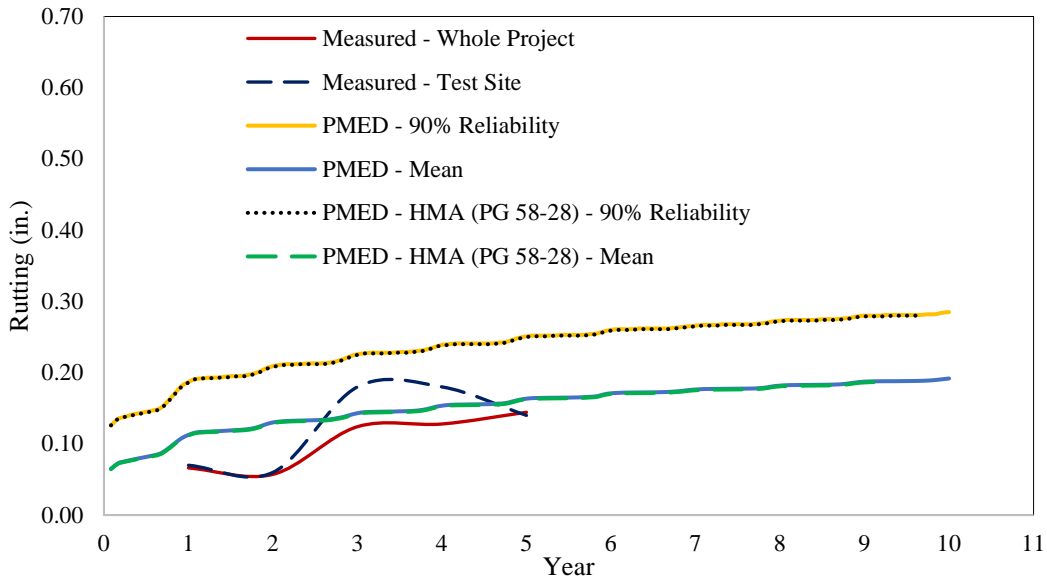


**Figure 121. Total Rutting at SH 86 Kiowa (Eastbound) Showing Amount of Measured and PMED Predicted Rutting**

The measured and the PMED-predicted fatigue cracking of SH 86 Kiowa (Eastbound) are presented in Figure 122 below. The measured fatigue cracking values on the whole project are very similar to the PMED-predicted fatigue cracking values at 90% reliability. The PMED-predicted fatigue cracking values by HMA SX (75) PG 58-28 mix at mean level are very small (close to zero).

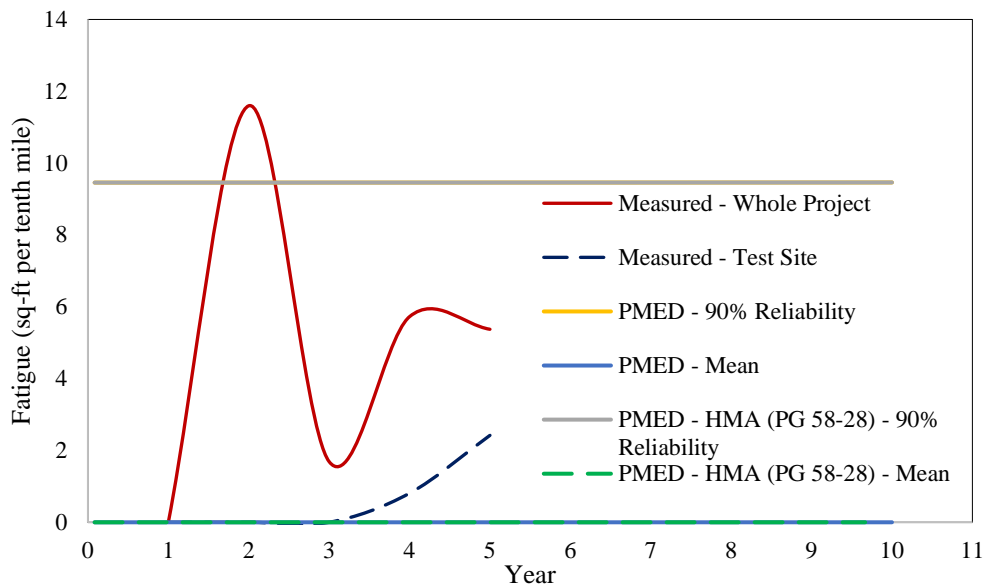


**Figure 122. Fatigue Cracking at SH 86 Kiowa (Eastbound) Showing Amount of Measured and PMED Predicted Cracking**

Site #5 I-25 South of Colorado City

The measured and the PMED-predicted IRI of I-25 South of Colorado City are presented in Figure 123 below. The PMED-outputs using the CIR and the HMA SX (75) PG 58-28 are similar, not the same as observed in the previous site. However, the HMA SX (75) PG 58-28 produces higher IRI compared to the CIR material. Figure 123 also shows the PMED-predicted IRI values at 90% reliability are higher than the measured IRI values. The PMED-predicted mean IRI values for both CIR and HMA SX (75) PG 58-28 consideration are in good agreement with the measured IRI values.

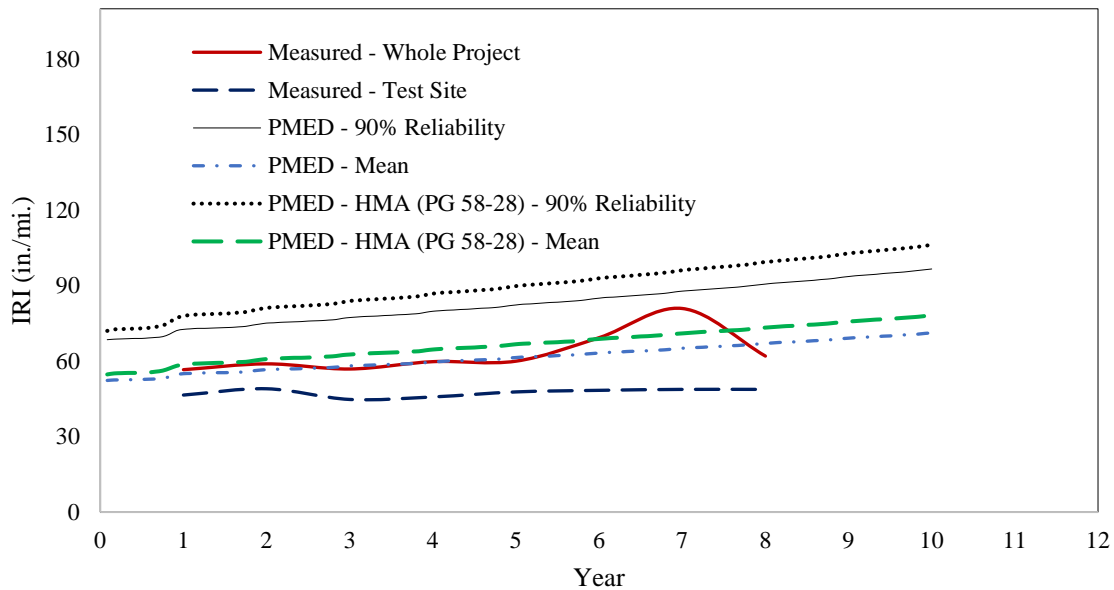


**Figure 123. IRI at I-25 South of Colorado City Showing Amount of Measured and PMED Predicted IRI**

The measured and the PMED-predicted total rutting of I-25 south of Colorado City are presented in Figure 124 below. The measured total rutting values are in good agreement with the PMED-predicted mean rutting values compared to the PMED-predicted IRI at 90% reliability. The PMED-predicted rutting values at 90% reliability for both HMA and CIR conditions are higher than the measured rutting values.

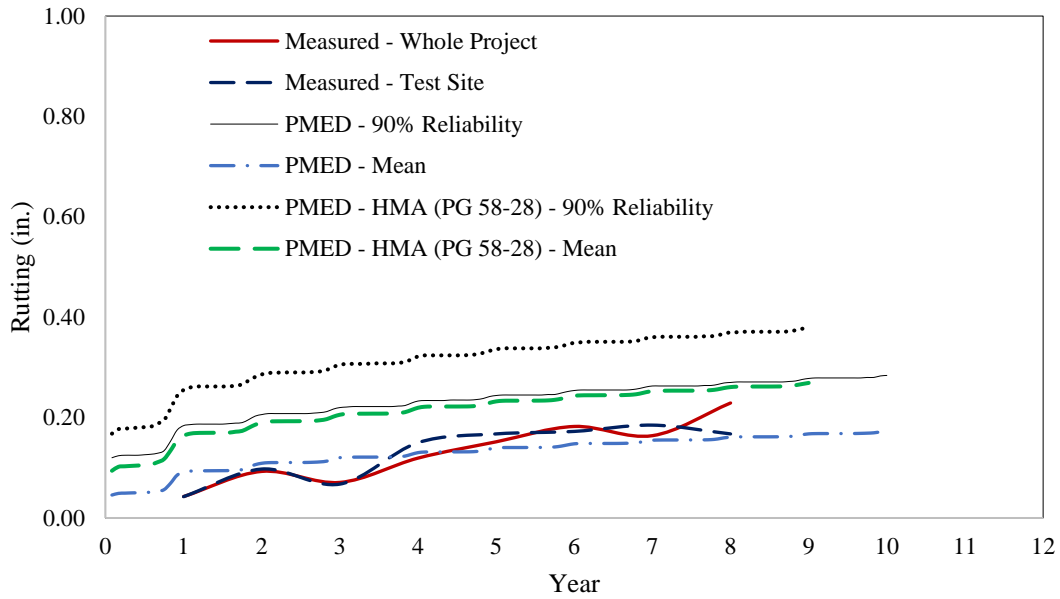


**Figure 124. Total Rutting at I-25 South of Colorado City Showing Amount of Measured and PMED Predicted Rutting**

The measured and the PMED-predicted fatigue cracking of I-25 south of Colorado City are presented in Figure 125 below. The measured fatigue cracking values on the whole project and test site are much higher than the PMED-predicted fatigue cracking values for any consideration. The PMED-predicted fatigue cracking values by both HMA and CIR mix at mean level are very small (close to zero), while at 90% reliability, they produce about 9.5 square feet per tenth-mile.

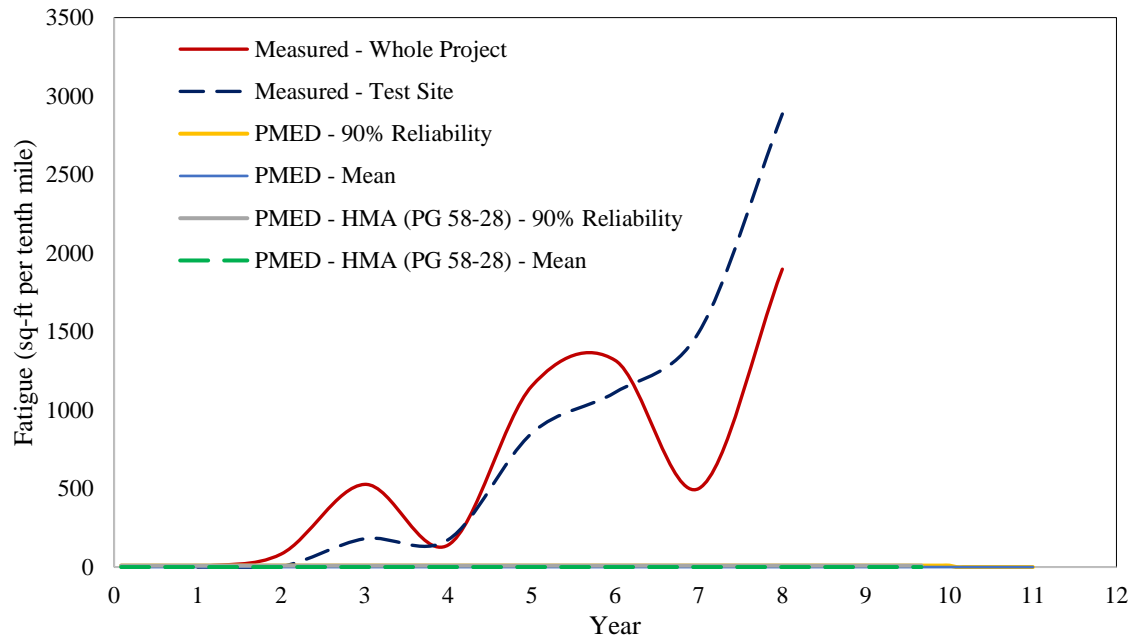


**Figure 125. Fatigue Cracking at I-25 South of Colorado City Showing Amount of Measured and PMED Predicted Cracking**

*Site #6 SH 50 Cerro Summit*

The measured and the PMED-predicted IRI of SH 50 Cerro Summit are presented in Figure 126 below. The first observation from this figure is that the PMED-outputs using the CIR and the HMA SX (75) PG 58-28 are almost the same. The measured IRI values are bounded by the PMED-predicted IRI values at 90% reliability level and at mean level. However, the PMED-predicted IRI values at 90% reliability are in better agreement with the measured IRI values compared to the PMED-predicted mean IRI values.

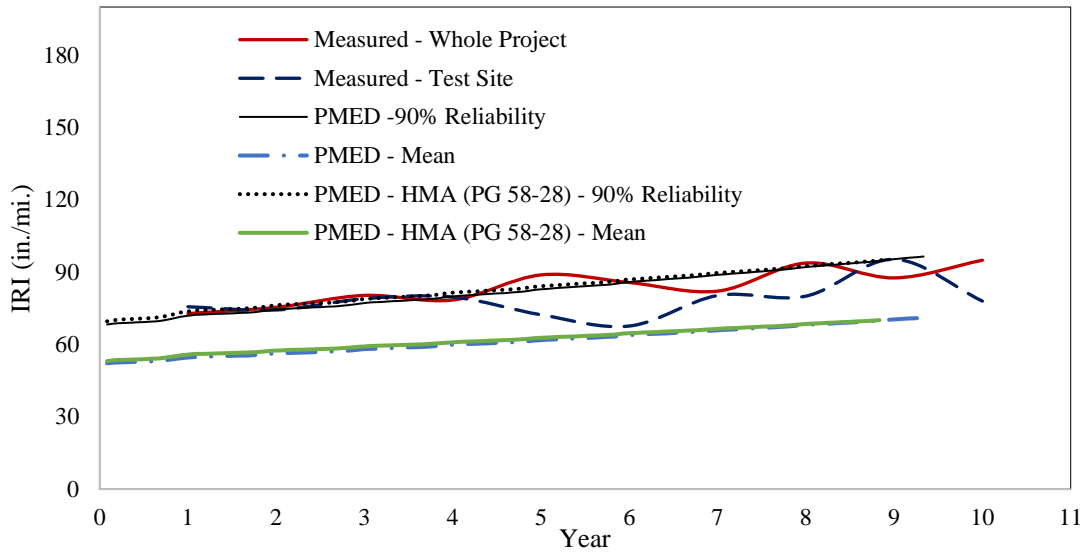


**Figure 126. IRI at SH 50 Cerro Showing Amount of Measured and PMED Predicted IRI**

The measured and the PMED-predicted total rutting of the SH 50 Cerro Summit are presented in Figure 127 below. The measured total rutting values are very close to the PMED-predicted mean rutting values; the PMED-predicted rutting values at 90% reliability are higher than the measured values (similar to the previous site (Site #5)).

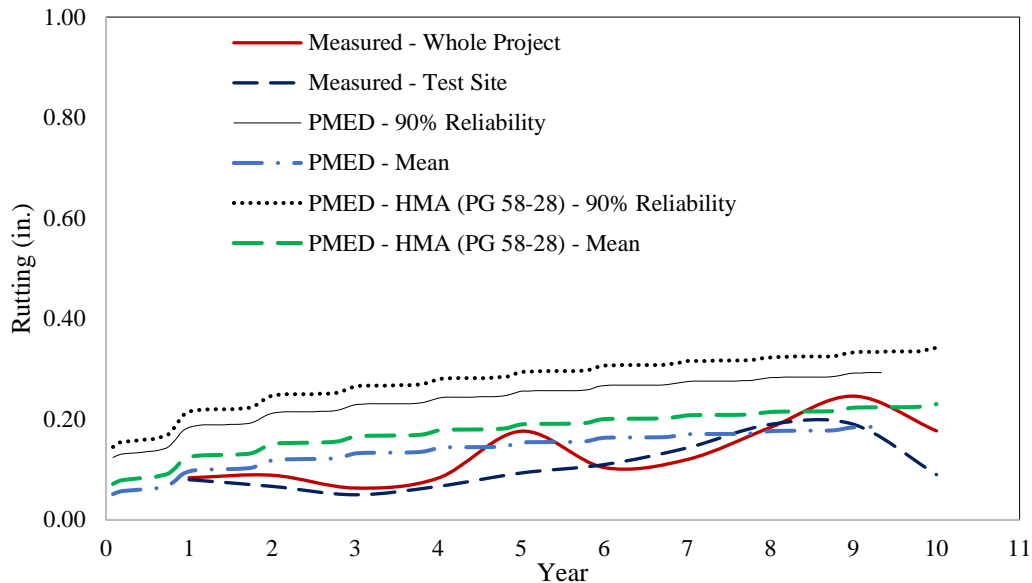


**Figure 127. Total Rutting at SH 50 Cerro Summit Showing Amount of Measured and PMED Predicted Rutting**

The measured and the PMED-predicted fatigue cracking of SH 50 Cerro Summit are presented in

Figure 128 below. The measured fatigue cracking values at the whole project and test site are higher than the PMED-predicted fatigue cracking values. The PMED-predicted fatigue cracking values by both HMA and CIR mix at mean level are very small (close to zero), while at 90% reliability, they produce about 9.5 square feet per tenth-mile.

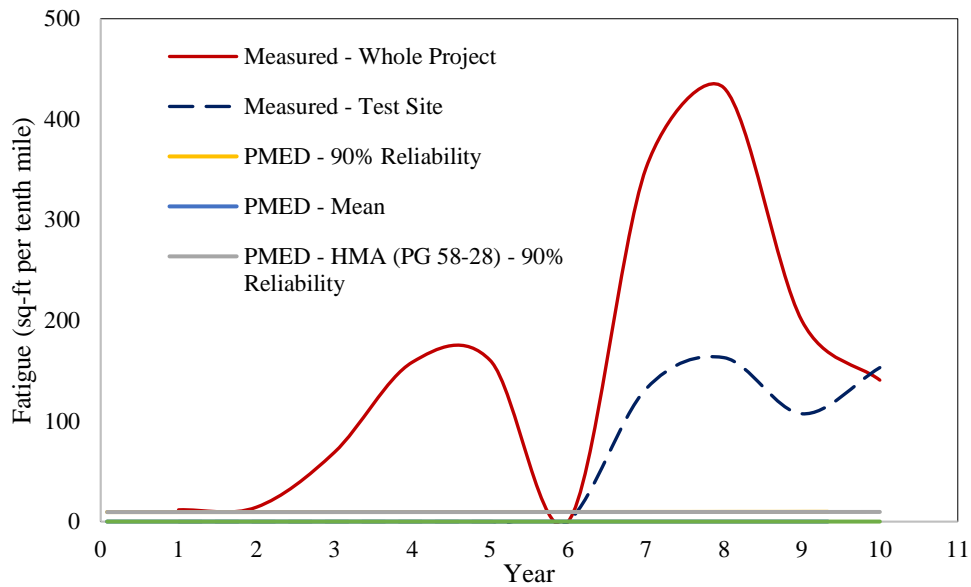


**Figure 128. Fatigue Cracking at SH 50 Cerro Summit Showing Amount of Measured and PMED Predicted Cracking**

Site #7 I-70 West of Mack

The measured and the PMED-predicted IRI of I-70 West of Mack are presented in Figure 129 below. It shows that the HMA SX (75) PG 58-28 produces higher IRI compared to the CIR material both at 90% reliability and at mean level. The PMED-predicted mean IRI values using both the CIR and HMA SX (75) PG 58-28 are very close to the measured IRI values.

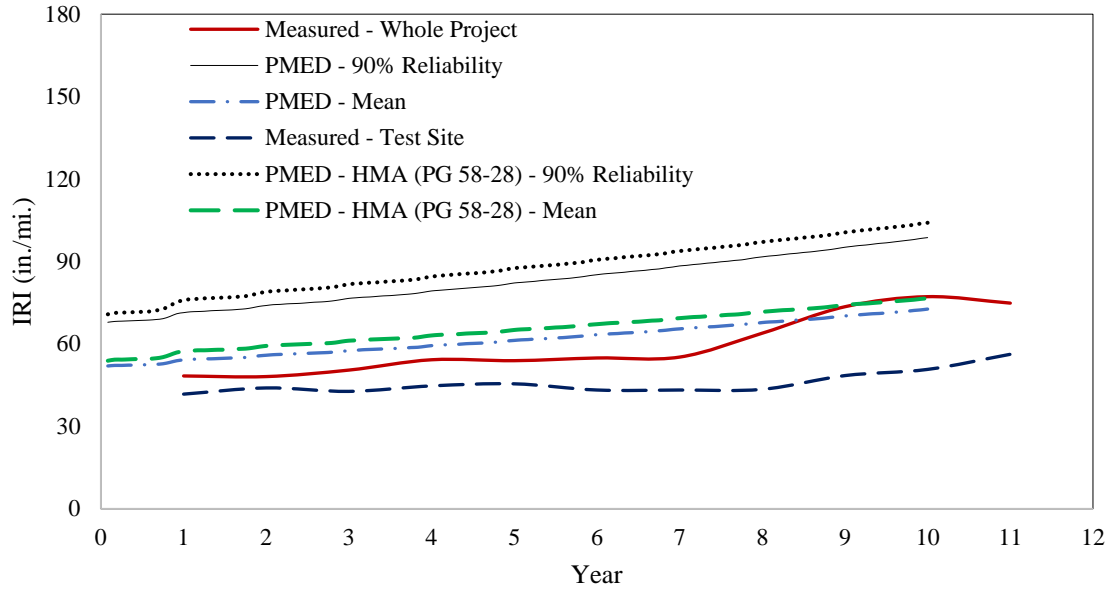


**Figure 129. IRI at I-70 West of Mack Showing Amount of Measured and PMED Predicted IRI**

The measured and the PMED-predicted total rutting of I-70 West of Mack are presented in Figure 130 below. The measured total rutting values are in good agreement with the PMED-predicted mean rutting values for all cases except the PMED-prediction at 90% reliability with HMA material. The PMED-predicted rutting values at 90% reliability for HMA material are slightly higher than the measured rutting values.

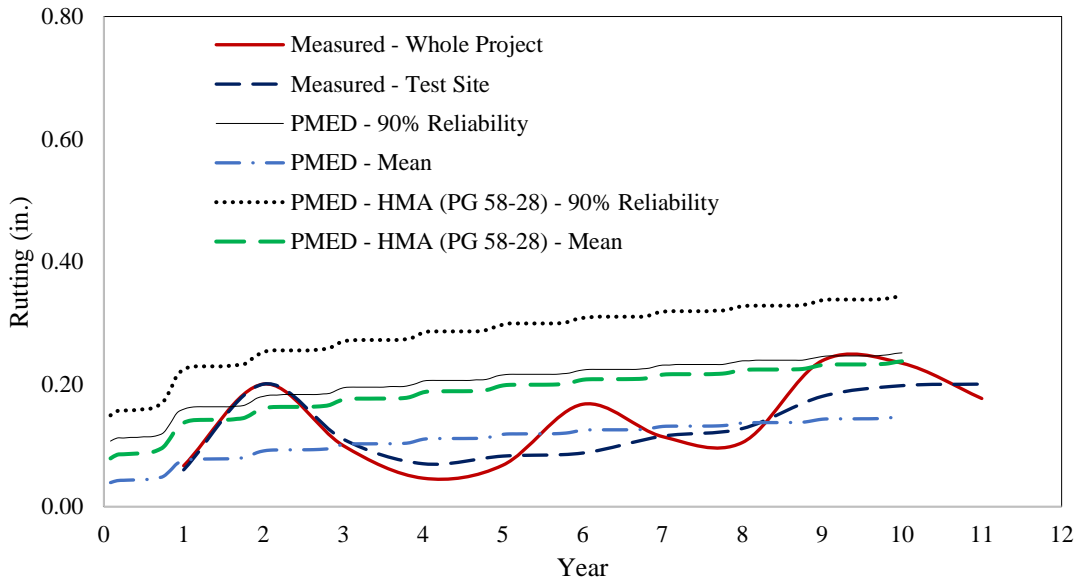


**Figure 130. Total Rutting at I-70 West of Mack Showing Amount of Measured and PMED Predicted Rutting**

The measured fatigue cracking values at the whole project and test site are higher than the PMED-predicted fatigue cracking values, Figure 131. The PMED-predicted fatigue cracking values by both HMA and CIR mix at mean level are very small (close to zero), while at 90% reliability, they produce about 9.5 square feet per tenth-mile.

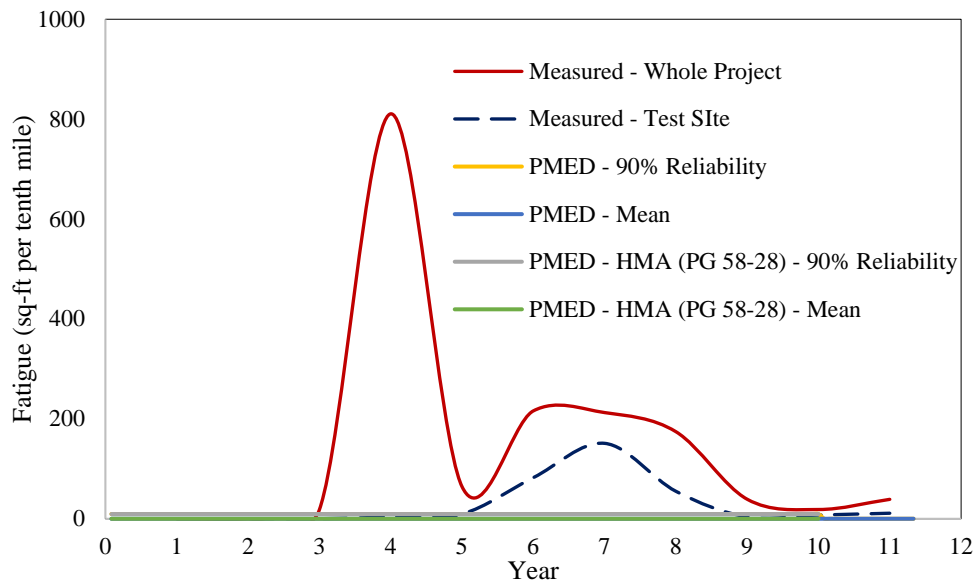


**Figure 131. Fatigue Cracking at I-70 West of Mack Showing Amount of Measured and PMED Predicted Cracking**

Site #8 I-70 Fruita to Clifton

The measured and the PMED-predicted IRI of Fruita to Clifton are presented in Figure 132 below. It shows that the PMED-predicted mean IRI values using the HMA SX (75) PG 58-28 are closer to the measured IRI values compared to the PMED-predicted IRI at 90% reliability. The PMED-predicted IRI values at 90% reliability using the HMA SX (75) PG 58-28 are higher than the measured IRI values.

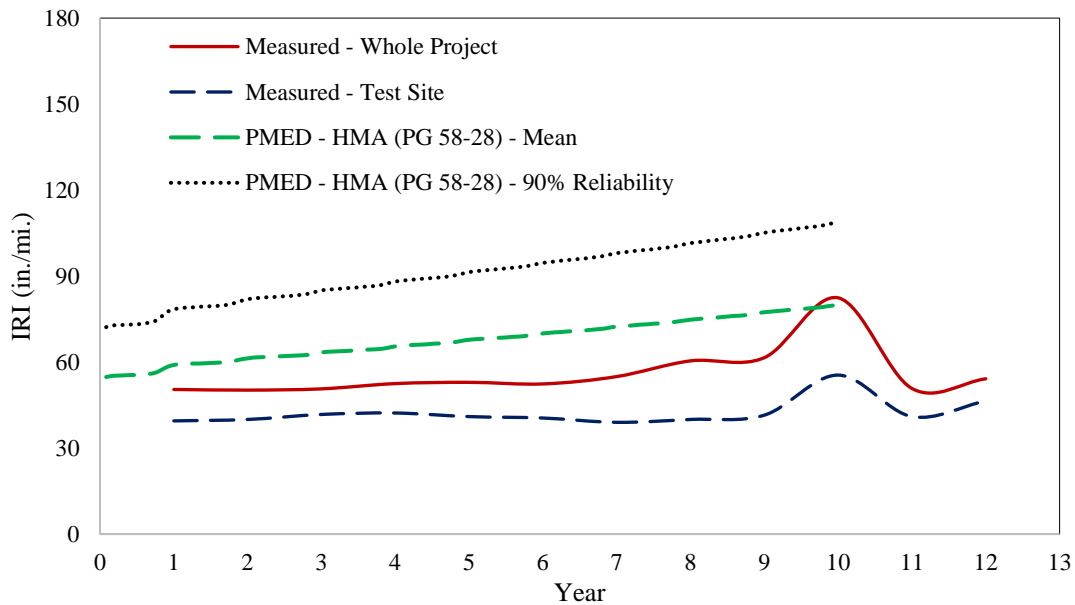


**Figure 132. IRI at I-70 Fruita to Clifton Showing Amount of Measured and PMED Predicted IRI**

The measured and the PMED-predicted total rutting of Fruita to Clifton are presented in Figure 133 below. The measured total rutting values are lower than the PMED-predicted rutting values using the HMA SX (75) PG 58-28 at both 90% reliability and mean level.

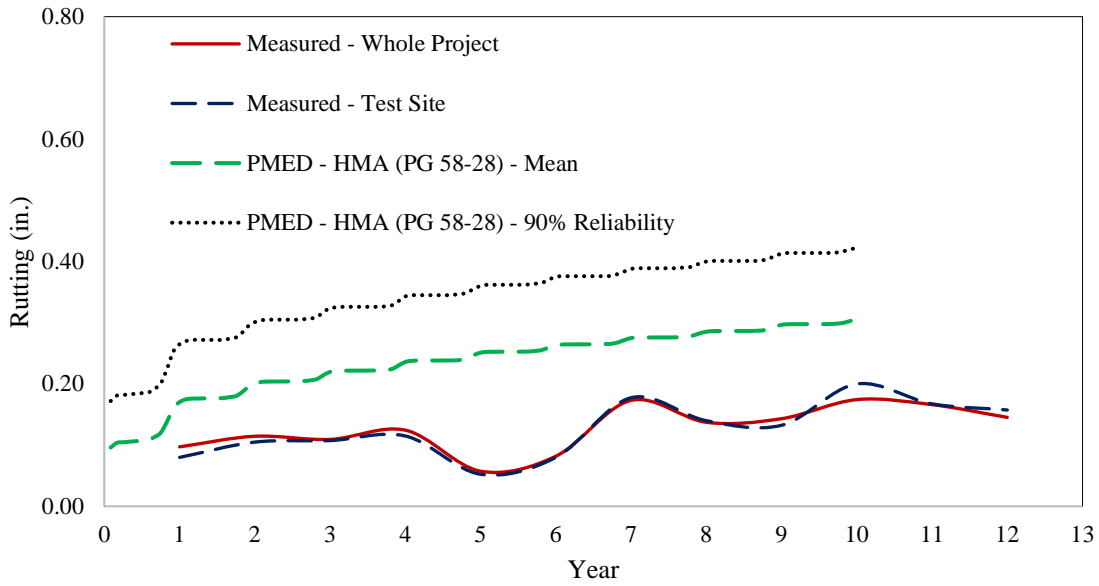


**Figure 133. Total Rutting at I-70 Fruita to Clifton Showing Amount of Measured and PMED Predicted Rutting**

The measured and the PMED-predicted fatigue cracking of Fruita to Clifton are presented in Figure 134 below. The measured fatigue cracking values are much higher than the PMED-predicted fatigue cracking values using the HMA SX (75) PG 58-28. The PMED-predicted fatigue cracking values by HMA SX (75) PG 58-28 mix at mean level are very small (close to zero), while at 90% reliability, they produce about 9.5 square feet per tenth-mile.

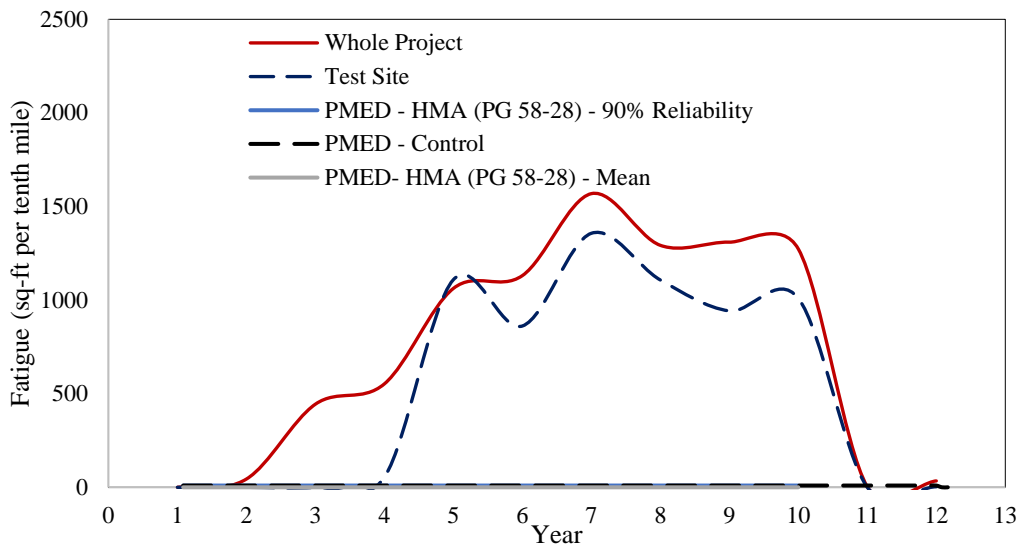


**Figure 134. Fatigue Cracking at I-70 Fruita to Clifton Showing Amount of Measured and PMED Predicted Cracking**

Site #9 SH 92 Delta (Eastbound)

The measured and the PMED-predicted IRI of SH 92 Delta are presented in Figure 135 below. The first observation from this figure is that the PMED-outputs using the CIR and the HMA SX (75) PG 58-28 are very close to each other. It also shows the PMED-predicted mean IRI values are in good agreement with the measured IRI values. The measured IRI values are lower than the PMED-predicted IRI values.

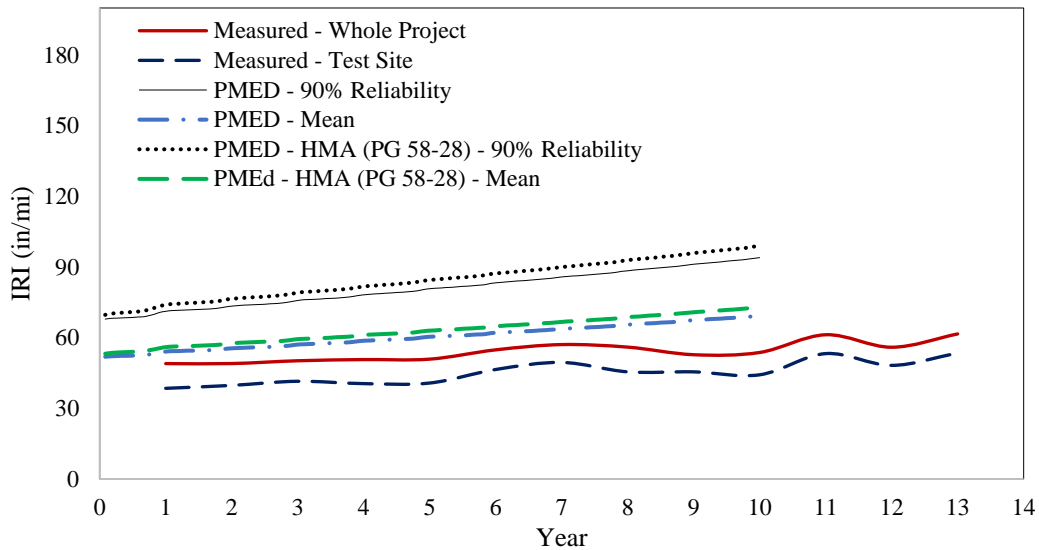


**Figure 135. IRI at SH 92 Delta (Eastbound) Showing Amount of Measured and PMED Predicted IRI**

The measured and the PMED-predicted total rutting of SH 92 Delta are presented in Figure 136 below. The measured total rutting values are in good agreement with the PMED-predicted total rutting values at different conditions. The predictions by CIR consideration and HMA consideration are close to each other.

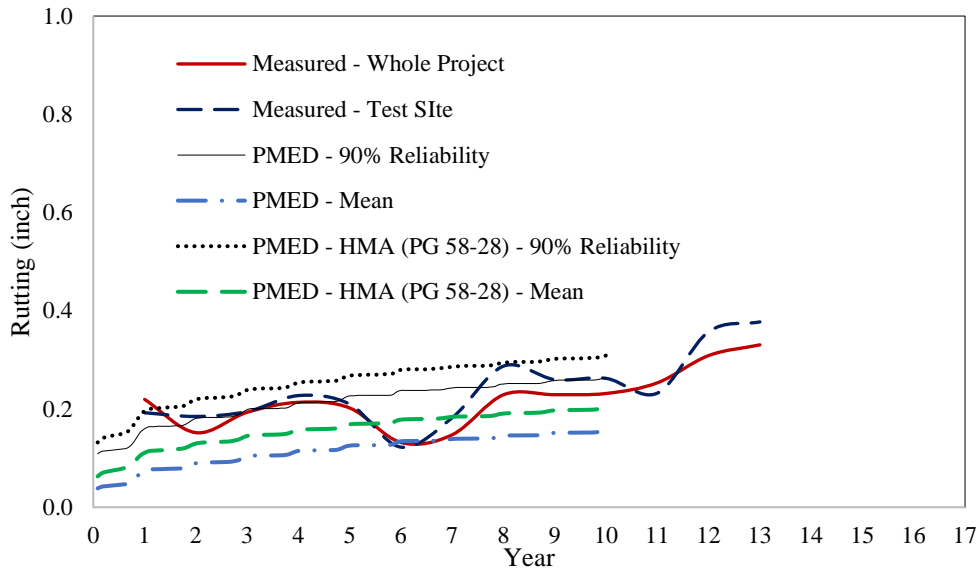


**Figure 136. Total Rutting at SH 92 Delta (Eastbound) Showing Amount of Measured and PMED Predicted Rutting**

The measured fatigue cracking values at the whole project and test site are higher than the PMED-predicted fatigue cracking values, Figure 137. The PMED-predicted fatigue cracking values by both HMA and CIR mix at mean level are very small (close to zero), while at 90% reliability, they produce about 9.5 square feet per tenth-mile.

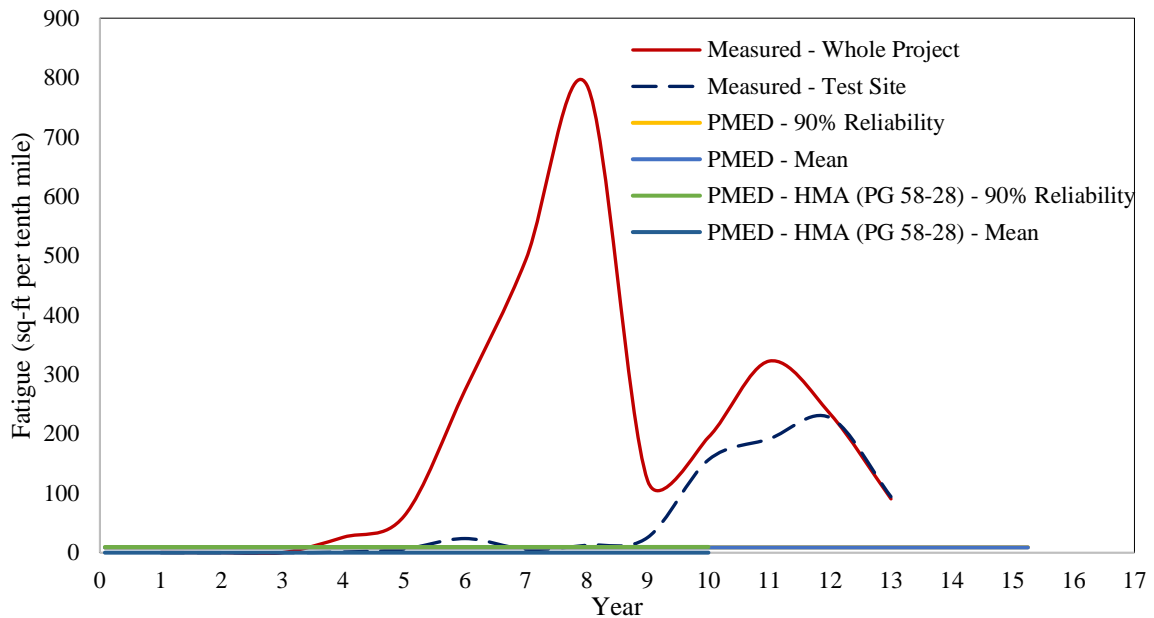


**Figure 137. Fatigue Cracking at SH 92 Delta (Eastbound) Showing Amount of Measured and PMED Predicted Cracking**

Site #10 SH 133 North of Hotchkiss

The measured and the PMED-predicted IRI of SH 133 Hotchkiss are presented in Figure 138 below. The PMED-outputs using the CIR and the HMA SX (75) PG 58-28 are almost the same. The measured IRI values are in between the PMED-predicted total IRI at mean level and at 90% reliability.

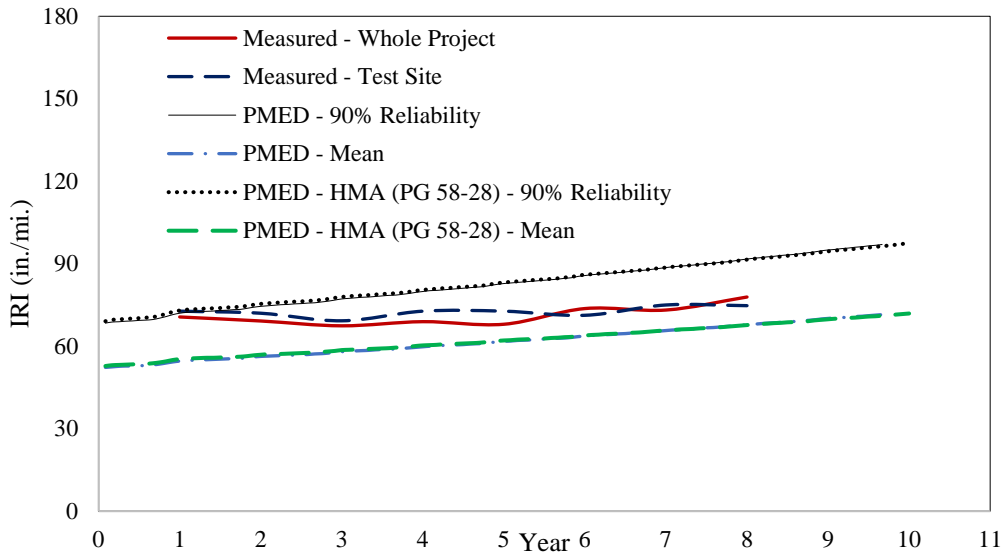


**Figure 138. IRI at SH 133 North of Hotchkiss Showing Amount of Measured and PMED Predicted IRI**

The measured and the PMED-predicted total rutting of SH 133 Hotchkiss are presented in Figure 139 below. The PMED-outputs using the CIR and the HMA SX (75) PG 58-28 are very close to each other. The PMED-outputs using the CIR and the HMA SX (75) PG 58-28 are very close to each other. The measured rutting values are in between the PMED-predicted rutting values.

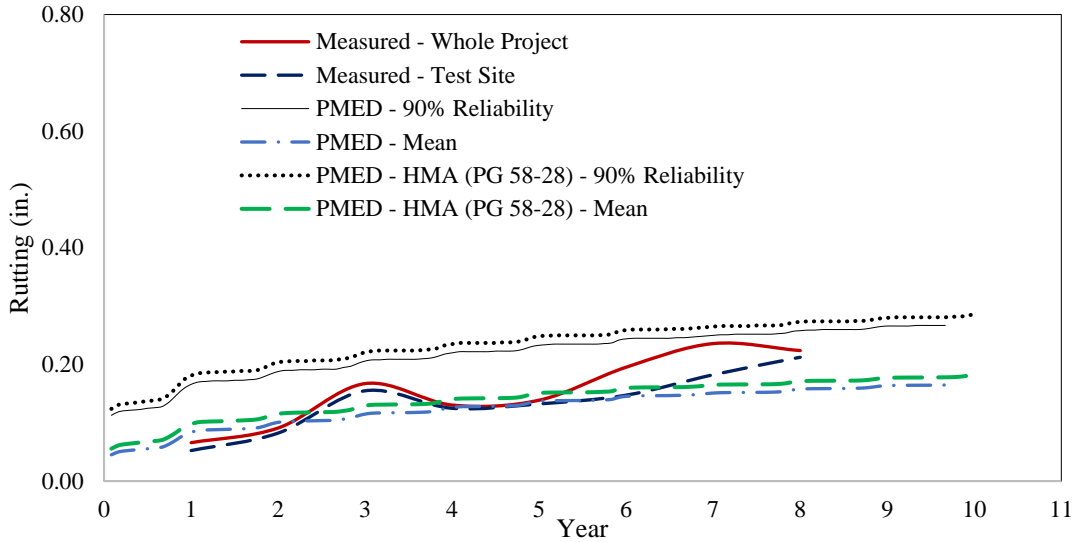


**Figure 139. Total Rutting at SH 133 North of Hotchkiss Showing Amount of Measured and PMED Predicted Rutting**

The measured and the PMED-predicted fatigue cracking of SH 133 Hotchkiss are presented in Figure 140 below. The measured fatigue cracking values are similar to the PMED-predicted fatigue cracking values at 90% reliability. The PMED-predicted fatigue cracking values by both HMA and CIR mix at mean level are very small (close to zero), while at 90% reliability, they produce about 9.5 square feet per tenth-mile.

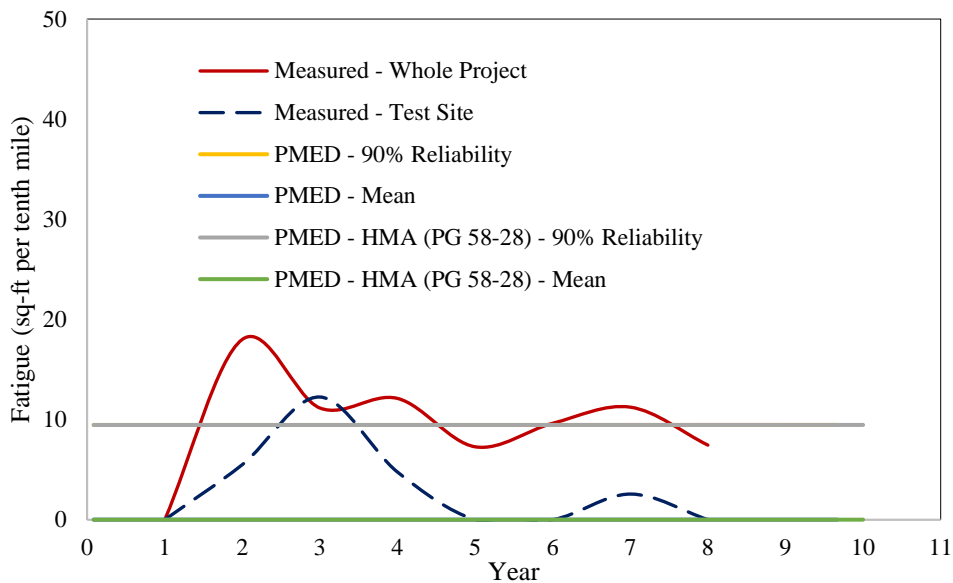


**Figure 140. Fatigue Cracking at SH 133 North of Hotchkiss Showing Amount of Measured and PMED Predicted Cracking**

## Summary

The PMED-predicted IRI and total rutting values are close or similar to the measured values. Thus, it can be said that the CDOT-calibrated PMED software for overlay design is good for the IRI and the total rutting with CIR materials as well. From the comparison of CIR and HMA SX (75) PG 58-28, it can be said that both materials behave almost the same for most of the sites and thus, can be used one in place of other.

The PMED-predicted fatigue cracking values are less than the measured data at the CIR whole project and test site. There may be several reasons for PMED low prediction. One reason is that a local calibration coefficient used in the fatigue equation, BF1 ( $\beta_{f1}$ ) is 130.3674 which is 1.0 for global calibration. A lower value of this coefficient may be appropriate for CIR material. Since calibration of the PMED software for CIR overlay design was not performed in this study, a more rigorous study is required for recalibration of the PMED software so it is compatible with CIR materials. Recalibration of the PMED software for overlay design with CIR materials is necessary for better cracking prediction.

## SECTION 8: CONCLUSIONS AND RECOMMENDATIONS

### Conclusions

This study evaluated the CIR material by conducting field performance data analysis, laboratory testing, and PMED software analysis. This study also developed a dynamic modulus master curve using test data from ten sites. Based on the study, the following conclusions are made:

- (a) Measured distresses of CIR rehabilitation techniques are mostly below the threshold values during the service period. IRI, Rutting and Transverse Cracking never exceeded the threshold values during the studied period. Only two CIR pavements exceeded the threshold values for fatigue cracking after 8-10 years of service.
- (b) Measured distresses of CIR rehabilitation techniques are similar to conventional pavement.
- (c) The CIR has smaller dynamic modulus compared to the conventional asphalt mixture at low temperature (or high frequency).
- (d) The generated master curve of the dynamic modulus has the following fitting parameters:
  - Max.  $E^*$  (ksi): 3,102.4
  - Min.  $E^*$  (ksi): 0.5
  - Beta,  $\beta$ : - 1.34372
  - Gamma,  $\gamma$ : -0.19225
  - $\Delta E_a$ : 241,692
- (e) CDOT calibrated PMED software is good to predict the IRI and the rutting of CIR overlaid pavement. The PMED prediction is mostly less for the fatigue cracking.
- (f) CIR materials investigated in this study behave very similar to the HMA SX (75) PG 58-28 mix and thus may be used in place of CIR.

## **Recommendations for Future Studies**

The conclusions drawn in the previous section are based on limited data available from the current study. Therefore, future studies are recommended and summarized below:

- (a) The current study used emulsified-CIR materials. Future research should incorporate cement treated or foam treated CIR material to determine the best CIR product. Effect of emulsion content may also be studied.
- (b) In future studies, CDOT may correlate pavement performance with dynamic modulus for both CIR sites and control sites. This may show how performance is correlated with dynamic modulus.
- (c) The PMED software analysis showed the PMED-predicted IRI and rutting values are close to the values measured in field. However, PMED-predicted fatigue cracking values are less than values measured in field. Therefore, recalibration of the PMED software for designing overlay using CIR is recommended.

## **Implementation Plans**

Based on this study, the following implementation plans are recommended:

- (a) CIR rehabilitation may be used in rehabilitation projects for low volume roads.
- (b) The dynamic moduli of CIR materials from this study can be used for CIR rehabilitation pavement designs.
- (c) The best-fitted dynamic modulus may be used for CIR overlay design.
- (d) The base and subgrade properties measured in this study may be used in pavement design at locations similar in elevation, geometry, traffic volume, etc.
- (e) The CDOT-calibrated PMED software may be used to predict the IRI and the rutting of CIR pavement overlays.

## SECTION 9: REFERENCES

1. Roberts, F.L., Kandhal, P.S., Brown, E.R., Lee, D-Y. and Kennedy, T. W. (1996) Hot Mix Asphalt Materials, Mixture Design, and Construction. NAPA Research and Education Foundation.
2. Cross, S. A. and Jakatimath, Y. (2007). Evaluation of Cold In-Place Recycling for Rehabilitation of Transverse Cracking on US 412, Report No. FHWA/OK 07 (04), Oklahoma Department of Transportation, Planning & Research Division, Oklahoma City, OK.
3. ARRA. (2014). Basic Asphalt Recycling Manual, 2nd Edition, Asphalt Recycling & Reclaiming Association (ARRA), Annapolis, Maryland.
4. Giani, M., Dotelli, G., Brandini, N., and Zampori, L. (2015). Comparative life cycle assessment of asphalt pavements using reclaimed asphalt, warm mix technology and cold in-place recycling, *Resources, Conservation and Recycling*, Vol. 104, pp. 224–238.
5. Schwartz, C. W. (2016). Structural Characteristics and Environmental Benefits of Cold-Recycled Asphalt Paving Materials. National Pavement Preservation Conference, October 12-14, 2016, Nashville, TN.
6. Bhavsar, J. (2015). Comparing Cold In-Place Recycling (CIR) and Cold In-Place Recycling with Expanded Asphalt Mixture (CIREAM), MS Thesis, Department of Civil Engineering, University of Waterloo, Ontario, Canada.
7. Kim et al (2010), Long-Term Field Performance of Cold In-Place Recycled Roads in Iowa, *Journal of Performance of Constructed Facilities*, Vol. 24, No. 3, 265–274.
8. Ma, T., Wang, H., Zhao, Y., Huang, X., and Pi, Y. (2015). Strength Mechanism and Influence Factors for Cold Recycled Asphalt Mixture, *Advances in Materials Science and Engineering*, Volume 2015, Article ID 181853, pp. 1-10.
9. Kim, Y., Lee, H., and Heitzman, M. (2007). "Validation of New Mix Design Procedure for Cold In-Place Recycling with Foamed Asphalt." *J. Mater. Civ. Eng.*, 19:11, 1000-1010.
10. Kim, Y., Lee, H., and Heitzman, M. (2009). "Dynamic Modulus and Repeated Load Tests of Cold In-Place Recycling Mixtures Using Foamed Asphalt." *J. Mater. Civ. Eng.*, 21:6, 279-285.
11. Kim, Y., and Lee, H., (2012). Performance evaluation of Cold In-Place Recycling mixtures using emulsified asphalt based on dynamic modulus, flow number, flow time, and raveling loss, *KSCE Journal of Civil Engineering*, Vol.16, No. 4, pp. 586–593.

12. Kim, Y, and Lee, H. (2011). Influence of Reclaimed Asphalt Pavement Temperature on Mix Design Process of Cold In-Place Recycling Using Foamed Asphalt, *Journal of Materials in Civil Engineering*, Vol. 23, No. 7, 961 – 968.
13. CDOT 2017, CDOT M-E Pavement Design Manual, Colorado Department of Transportation, Denver, CO.